REJECTION OF PERIODIC DISTURBANCES IN UNCERTAIN NONLINEARLY PERTURBED STABLE INFINITE DIMENSIONAL SYSTEMS

BY

VIVEK NATARAJAN

DISSERTATION

Submitted in partial fulfillment of the requirements
for the degree of Doctor of Philosophy in Mechanical Engineering
in the Graduate College of the
University of Illinois at Urbana-Champaign, 2012

Urbana, Illinois

Doctoral Committee:

Professor Joseph Bentsman, Chair and Director of Research
Professor M. Tamer Başar
Professor Naira Hovakimyan
Associate Professor Prashant G. Mehta

ABSTRACT

A motion distortion problem in the mold oscillation system of a continuous caster is addressed. The mold oscillation system consists of a subsystem of beams hinged at the center supporting the mold at one end and excited by an electro-hydraulic actuator at the other end. The actuator piston is attached to the beam subsystem and tracks a reference sinusoid, typically via proportional feedback. When the reference sinusoid frequency is near a submultiple of a beam resonance frequency, the mold velocity profile exhibits distortions. Eliminating these distortions will permit the safe operation of the oscillation system in production using reference sinusoids of larger frequency. This will improve the surface quality of the cast steel slabs which in turn will enable casting of newer grades of steel.

An experimental testbed, a simplified construction of the mold oscillation system, consisting of a hollow beam hinged at the center, supporting a mass resembling the mold at one end and excited by an electro-hydraulic actuator at the other end was built by the steel company. This testbed exhibits distortions similar, albeit more pronounced, to the mold oscillation system. Eliminating these distortions from the testbed is a prerequisite for gaining access to the mold oscillation system. Furthermore, access to the mold oscillation system is limited in general. Hence the modeling, problem formulation, controller synthesis, controller validation and rigorous analysis are carried out for the testbed. Then the controller is transitioned, under reasonable assumptions, to eliminate distortions in the mold oscillation system.

A fundamentally based analytical model of the testbed was developed as a system of coupled linear partial differential equations and nonlinear ordinary differential equations. Using experimental data it was hypothesized, and then verified using model simulations, that the major

source of distortion was the nonlinear actuator dynamics. The nonlinear effects, though insignificant in general, lead to the creation of small amplitude harmonics in the piston position signal that get amplified by the beam to create large distortions in the mold position and velocity profiles. Hence the overall system dynamics, with the piston position as the output, was justified to be that of a nonlinearly perturbed linear infinite dimensional system from whose output the harmonics created by the nonlinearity must be eliminated.

First a non-model based control scheme, using the plant gain at the frequency of interest alone, is developed to reject bandlimited periodic disturbances from the output of a nonlinearly perturbed finite dimensional plant. The stability of the closed loop is obtained via block diagram manipulations and small gain theorem. Next this scheme is shown to be applicable for tracking of periodic signals by regular linear systems, a fairly large class of infinite dimensional linear systems, using tools from infinite dimensional control theory. Quantifiable robustness margins, valuable in application, are derived. Finally a class of nonlinearly perturbed regular linear systems, matching the phenomenology of the application, is introduced. Its stability and response to periodic excitation are characterized and the proposed control scheme is rigorously shown to be applicable for rejecting unwanted harmonics from this class.

The testbed model is shown, under reasonable assumptions, to belong to the class of systems introduced above. Therefore applying the proposed control scheme in simulations to the testbed model and in experiments to the testbed is justified and is carried out to eliminate the unwanted harmonic. The mold oscillation system and the testbed have a similar structure - flexible components, electro-hydraulic actuator, and end mass. Therefore transitioning the control scheme, developed for the testbed, to the mold oscillation system is reasonable and is performed in the absence of steel to eliminate the unwanted harmonics, thereby removing the

distortions from the mold velocity profile. Finally, after refining the code to include calculation of the controller coefficients using explicit functions of the excitation frequency, the control scheme is implemented in production, i.e. in the presence of molten steel, to achieve visibly noticeable improvement in the surface quality of the steel slabs.

To my parents

ACKNOWLEDGEMENTS

I wish to thank my adviser Professor Joseph Bentsman for his guidance and encouragement during the course of my PhD. His constant support in all research matters enabled me to face the uncertainties encountered during my work confidently. I am thankful to him for always offering any help he could provide whole heartedly. I appreciate the freedom he gave me to pursue my research interests. I am indebted to him for introducing me to the area of control of PDEs.

I am grateful to Professors Tamer Basar, Naira Hovakimyan and Prashant Mehta for kindly agreeing to be on my doctoral committee. I thank them for their valuable comments and suggestions.

I thank Professor Eduard Kirr for giving me the opportunity to work with him on some very interesting problems. I learned a lot about PDEs both by working with him and from his courses. Our weekly meetings were an intense learning experience for me. I deeply appreciate the encouragement and support he so willingly provided me when I was exploring my career options. His guidance in this matter was invaluable.

I thank Dr. Ronald O'Malley and Nucor Steel, Decatur for the opportunity to work on the oscillator project which forms the basis for this dissertation. The financial support from Nucor Steel is gratefully acknowledged. Working with all the Nucor personnel has been a pleasure and I will certainly miss it.

Glynn Elliott has been a part of all the ups and downs in the oscillator project. His willingness to let me implement any new idea on the experimental setup and his patience when things did not go as planned (resulting in broken equipment, oil leaks, etc) made it a pleasure to work with him. I will vividly remember the day when we had our first successful experiment and

the day when we finally managed to prove our ideas in production. He has been more than a colleague and I will miss working with him. I thank him and Kathy for making my visits to Decatur enjoyable. I am also indebted to Sunil Hanumanthe for his invaluable support to the project.

Sincere thanks to the staff in the Mechanical Engineering department, especially Kathy Smith, for their assistance during my stay at Illinois.

My stay in Champaign would not have been pleasant but for the company of my friends Jagan, Kunal, Anil, Mamta, Gayathri, JK, Sathe, Jayanand, RG, Anand, Vijay, Sreeram, Shankar, Praveen, Venkat, Dwarak, Pritam and Ramki. My friends in the department Cheng, Huan, Barno, Ali, Ray and Rajneesh made my stay memorable. I thank my lab mates Bryan, Insu, Dong and Shu for the many interesting conversations.

Finally I would like to thank my family for their unwavering belief in me. It was comforting to know that I could always count on them. I am grateful to my wife Nandhini for her support over the past few strenuous months.

TABLE OF CONTENTS

LIST OF SYMBOLS

$\mathcal{L}(X,Y)$	Space of bounded linear operators from X to Y. Let $\mathcal{L}(X,X)=\mathcal{L}(X)$,
$L^2([t,T),X)$ / $L^\infty([t,T),X)$	Space of square integrable / essentially bounded functions from $[t,T)$ to X with the usual norm,
$L^2_{loc}([0,\infty),X)$	Space of locally square integrable functions from $[0,\infty)$ to X,
$L^2_\alpha([0,\infty),X)$	$\left\{ f \in L^2_{loc}([0,\infty),X) : \int_0^\infty \|f(t)\|_X^2 \, e^{-2\alpha t} dt < \infty \right\}$,
$H^n(a,b)$	Sobolev space of order n on (a,b),
$D(A)$ / $\rho(A)$	Domain / resolvent set of an operator A,
$\|\bullet\|_X$ / $\|\bullet\|_{op}$	Norm in space X / norm of the operator,
$\mathbb{R}$ / $\mathbb{C}$	Space of real / complex numbers,
$\mathbb{C}_\alpha$ / $\mathbb{C}_\alpha^+$	$\{s \in \mathbb{C} : \text{real}(s) > \alpha\}$ / $\{s \in \mathbb{C} : \text{real}(s) \geq \alpha\}$,
H_α^∞	Space of analytic functions from $\mathbb{C}_\alpha$ to $\mathbb{C}$ bounded in the supremum norm. Let $H_0^\infty = H^\infty$,
$\overline{x}$	Complex conjugate of x,
$B(a,b)$ / $B_c(a,b)$	Open / closed ball with center a and radius b, in the space being considered,
$\|x\|_{L^2[0,T)}$	Same as $\|x(t)\|_{L^2([0,T),X)}$, when X is clear,
$\|x\|_{X,\infty}$	Same as $\|x(t)\|_{L^\infty([0,\infty),X)}$,
$\|x([T,\infty))\|_{X,\infty}$	Same as $\|x(t)\|_{L^\infty([T,\infty),X)}$,

$C_B\left([0,\infty),X\right)$	Banach space of continuous bounded functions from $[0,\infty)$ to X with $\|\bullet\|_{X,\infty}$ as norm and
$C\left([0,t],D\right)$	Space of continuous functions from $[0,t]$ to $D \subseteq X$ with norm $\left\|x\left([0,t]\right)\right\|_{X,\infty}$.
TF	Transfer function
BIBO	Bounded input bounded output
SISO	Single input single output
MIMO	Multi input multi output

LIST OF FIGURES

LIST OF TABLES

CHAPTER 1

INTRODUCTION

Periodically excited structures, an integral component of many industrial systems, are typically affected by periodic disturbances. Rejection of such a disturbance from a flexible structure, mold oscillation system, used in the continuous casting of steel at Nucor Steel, Decatur is the subject of this dissertation. For the safe operation of the caster, the mold displacement and velocity profiles must be undistorted sinusoids of specified frequency and amplitude. The controller presently used at Nucor Steel cannot satisfy this essential requirement in certain frequency range of excitation of the mold oscillation system thereby enforcing hard constraints on the caster operation and consequently on the grades of steel that can be cast. The goal is to develop a controller that can provide undistorted mold displacement and velocity profiles over the desired frequency range of excitation.

To study this problem Nucor Steel built an industrial scale physical testbed, exhibiting distortions in the mold profiles similar to those in the mold oscillation system. The two systems, mold oscillation system and testbed, are similar but not identical. Since the mold oscillation system is a critical component of the caster, access to it is restricted. Nucor stipulated that a control scheme be developed to address the distortion problem in the testbed first, its disturbance rejection capabilities be demonstrated in experiments and then the same scheme be transitioned to the mold oscillation system with minimal testing. To enable this, a source of disturbance based on the similarities between the two systems must be identified and addressed. The differences between the two systems suggested that the developed control scheme be not plant model based

to simplify its transitioning between the systems. Furthermore a non-model based data driven scheme can be easily automated and integrated with the overall process control.

An analytical model of the testbed was developed to understand the distortion problem, identify its cause and test various solution approaches. Based on this model and the results from experiments and model simulations, the testbed was characterized as a nonlinearly perturbed linear infinite dimensional structure. Under sinusoidal excitation, the nonlinear perturbation generates harmonics in the system output which excite the infinite dimensional structure near a resonance causing distortion in the mold profiles. Hence the control objective is to eliminate the harmonic near the resonance frequency from the system output.

Tracking and rejection of periodic signals with zero steady state error based on internal model principle (IMP) [1] introduces the generator of the signal into the closed-loop. IMP has been used to track and reject periodic signals in finite dimensional linear [2]-[7] and nonlinear systems [8]-[10] when the plant model is known. When the plant model is linear finite dimensional but unknown, the methodology for applying IMP using only the TF gains at the frequencies of interest, to track bandlimited periodic signals was developed in [11]-[13]. This methodology has been extended to exponentially stable regular linear systems (a large subset of well-posed linear system) in [14] (only for step reference), to the class of stable plants with TF in Callier-Desoer algebra in [15], and to exponentially stable well-posed linear systems in [16].

The aforementioned non-model based techniques focus on linear systems, require the tuning of a non-intuitive parameter for stability, and do not provide quantitative robustness estimates that are essential in application. These shortcomings are addressed by introducing a class of nonlinearly perturbed infinite dimensional systems, developing a non-model based control scheme for linear infinite dimensional systems with quantifiable robustness and graphical

interpretation for the tuning parameter, and then rigorously establishing the applicability of this scheme to the class of nonlinear systems. Finally, the testbed model is classified as belonging to this class. This justifies implementing the proposed control scheme on the testbed, and on the mold oscillation system owing to its structural similarity with the testbed, to eliminate distortions in the mold profiles. Accomplishing this has enabled the production of steel with better surface quality at Nucor.

1.1 Dissertation outline

The organization of the dissertation is as follows. In Chapter 2 continuous casting of steel, the process of interest, is discussed. In particular the mold oscillation system, a subsystem of beams supporting the mold and excited by an electro-hydraulic actuator, which is affected by periodic disturbances is described. The influence of the frequency and amplitude of oscillation and the presence of distortions in the mold velocity profile on the casting process are explained. Next a testbed for the mold oscillation system consisting of a beam with an end mass, called mold, and excited by an electro-hydraulic actuator is presented. The testbed exhibits distortions in the mold profiles similar to the mold oscillation system. A fundamentally based analytical model of the testbed as a system of coupled linear partial differential equations and nonlinear ordinary differential equations is developed. In simulation, this model shows the distortions seen in the testbed and hence can act as a platform for understanding the dynamics and testing control schemes. Using experimental data from the testbed and computational data from the testbed model the cause of distortion is identified. Based on the system dynamics the abstract mathematical problem statement for controller synthesis is formulated as the rejection of bandlimited periodic disturbances from a nonlinearly perturbed infinite dimensional system.

In Chapter 3 the controller synthesis problem is addressed by assuming that the plant model is a nonlinearly perturbed finite dimensional system. The proposed non-model based solution methodology is motivated by the repetitive control architecture, the delay block in which is replaced by an appropriately chosen filter. The control scheme assumes no knowledge of the given closed-loop system, other than that it behaves like a stable perturbed finite dimensional linear system and its gain at the frequency interest, readily found in experiments, is non-zero. The controller synthesis is presented in detail, providing insights and motivating the concise feedback architectures considered in the infinite dimensional case. The proof technique is based on block diagram manipulations and small gain theorem. A discussion comparing the proposed methodology with the previous works is included.

The control scheme proposed in Chapter 3 is shown in Chapter 4 to be applicable to tracking of bandlimited periodic signals by plants in the class of regular linear systems (RLS), a large class of infinite dimensional systems encompassing many physical models. Results on the feedback interconnection of RLS are used to establish the stability of the closed loop. The controller uses only the plant gain at the frequency of interest and quantitative robustness estimates are derived in terms of permissible variations in this plant gain. Guidance for choosing the controller parameters is presented.

To rigorously address the problem statement in Chapter 2, a class of systems - nonlinearly perturbed regular linear system (NPRLS) - that directly matches the phenomenology of the application of interest is defined and a detailed characterization of its stability and response to periodic excitation is presented in Chapter 5. The robust control scheme from Chapter 4 is then applied to plants in this class and conditions for closed loop stability and rejection of unwanted harmonics in the output are rigorously ascertained. This is accomplished by first considering the

closed loop without the nonlinear perturbation and then analyzing the effect of the perturbation on stability and performance using the aforementioned characterization of NPRLS.

The testbed model is shown under reasonable assumptions to be a NPRLS in Chapter 6. A major step in this is to characterize the state operator associated with the linearization of the model. The state operator is shown to be the sum of a maximal dissipative operator and a bounded operator and hence the infinitesimal generator of a strongly continuous semigroup by Lumer-Phillips theorem. The exponential stability of the semigroup is then justified under reasonable assumptions. The other assumptions that must be verified to establish that the testbed model is a NPRLS follow directly.

Chapter 7 presents the computational and experimental results. Since the testbed model is a NPRLS, it is justified to apply the control scheme in Chapter 5 to the testbed to reject unwanted harmonics and eliminate distortions in the mold profiles. Validation of the controller, both computationally on the testbed model and experimentally on the testbed, is presented. Owing to the similarity between the structure of the testbed and the mold oscillation system, it is reasonable to assume that the control scheme developed for the former applies to the latter. Results of implementing the control scheme on the mold oscillation system, first in the absence of steel in the mold and then with steel during the casting process, are presented. The results indicate that the distortions in the mold profiles over the desired frequency range of operation are eliminated, thereby enabling the production of steel slabs with an improved surface quality. Practical aspects of controller implementation are discussed in detail. The role played by the robustness estimates derived in Chapter 4 in choosing the controller parameters is clarified.

A summary of the dissertation and suggestions for future work are presented in Chapter 8.

Some of the results in this dissertation have previously appeared in [17]-[19] and are also included in [20], [21].

CHAPTER 2

INDUSTRIAL APPLICATION AND PROBLEM STATEMENT

The industrial process of interest, continuous casting of steel, and the mold oscillation system which is an integral part of this process are introduced. The mold oscillation system is affected by periodic disturbances which distort the mold displacement and velocity profiles and must be rejected. The experimental testbed for the mold oscillation system which exhibits similar distortions in the mold profiles and the analytical model of the testbed are presented. The cause of distortions in the testbed is identified using data from experiments and simulations. On the basis of this identification the problem statement for controller synthesis is formulated.

2.1 Continuous casting of steel

Continuous casting is a widely used industrial process for transforming molten steel continuously into slabs. In this process molten steel is poured from above into a tall hollow rectangular copper mold which is open in the top and the bottom and is water cooled on the sides. As the steel flows down the mold, it freezes on contact with the mold walls and forms a solid shell with a liquid core. This shell is continuously pulled out from the bottom of the mold at a constant rate, called the casting speed. The casting speed and the rate at which molten steel is poured into the mold are matched, resulting in continuous casting. During this process the mold executes a sinusoidal vertical motion imposed by a mold oscillation system, which prevents the sticking of the shell to the mold wall. The amplitude and frequency of oscillation are chosen to obtain guaranteed negative strip time and reduce the oscillation marks.

The negative strip time is that period during each cycle of oscillation during which the mold moves down faster than the shell. During this time the mold exerts a compressive force on the shell and any steel sticking to the mold wall will be stripped off it and squeezed on to the existing shell [22]. This prevents tearing of the shell. Clearly the negative strip time depends both on the casting speed and the oscillation frequency and amplitude. To provide a guaranteed constant negative strip time, the sinusoidal profiles of the mold displacement and the corresponding velocity are required to be undistorted. An unexpected distorted velocity profile can result in a shorter than safe negative strip time and cause the tearing of the shell.

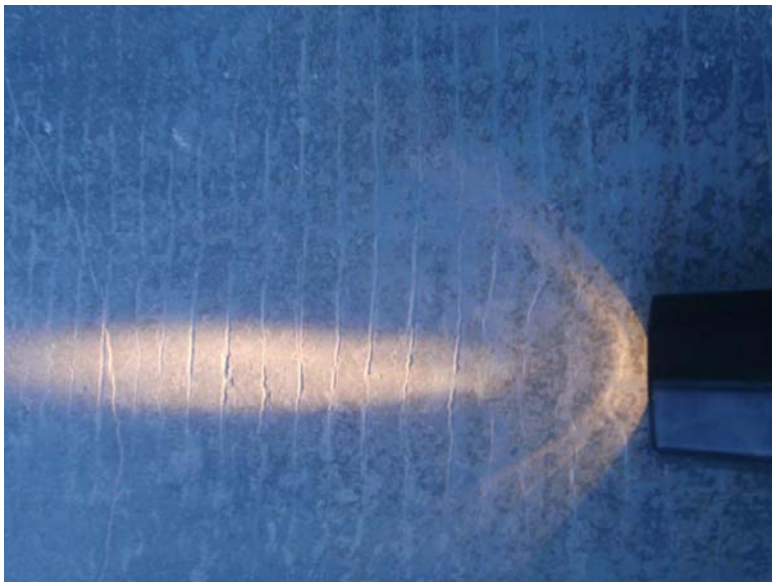

Figure 2.1: Oscillations marks (vertical lines in the picture) on the surface of the cast steel slab

The periodic oscillation of the mold leads to the formation of periodic depressions on the steel surface perpendicular to the direction of casting referred to as oscillation marks, as shown in Figure 2.1. These marks can act as initiation sites for cracks. Hence shallower oscillation marks are desirable and can be obtained by decreasing the amplitude and increasing the

frequency of oscillation. Detailed description of the continuous casting process can be found in [23].

2.2 Mold oscillation system

The mold oscillation system in the caster at Nucor Steel, Decatur, consists of a subsystem of beams that supports a heavy mold (~25,000 Kg) at one end and is driven by an electro-hydraulic actuator with its piston attached to this subsystem at the other end. Figure 2.2 and Figure 2.3 show the sideview and the backview, respectively, of the oscillation system assembled at a workshop. Both primary beams are hinged at the center and support the mold table, on which the mold is typically mounted, on one end. A steel structure called the counterweight (not in pictures), is placed across the two primary beams at the other end. The actuator is positioned symmetrically between the beams below the counterweight and is attached to it. The secondary beams assist in holding the mold table vertical.

Figure 2.2: Sideview of the caster mold oscillation system assembled at the workshop

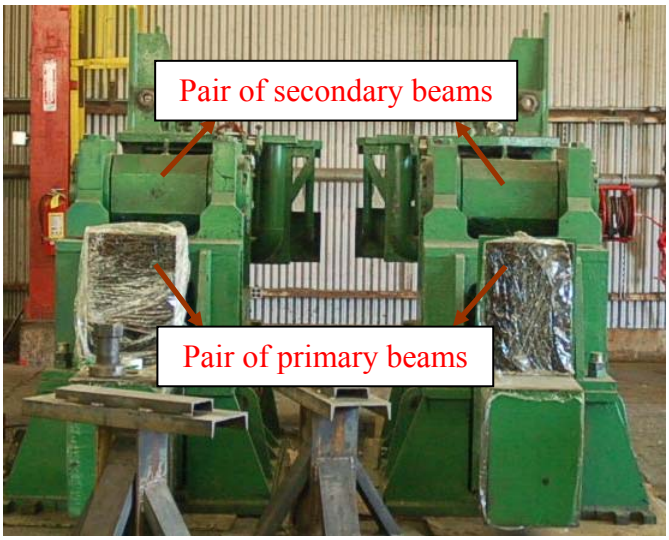

Figure 2.3: Backview of the caster mold oscillation system assembled at the workshop

The desired sinusoidal profile for the mold position is given as the reference input to the actuator piston for tracking, which is enforced using a controller. The present controller at Nucor Steel provides reasonable mold displacement and velocity profiles when the frequency of the reference input is below 3.8 Hz. To make the oscillation marks shallower - which will improve the surface quality, reduce the probability of surface crack formation and hence enable the casting of newer crack sensitive grades of steel - it is required that the frequency of the reference input be larger (up to 5.2 Hz). In this higher frequency range (3.85 Hz – 5.2 Hz) the mold profiles generated by the present controller are heavily distorted and in fact a proportional controller performs significantly better (but not satisfactorily). Since the focus is on the higher frequency range, the mold profiles provided by a proportional controller will be used as the standard against which the performance of any new controller will be measured.

Since the beam subsystem is not rigid, there is an inherent scaling between the displacement and velocity profiles at the mold and the actuator ends. This scaling can be compensated for by modifying the amplitude of the sinusoidal reference input to the piston.

However, at some reference input frequencies, the mold velocity profile exhibits distortion. The distortion is prominent at frequencies that are near submultiples of the resonance frequency of the beams in the subsystem. For instance the beam subsystem has a resonance near 13 Hz. When the reference input amplitude is 3.5 mm and frequency is 4.4 Hz the mold velocity profile exhibits significant distortion (Figure 2.4). The goal is to identify the source of this distortion and eliminate it. Here a proportional gain of 0.7 was used as the controller for tracking.

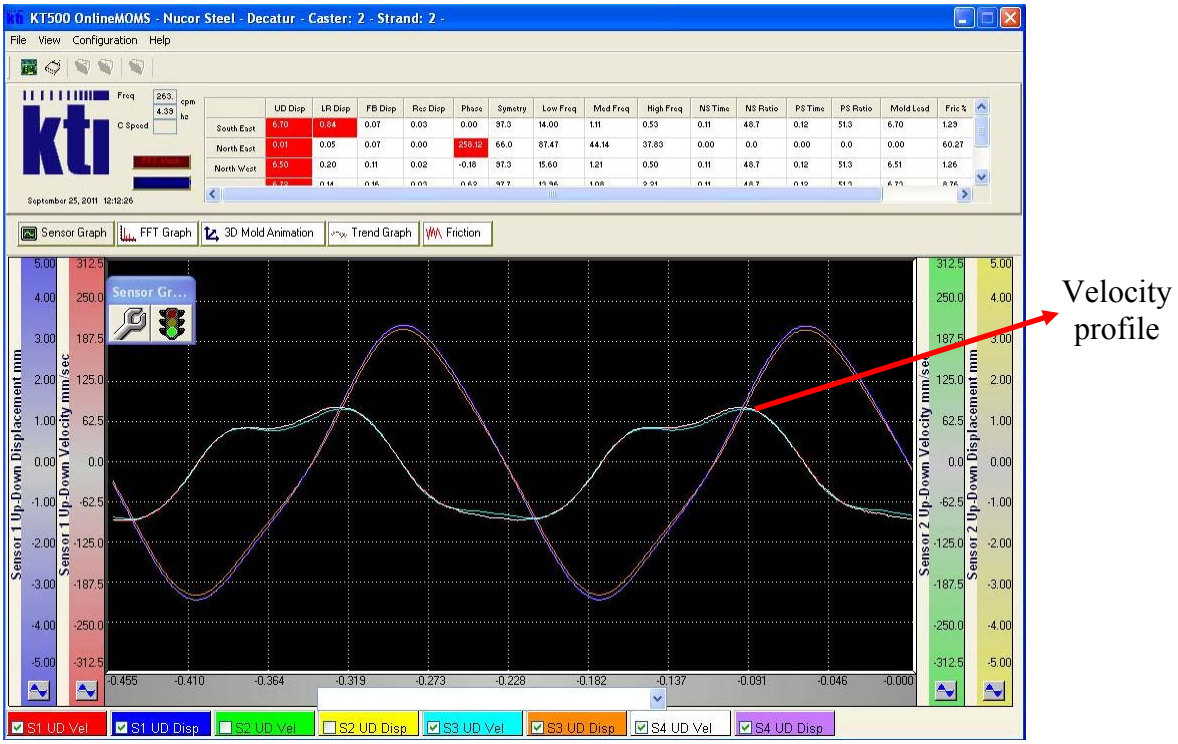

Figure 2.4: Screenshot of the mold displacement and velocity profiles displayed by the monitoring system at Nucor Steel

2.3 Experimental testbed

The mold oscillation system being one of the critical enabling components of the caster operation was not open to any experiments. Apart from a few screenshots, similar to Figure 2.4, showing

the distortion in the mold velocity profile at the caster, no other data was available at the beginning of the project. In fact, the occurrence of distortions in the mold velocity profile and its prominence at reference frequencies that are near submultiples of the beam resonance frequency are assumed to be true based on the reports by companies that had previously studied this problem and from the input from Nucor personnel.

As an alternative to providing access to the mold oscillation system, Nucor Steel built a physical testbed exhibiting a submultiples distortion problem to carry out controller development and testing. A prerequisite condition for gaining access to the caster mold oscillation system was solving the distortion problem in the testbed - a stipulation from Nucor, assuming the nature and source of distortion at the caster and the testbed are identical. The caster mold oscillation system differs from the testbed in being more rigid and complicated, thereby causing the distortions at the testbed to be more severe, suggesting that the developed controller ideally be not plant model based or, inasmuch as possible, make minimal use of the plant model.

The testbed (Figure 2.5) has a hinged hollow beam that supports a heavy mass (~2500 Kg), resembling a mold, on one end and is driven by an electro-hydraulic actuator with its piston attached to the beam at the other end. It exhibits the submultiples problem present in the mold oscillation system, albeit much more pronounced. When the frequency of the reference sinusoid to the actuator piston is near a submultiple of the beam resonance frequency, the mold displacement and velocity profiles exhibit significant distortions. For instance the first resonance frequency of the beam is near 9.2 Hz. When the reference to the piston is a sinusoid of 3 mm amplitude and 4.6 Hz frequency, i.e. at submultiple 2 of the beam resonance frequency, the mold displacement profile is heavily distorted (Figure 2.6). The tracking in this case is enforced by a proportional controller with gain 2.

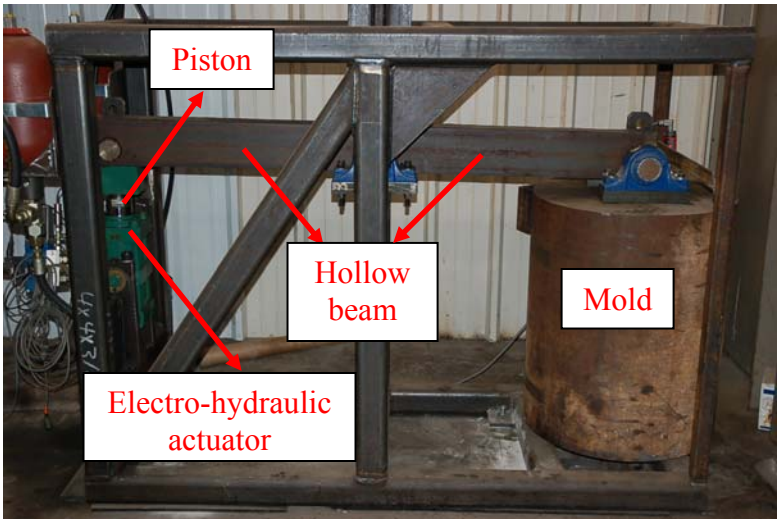

Figure 2.5: Testbed for the mold oscillation system

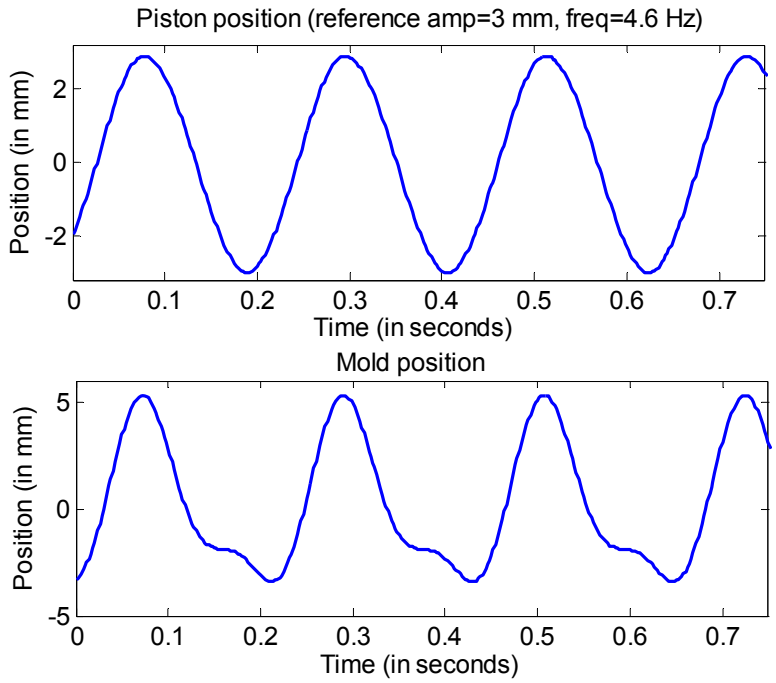

Figure 2.6: Experimental data from testbed - piston and mold position with piston reference at 4.6 Hz

Owing to the restricted access to the mold oscillation system, the controller development and all the related analysis will be performed for eliminating the distortions from the testbed. Under suitable justifications the proposed controller will then be transitioned to the mold

oscillation system. Although the variable of interest is the mold velocity profile, the focus henceforth will be on eliminating distortions from the mold displacement profile. This will consequently render the velocity profile distortion free.

2.4 Testbed model

A fundamentally based analytical model of the testbed as a system of coupled linear partial differential equations and nonlinear ordinary differential equations is developed. This model plays an important role in understanding the testbed dynamics and acts as a platform for controller testing.

2.4.1 Electro-hydraulic actuator model

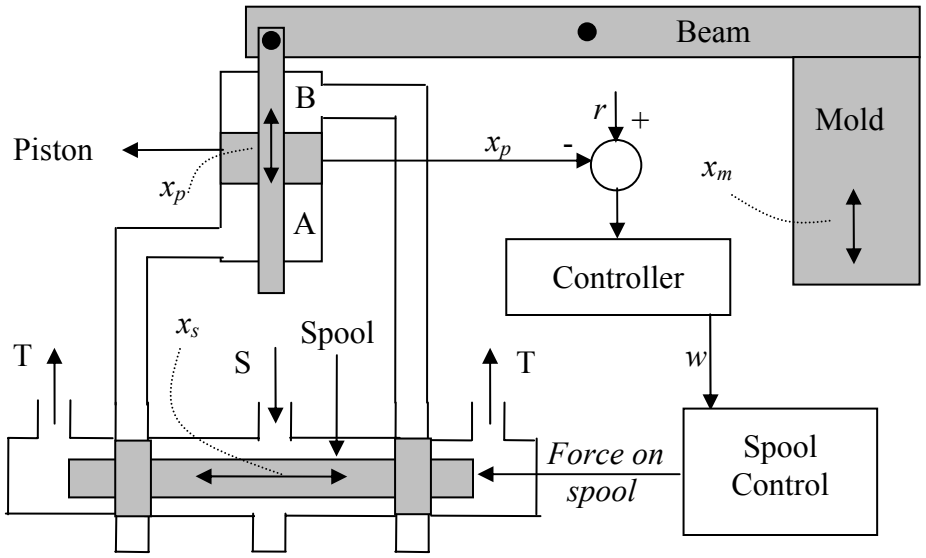

Figure 2.7: Detailed schematic of the testbed

A layout of the coupled actuator and beam system is shown in Figure 2.7, where 'S' and 'T' refer to the supply of the pressurized fluid and the fluid on the tank side, respectively. The hydraulic

actuator functions as follows [24], [25]. When the spool moves to the right, 'S' is connected to chamber 'B' and the piston is pushed down. When the spool moves to left, 'S' is connected to chamber 'A' and the piston is pushed up. Hence, the appropriate motion of the spool can cause the piston to oscillate.

The actuator typically functions in the closed loop. The error between the desired and the actual piston position is used to control the spool position. Piston position x_p is governed by the equation

$$m_p\ddot{x}_p + b\dot{x}_p = \left(P_A - P_B\right)a_p - m_p g + F_B \tag{2.1}$$

where m_p, b, P_A, P_B, a_p, g, F_B stand for the piston mass, damping, pressure in chamber 'A', pressure in chamber 'B', piston area, gravity, and force from the beam, respectively. When x_p is zero, chambers 'A' and 'B' have equal volumes. The pressures in chambers 'A' and 'B' are governed by

$$\begin{aligned} \dot{P}_A &= \beta\left(q_A - a_p\dot{x}_p\right)\Big/\left(V_A + a_p\left(L + x_p\right)\right), \\ \dot{P}_B &= \beta\left(-q_B + a_p\dot{x}_p\right)\Big/\left(V_B + a_p\left(L - x_p\right)\right), \end{aligned} \tag{2.2}$$

where β, q_A, q_B, V_A, V_B, L are bulk modulus of the actuator fluid, flow rates into chamber 'A' and out of chamber 'B', volumes of tubes connected to chambers 'A' and 'B', and half the stroke length of the piston, respectively. Assuming turbulent flow conditions, the flow rates q_A and q_B are given by

$$q_A = \begin{cases} c\left(d - x_s\right)\sqrt{P_s - P_A}, & x_s < -d, \\ c\left(d - x_s\right)\sqrt{P_s - P_A} - c\left(x_s + d\right)\sqrt{P_A - P_t}, & -d < x_s < d, \\ -c\left(x_s + d\right)\sqrt{P_A - P_t}, & x_s > d, \end{cases} \tag{2.3}$$

and $$q_B = \begin{cases} c(d - x_s)\sqrt{P_B - P_t}, & x_s < -d, \\ c(d - x_s)\sqrt{P_B - P_t} - c(x_s + d)\sqrt{P_s - P_B}, & -d < x_s < d, \\ -c(x_s + d)\sqrt{P_s - P_B}, & x_s > d, \end{cases} \tag{2.4}$$

with $c = c_d w\sqrt{2/\rho}$. Here c_d, w, ρ, d, P_s, P_t, x_s are the effective discharge coefficient, width of port for fluid flow between chambers 'A'/'B' and 'S'/'T', density of the fluid, spool underlap length, supply pressure, tank pressure, and spool position, respectively. In Chapter 6 modifications to this equation when the pressure difference is small are discussed. The spool position dynamics including the spool control is assumed to be governed by a second order system:

$$\ddot{x}_s + 2\zeta_s\omega_s\dot{x}_s + \omega_s^2 x_s = \omega_s^2 w. \tag{2.5}$$

Here w is the input generated by a controller using error between x_p and desired reference signal r, as seen in Figure 2.7. Typically, a proportional control law

$$w = k(x_p - r) \tag{2.6}$$

is used where k is the proportional gain. In Figure 2.7 x_m is the mold position.

2.4.2 Beam model

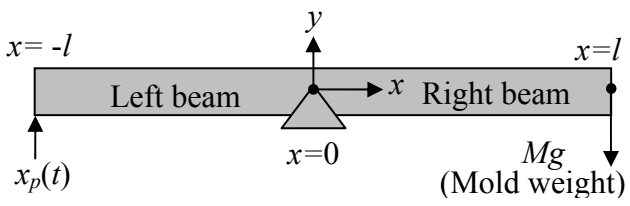

Figure 2.8: Beam schematic

The hollow beam in the testbed is modeled as two beams attached at the hinge, each using Timoshenko beam model consisting of two coupled second order PDEs [26]. The coordinate along the length of the beams is x. The beams are coupled via the boundary conditions at the hinge location x=0 that ensure that the torque and angular displacement at this location are the same. Thus, the model of the hinged beam of length 2l shown in Figure 2.8, with the vertical and the angular displacements to the left and to the right of the hinge denoted by (y_L,ψ_L) and (y_R,ψ_R), respectively, is given by a set of four coupled PDEs of the form

$$m_b\frac{\partial^2 y_L}{\partial t^2}+\gamma_y\frac{\partial y_L}{\partial t}=\frac{\partial}{\partial x}\left(k'Ga_b\left(\frac{\partial y_L}{\partial x}-\psi_L\right)\right)-m_b g\,,$$

$$\frac{I}{a_b}m_b\frac{\partial^2\psi_L}{\partial t^2}+\gamma_\psi\frac{\partial\psi_L}{\partial t}=\frac{\partial}{\partial x}\left(EI\frac{\partial\psi_L}{\partial x}\right)+k'Ga_b\left(\frac{\partial y_L}{\partial x}-\psi_L\right),$$

$$m_b\frac{\partial^2 y_R}{\partial t^2}+\gamma_y\frac{\partial y_R}{\partial t}=\frac{\partial}{\partial x}\left(k'Ga_b\left(\frac{\partial y_R}{\partial x}-\psi_R\right)\right)-m_b g\,,$$

$$\frac{I}{a_b}m_b\frac{\partial^2\psi_R}{\partial t^2}+\gamma_\psi\frac{\partial\psi_R}{\partial t}=\frac{\partial}{\partial x}\left(EI\frac{\partial\psi_R}{\partial x}\right)+k'Ga_b\left(\frac{\partial y_R}{\partial x}-\psi_R\right).$$

The mold is attached to the beam using a hinge joint at x=l and the mold dynamics gives rise to the following boundary conditions for the beam at this location:

$$k'Ga_b\left(\frac{\partial y_R(l)}{\partial x}-\psi_R(l)\right)+Mg+M\frac{\partial^2 y_R(l)}{\partial t^2}+\gamma_m\frac{\partial y_R(l)}{\partial t}=0\qquad\text{and}\qquad EI\frac{\partial\psi_R(l)}{\partial x}=0\,,$$

where the first equation follows from force equilibrium while the second equation indicates the absence of external torque at the hinge joint. The boundary conditions at x=-l where the piston attaches to the beam via a hinge joint are

$$y_L(-l)=x_p(t)\qquad\text{and}\qquad EI\frac{\partial\psi_L(-l)}{\partial x}=0\,.$$

The boundary conditions at the hinge at x=0 are

$$y_L(0)=0,\quad y_R(0)=0,\quad \psi_L(0)=\psi_R(0),\quad \text{and}\quad EI\frac{\partial\psi_L(0)}{\partial x}=EI\frac{\partial\psi_R(0)}{\partial x},$$

which indicate that the displacement at this hinge is zero, the rotation of the two beams at the hinge is the same and that there is no external torque at the hinge.

In the equations m_b, a_b, G, E, I, γ_y/γ_ψ, γ_m, k', M stand for mass of beam per unit length, area of cross section of beam, shear modulus, Young's modulus, moment of inertia of beam, beam vertical/angular displacement damping, mold damping, shear constant, and mold mass. The coupling between the nonlinear actuator and the beam is via the piston displacement entering the boundary condition for the left beam and the force F_B from the beam acting on the piston where

$$F_B=k'Ga_b\left(\frac{\partial y_L(-l)}{\partial x}-\psi_L(-l)\right). \tag{2.7}$$

2.4.3 Simulation of the model

Simulation of the testbed model is performed using parameter values shown in Table 2.1 (some actuator parameter values are from [27]). The initial chamber pressures are set at $P_A=P_B=50\,P_t$. All other initial conditions are zero.

The linear PDEs are discretized in space with a step size of 0.0251 m using a second order finite difference scheme to obtain a set of linear ODEs in time. The latter are simulated with the electro-hydraulic actuator ODEs in MATLAB Simulink using a fixed step fourth order Runge-Kutta solver with step size 5×10^{-7} seconds. The actuator simulation, which must run in closed loop, uses a proportional controller with the value of w in Eq. (2.5) given by $w=0.6\left(x_p-r(t)\right)$ where $r(t)$ is a sinusoid of 3 mm magnitude and 4.6 Hz frequency, and the controller gain is 0.6

rather than 2 used in the testbed. Figure 2.9 shows the mold position distortions similar to those in Figure 2.6, although not identical due to plant/model mismatch. Therefore, the model presented adequately exhibits the submultiples problem at submultiple 2 and can be used as a platform for testing control strategies.

Table 2.1: Values of the testbed model parameters used in simulation

Variable	Nominal value	Units
m_p	2	Kg
b	1000	N.sec/m
a_p	0.0046	m^2
g	9.8	m/sec^2
β	$1.5x10^9$	Pa
V_A	$4.7113x10^{-5}$	m^3
V_B	$7.0464x10^{-5}$	m^3
L	0.015	M
c	$3x10^{-4}$	-
d	$1.27x10^{-6}$	M
P_s	20684250	Pa
P_t	206842	Pa
m_b	23.0853	Kg/m
a_b	0.0029	m^2
G	$7.7\ x10^{10}$	Pa
E	$2\ x10^{11}$	Pa
I	$1.7668\ x10^{-5}$	m^4
γ_y	10	Kg/m/sec
γ_ψ	10	Kg.m/sec
γ_m	2250	Kg/sec
k'	0.83	-
M	2250	Kg
l	0.88	M
ζ_s	0.6	-
ω_s	255	rad/sec

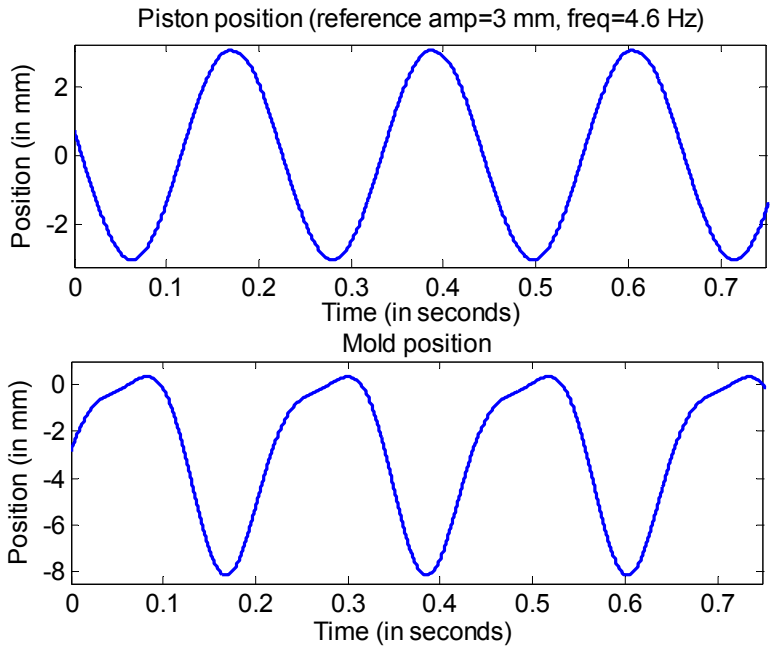

Figure 2.9: Simulation data from testbed model - piston and mold position with reference at 4.6 Hz

2.5 Source of disturbance and problem statement

The input to the testbed is a sinusoidal reference r and the outputs of interest are the piston position x_p and the mold position x_m. Purely on the basis of the problem description, it was naively expected that the nonlinearities in the actuator (Eqs. (2.2), (2.3) and (2.4)) generate harmonics of the reference frequency in the piston position signal thereby distorting it and the mold position profile. But as seen in Figure 2.6, where a reference sinusoid of frequency 4.6 Hz is used, while the mold position is heavily distorted the piston position looks perfect leading one to suspect that the actuator is not the source of the disturbance. This view is further supported by the magnitude spectrum plots of the two signals shown in Figure 2.10, where the spectrum of the mold position has a peak at 9.2 Hz which causes the distortion seen in Figure 2.6 and no such peak is apparent in the spectrum of the piston position.

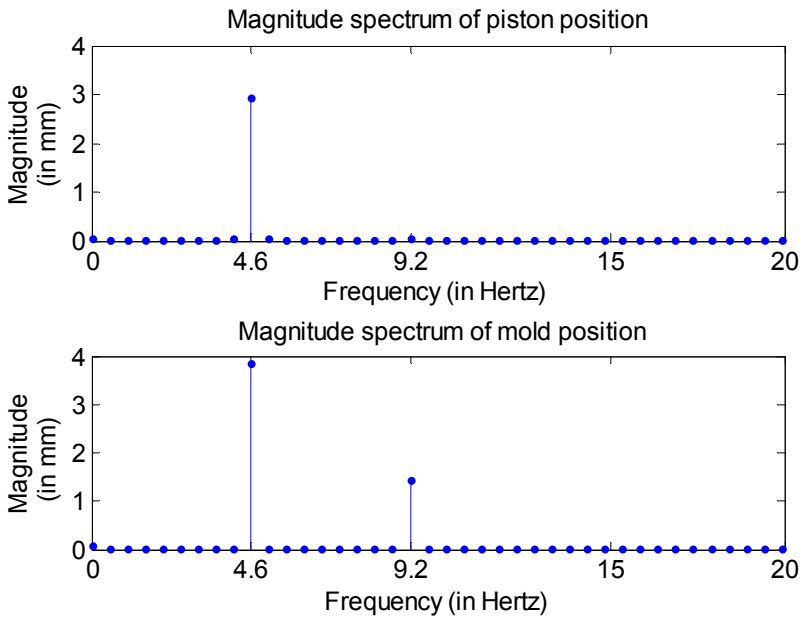

Figure 2.10: Experimental data from testbed - magnitude spectra of the piston and mold position shown in Figure 2.6

But a closer look at the magnitude spectrum of the piston position, shown in Figure 2.11, reveals a small peak of about 36 microns at 9.2 Hz. It is conjectured that this peak caused by the nonlinear characteristics of the actuator, being near the beam resonance frequency, is amplified by the beam to cause the large peak in the magnitude spectrum of the mold position. This is plausible given the large resonance amplification factor (about 40) of the beam.

The piston and mold position signals obtained by model simulations (Figure 2.9) show features similar to the testbed signals – the mold position signal exhibits distortions while the piston position signal appears to be perfect. The magnitude spectrum of the simulated signals, Figure 2.12, reveals that the spectrum of the piston position has a small peak at 9.2 Hz caused by the nonlinear actuator. Since this peak gets amplified by the linear beam model and causes the distortions in the mold position profile, the conjecture about the distortions in the testbed is verified.

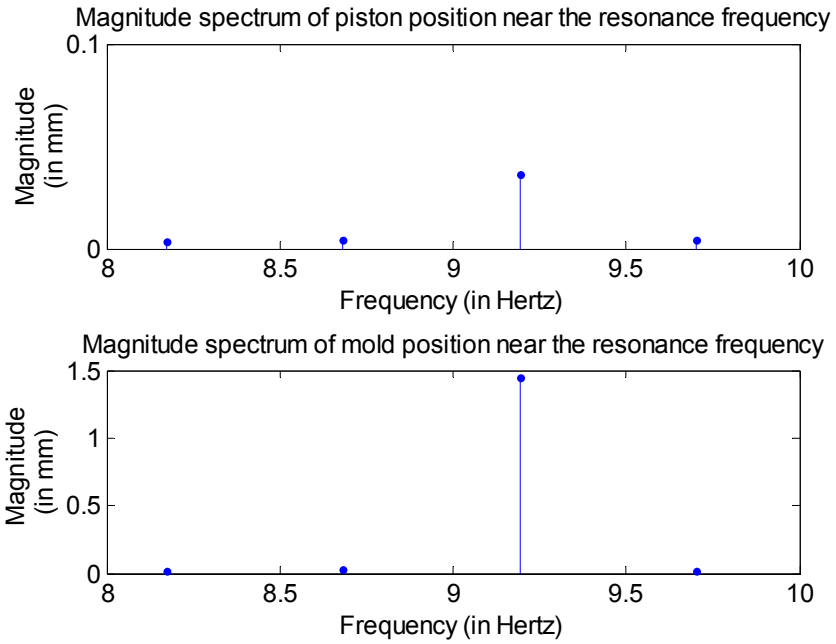

Figure 2.11: Experimental data from testbed - magnitude spectra of the piston and mold position shown in Figure 2.6 near the beam resonance frequency

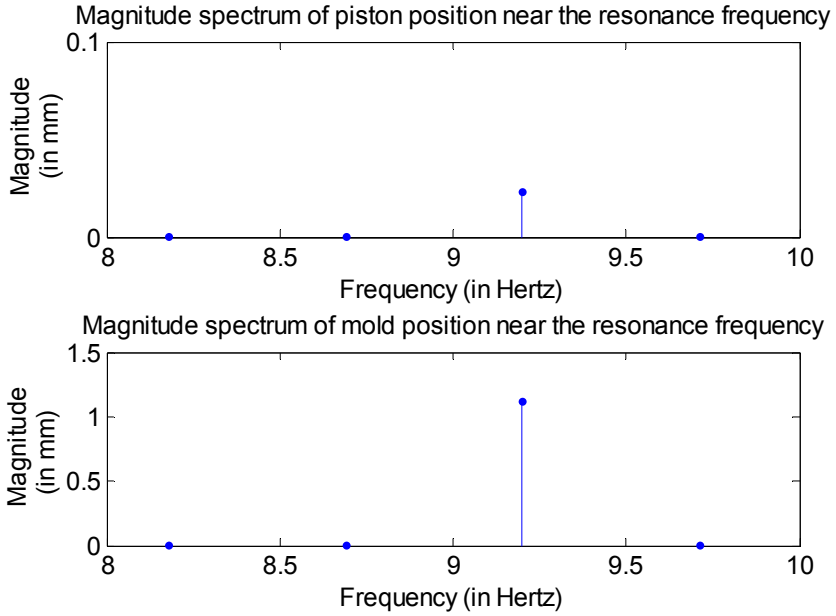

Figure 2.12: Simulation data from testbed model - magnitude spectra of the piston and mold position shown in Figure 2.9 near the beam resonance frequency

Figure 2.13 shows the feedback diagram corresponding to the schematic of the testbed in Figure 2.7. Based on the aforementioned conjecture, to reduce the distortion in the mold position x_m of the testbed, the peak near the resonance frequency of the beam in the spectrum of the piston position x_p must be eliminated. Hence, although the variable of interest is x_m, x_p is the variable to be controlled to eliminate the distortions.

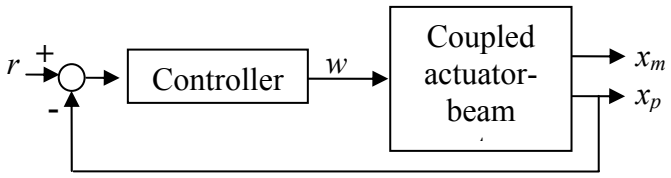

Figure 2.13: Feedback representation of the testbed

Electro-hydraulic actuators are designed to exhibit stable linear behavior in a nominal range of operation under feedback, implemented typically using a proportional controller as is done throughout this work. Various linear models of such actuators [24], [25], [28], provide a reasonably accurate frequency response at low frequencies for relatively small displacements. The latter conditions characterize the oscillations in the testbed. The effect of the beam on the piston is predominantly linear in the operating range, making a stable linear system perturbed by small nonlinearity a plausible model for the input-output behavior of the testbed where the reference *r* is the input and the variable to be controlled, x_p, is the output. This is supported, both in simulations and experiments, by the absence of any significant nonlinear effects in the output. For instance there are no visible distortions in the piston position profile (Figure 2.6 and Figure 2.9) and the peaks at the harmonic frequencies in the corresponding magnitude spectrum (Figure 2.10 and Figure 2.12) are small. In fact, in Figure 2.10 the magnitude of the signal at 9.2 Hz in the piston position is 0.036 mm, about 80 times smaller than the 3 mm magnitude at 4.6 Hz, the

frequency of the reference input. Furthermore, both in the experiment and simulation, the piston does track the reference input sinusoid at 4.6 Hz except for the presence of a small magnitude harmonic at 9.2 Hz. Hence the control objective is to eliminate the unwanted harmonics from the output of a sinusoidally excited nonlinearly perturbed linear system.

Although the electro-hydraulic actuator modeled as a finite dimensional system introduces the nonlinear effects into the testbed output, x_p, its dynamics is coupled to the beam modeled as an infinite dimensional system (Figure 2.14). Hence, to be rigorous, the problem for controller synthesis must be formulated to address the rejection of harmonics from the output of a nonlinearly perturbed linear infinite dimensional system.

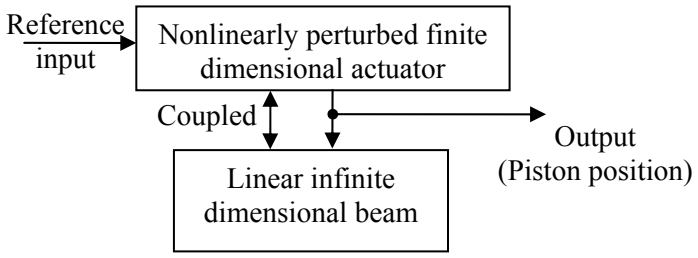

Figure 2.14: Simplified schematic of the testbed illustrating key features of the system dynamics

Based on the above discussion the abstract mathematical *problem statement* for controller synthesis is formulated:

Given a nonlinearly perturbed stable infinite dimensional linear system that tracks the input sinusoid of frequency ω satisfactorily, but for the presence of an internally generated small magnitude higher harmonic at ω_r - a nonlinear effect - in the output, design a control scheme that eliminates the harmonic at ω_r from the output without affecting the system stability and tracking performance at frequency ω. Here ω_r is an r-integer multiple of ω.

This problem statement is addressed in Chapter 3, assuming that the plant is finite dimensional, by developing a non-model based control scheme. This scheme is motivated by the repetitive control architecture and uses the plant gain at the frequency ω_r, alone. Once the control scheme has been fully developed in a finite dimensional setting, which is simpler, it is rigorously shown to be applicable to plants belonging to a newly introduced class of nonlinearly perturbed infinite dimensional systems in Chapters 4 and 5 to completely address the problem statement. Although only a single harmonic at ω_r, the first resonance frequency of the beam, must be eliminated in the testbed to remove distortion from the mold profiles, the proposed control scheme can be extended directly to reject a finite number of harmonics from the output as discussed in Chapter 4.

The conjecture on the cause of distortion in the mold profiles in the testbed, which is the basis for the problem statement, is based on component characteristics (actuator nonlinearity and beam resonance) common to both the testbed and the mold oscillation system. Hence it is reasonable to expect that the conjecture explains the source of disturbance in both systems, thereby making the above problem statement relevant to the mold oscillation system.

CHAPTER 3

REJECTION OF A SINUSOID FROM NONLINEARLY PERTURBED FINITE DIMENSIONAL PLANTS

In this chapter the periodic disturbance rejection problem formulated in Chapter 2 is partially addressed by considering nonlinearly perturbed finite, instead of infinite, dimensional plants. Assuming no knowledge of the plant dynamics other than being that of a stable perturbed linear system and its gain at the frequency of interest being known and non-zero, a control approach based on the internal model principle is proposed that rejects a sinusoidal disturbance of known frequency from the output of the periodically excited plant. The control schemes are presented in the form of two theorems. The results in Chapters 4 and 5 generalize these theorems to infinite dimensional plants using more sophisticated mathematical tools but do not emphasize the intuition behind the controller design as is the case in this chapter.

3.1 Description of the control scheme

The plant is the coupled electro-hydraulic actuator and beam system under proportional feedback (Figure 2.13). The output of interest in this stable closed loop is the actuator piston position from which the unwanted harmonic must be eliminated.

The proposed solution consists in introducing a novel topology obtained by partitioning the feedback path of the closed loop system into two weighted paths by appropriately choosing the stable partitioning filter Γ (Figure 3.11) and inserting between these paths a loop containing an internal model based filter. The resulting system (Figure 3.12), further referred to as the augmented partitioned system, is an outgrowth of the augmented unpartitioned system (Figure

3.2) which is motivated by the linear feedback structure in repetitive control [2]. Focusing on disturbance rejection in nonlinear systems at a single frequency, ω_r, the infinite dimensional delay block used in [2] is replaced by a second order filter to get the augmented unpartitioned system. By appropriately shaping the second order filter the plant response at frequencies away from ω_r is nearly unaffected and the scheme can be rendered non-model based.

The stability of the augmented unpartitioned system is shown to be guaranteed if the unaugmented closed loop gain at frequency ω_r, further referred to for brevity as g_{nl}, satisfies a certain bound condition. If this condition is violated, feedback path partitioning described above is applied. The stability of the augmented partitioned system is then guaranteed by an appropriate choice of the partitioning filter, provided g_{nl} is non-zero, thereby extending the applicability of the augmentation procedure. Stability of the augmented loop ensures the rejection of the sinusoidal disturbance at frequency ω_r from the given nonlinearly perturbed linear system. Although the theorems are stated for rejecting a single harmonic, addressing the rejection of a finite number of harmonics follows directly.

The control schemes in [11]-[16] address the rejection of a finite number of sinusoids from linear plants requiring the same plant information as in the present work. But the fundamentally different proof techniques in the present work enable the graphical verification of stability using gain plots. This makes transparent the tuning of a small control parameter, common to all the approaches, by clarifying its influence in terms of gain plots and enables obtaining quantitative estimates for the robustness of the scheme. This is discussed in detail in Chapter 4. Furthermore the present work considers a nonlinear perturbation which is essential as the source of the small amplitude harmonic to be rejected and dramatically influences the application considered. In the presence of the perturbation, establishing stability of the control scheme becomes involved. For

instance, it must be shown that the interaction between the controller poles, which tend towards the imaginary axis as the tuning parameter tends to zero, and the nonlinear perturbation does not cause instability. This is addressed in Theorem 1 and Lemma 3.

3.2 Controller design and analysis

The stable nonlinearly perturbed finite dimensional system is governed by the equation:

$$\begin{aligned} \dot{x} &= Ax + Bu + \varepsilon g(x), \qquad x(0) = x_0, \\ y &= Cx, \end{aligned} \tag{3.1}$$

where $x \in \mathbb{R}^n$, $u \in \mathbb{R}^m$, $y \in \mathbb{R}^k$, A is a $n \times n$ Hurwitz matrix satisfying $\left\| e^{At} \right\|_{\mathcal{L}(\mathbb{R}^n)} < Me^{-at}$ with $M \geq 1$ and $a > 0$, B is a $n \times m$ matrix, C is a $k \times n$ matrix, ε is a small constant and $g(x) : \mathbb{R}^n \to \mathbb{R}^n$ is a locally Lipschitz function, with $g(0) = 0$. Hence for any bounded domain $D \subset \mathbb{R}^n$, there exists $L(D)$ so that $\left\| g(x) - g(y) \right\|_{\mathbb{R}^n} < L(D) \left\| x - y \right\|_{\mathbb{R}^n}$, $\forall\ x, y \in D$.

Lemma 1 states that for sufficiently small ε, if the input, u, to the system in Eq. (3.1) is *T*-periodic, so is the state, x (asymptotically). This implies that the output, y, is also *T*-periodic (asymptotically) which is a main premise in this work.

Lemma 1: Consider the nonlinearly perturbed system given in Eq. (3.1) and the associated nonlinear integral map $q = \mathbb{I}(p)$ *defined* $\forall t \in [0, \infty)$ *as*:

$$q(t) = p(t) - e^{At} x_0 - \int_0^t e^{A(t-\tau)} Bu(\tau)\, d\tau - \varepsilon \int_0^t e^{A(t-\tau)} g\left(p(\tau)\right) d\tau .$$

Let $\|x_0\|_{\mathbb{R}^n} < C_0$ *and* $u:[0,\infty) \to \mathbb{R}^m$ *be a continuous T-periodic function. Then for some* $\bar{N} > 0$, $\left\| \int_0^t e^{A(t-\tau)} Bu(\tau)\, d\tau \right\|_{\mathbb{R}^n,\infty} < \bar{N}\|u\|_{\mathbb{R}^n,\infty}$. *Hence the map* $\mathbb{I}$ *is well defined from* $C_B\left([0,\infty),\mathbb{R}^n\right)$ *to itself. Assume that* ε *is small enough so that for some* $0<\alpha<1$ *and* $D_0 = \left\{ x \in \mathbb{R}^n : \|x\|_{\mathbb{R}^n} \le \left(C_0 + \left(MC_0 + \bar{N}\|u\|_{\mathbb{R}^n,\infty} \right) \right) \Big/ (1-\alpha) = d_0 \right\}$, $(\varepsilon M L_0)/a < \alpha$. *Here* L_0 *is the Lipschitz constant of* $g(x)$ *for the domain* D_0. *Then,* $\exists x, \hat{x} \in C_B\left([0,\infty),\mathbb{R}^n\right)$ *with* $\mathbb{I}(x) = 0$ *and* $\hat{x}$ *a T-periodic function with* $\|\hat{x}\|_{\mathbb{R}^n,\infty}$ *independent of* x_0, *such that for any given* $\lambda > 0$, $\exists\, \hat{t} > 0$ *such that* $\left\| x[\hat{t},\infty) - \hat{x}[\hat{t},\infty) \right\|_{\mathbb{R}^n,\infty} < \lambda$.

Proof: The function x satisfying $\mathbb{I}(x) = 0$, is the solution to the state equation in Eq. (3.1). This lemma states that when u is *T*-periodic, so is the state x and consequently the output y (asymptotically). The conclusions of this lemma can be equivalently obtained by using a general finite dimensional result in [29]. However, focusing on perturbed linear systems, a less general class of systems, makes it possible to present a more direct and self-contained proof, illustrating clearly the role played by the assumptions on the magnitude and the smoothness of the perturbation. The smoothness assumptions are subsequently compared to the smoothness of the testbed model presented in Chapter 2 to obtain a better understanding of the physical testbed which yields *T*-periodic response to *T*-periodic input. The details of the proof are presented in Chapter 5 where this lemma is established, more generally, for a class of nonlinearly perturbed infinite dimensional systems. □

Next the control schemes that address the periodic disturbance rejection problem are presented. The plant is assumed to be a SISO system, matching the requirements of the application. Hence in Eq. (3.1), $m = k = 1$. To ensure presentation clarity the results are given in the form of two theorems. Theorem 1 deals with the topology directly motivated by [2] where the feedback signal is not partitioned (Figure 3.1), while Theorem 2 generalizes Theorem 1 by considering a partitioned feedback path (Figure 3.11). The controllers in Theorems 1 and 2 are motivated by the predominant linearity of the plant and naturally apply to linear plants. However, rigorously establishing their applicability to perturbed linear plants is nontrivial, as seen from the proof of Theorem 1, presented below. The proof of Theorem 2 is analogous and is only briefly sketched.

To formulate Theorem 1, consider the closed loop system shown in Figure 3.1, referred to as the unpartitioned unaugmented system, where *P* is a nonlinear system, *K* is a controller that stabilizes the loop, *u* is the reference input, and *y* is the output. In the case of the testbed (Figure 2.13), *P*, *K*, *u* and *y* correspond to the coupled actuator-beam system, proportional controller, reference sinusoid, and actuator piston position, respectively. Let the closed loop in Figure 3.1 exhibit perturbed linear dynamics governed by Eq. (3.1).

Theorem 1: Let the following hold:

F1. The input u and initial condition x_0 *satisfy* $\|u\|_{L^\infty} < C_u$ *and* $\|x_0\|_{\mathbb{R}^n} < C_0$. *By Lemma 1, if* ε *is sufficiently small, the output y of Eq. (3.1) is bounded and if u is* T *periodic, so is y (in the limit* $t \to \infty$*).*

F2. The unpartitioned unaugmented system tracks input sinusoid of frequency ω, but its output contains small amplitude higher harmonics of ω, including ω_r, due to nonlinear effects. Here ω_r is an r-integer multiple of ω.

F3. When the input u in Eq. (3.1) is a sinusoid of frequency ω_r, the corresponding steady state periodic output y_{ss} contains sinusoid at that frequency, denoted by $S_{y,\omega_r}(t)$. Assume that the complex loop gain g_{nl} from u to $S_{y,\omega_r}(t)$, satisfies the condition

$$|1 - g_{nl}| < 1. \tag{3.2}$$

Next consider the feedback system shown in Figure 3.2, further referred to as the unpartitioned augmented system. Let F be the stable linear system with TF

$$G_F(s) = \frac{2\zeta\omega_r s}{s^2 + 2\zeta\omega_r s + \omega_r{}^2} \tag{3.3}$$

where $0 < \zeta \ll 1$. If in addition to the above assumptions ε is small, then, $\exists \zeta^*$ such that for all $\zeta \in (0, \zeta^*]$, the unpartitioned augmented system is stable and tracks the input sinusoid of frequency ω akin to the unaugmented system and its output possibly contains small magnitude higher harmonics of ω generated by the nonlinear perturbation, but the harmonic at frequency ω_r is asymptotically eliminated.

Remark 1: The specific choice of the amplitude a_u for u in F3 is not critical since the system considered is perturbed linear. As shown below, if ε is sufficiently small and Eq. (3.2) holds for some a_u, it holds for all amplitudes less than a_u.

Remark 2: F2 is true for the testbed where the reference to the piston is the input and the actual piston position is the output. Problem statement in Chapter 2 requires that given that F2 is true, adding the filter must affect the tracking at frequency ω only minimally. Here $0 < \zeta \ll 1$ assists

by shaping the filter bandwidth. As $\zeta \to 0$, *the contribution of the additional loop in Figure 3.2 at all frequencies except* ω_r *goes to zero. Note that F is in positive feedback in Figure 3.2 and generates poles at* $\pm j\omega_r$.

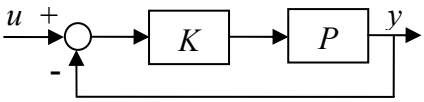

Figure 3.1: Block diagram of the unpartitioned unaugmented system

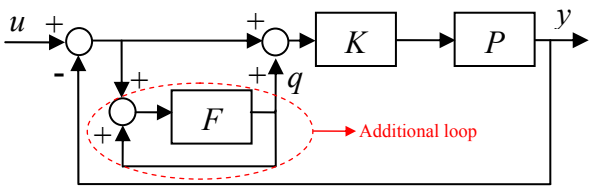

Figure 3.2: Block diagram of the unpartitioned augmented system

Proof: The proof is completed in 5 steps. In step 1, the given perturbed linear system is treated as the sum of its linearization (in terms of a linear system *L*) and a nonlinear system *N* with small BIBO gain. Relevant properties of both systems are obtained. Step 2 develops a convenient representation of the augmented system using *L* and *N*. In step 3 the linearization of the augmented system, with *N* removed, is shown to be stable provided $\zeta \in (0, \zeta^*]$. In step 4, *N* is introduced back and the stability of the augmented system is established for all $\zeta \in (0, \zeta^*]$ and a sufficiently small ε independent of ζ. This independence is not obvious since, as $\zeta \to 0$, two poles of G_F and consequently of the linearization of the augmented system, tend to the imaginary axis thereby rendering the robustness of the linearized augmented system, to even small perturbations, questionable. Step 5 establishes the asymptotic rejection of the harmonic at frequency ω_r from the output.

Step 1: Consider the block diagram shown in Figure 3.3 where the linear system *L*, with TF G_L is

$$\dot{l} = (A + BC)l + Bu_1, \qquad l(0) = x_0,$$
$$y_1 = Cl,$$

and the nonlinear system N is

$$\dot{n}_1 = An_1 + Bu + \varepsilon g(n_1), \qquad n_1(0) = x_0,$$
$$\dot{n}_2 = An_2 + Bu, \qquad n_2(0) = x_0,$$
$$y_2 = C(n_1 - n_2).$$

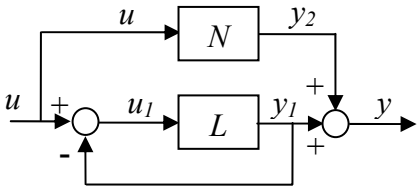

Figure 3.3: Block diagram separating linear and nonlinear dynamics

In Figure 3.3, $u_1 = u - y_1$. By block diagram simplifications, it follows that the loops in Figure 3.1 and Figure 3.3 are equivalent from input (u)-output (y) standpoint. For ε sufficiently small, it follows from Lemma 2 (in Section 3.3) that the output of the nonlinear system N is bounded by a constant proportional to ε, i.e. for some constant $C_N(C_0, C_u) > 0$,

$$\|y_2(t)\|_{L^\infty} = \|C(n_1(t) - n_2(t))\|_{L^\infty} \le \varepsilon C_N(C_0, C_u)(C_0 + C_u). \tag{3.4}$$

When u is a sinusoid of frequency ω_r (as in *F3*), let y_1, y_2, and y converge to the periodic functions $y_{1,ss}$, $y_{2,ss}$, and y_{ss}, respectively. Let $S_{y_2,\omega_r}(t)$ be the sinusoid of frequency ω_r contained in $y_{2,ss}$. From Lemma 1, the amplitude of $y_{2,ss}$ is independent of the initial condition. Hence using Eq. (3.4), it follows that $\|S_{y_2,\omega_r}\|_{L^\infty} \le 2\varepsilon C_N\left(0, \|u(t)\|_{L^\infty}\right)\|u(t)\|_{L^\infty}$ (this expression justifies Remark 1). Since from *F3*, the complex gain g_{nl} from u to $S_{y,\omega_r}(t)$ satisfies the

condition $|1-g_{nl}|<1$, it follows that if ε is small, then the complex gain $g_l = G_L(j\omega_r)/(1+G_L(j\omega_r))$ from u to $S_{y_1,\omega_r}(t)$ also satisfies $|1-g_l|<1$.

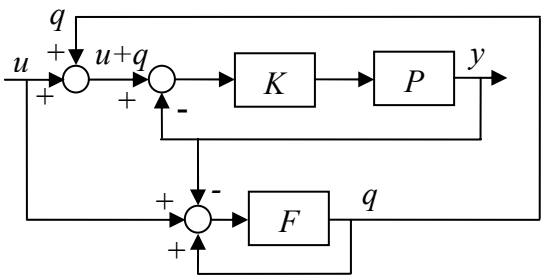

Figure 3.4: Modified block diagram of the unpartitioned augmented system

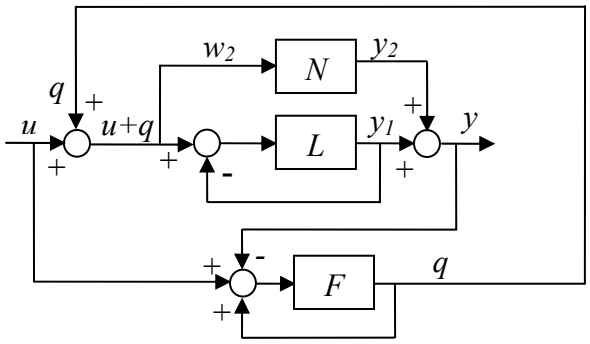

Figure 3.5: Block diagram of the unpartitioned augmented system with nonlinear part shown explicitly

Step 2: The systems shown in Figure 3.2 and Figure 3.4 are equivalent. In Figure 3.4, separating the linear and nonlinear dynamics using the definitions of L and N and Figure 3.3, an input-output equivalent block diagram shown in Figure 3.5 is obtained which after modifications yields the block diagram in Figure 3.6 which is equivalent to that in Figure 3.2. Figure 3.6 is used for analysis.

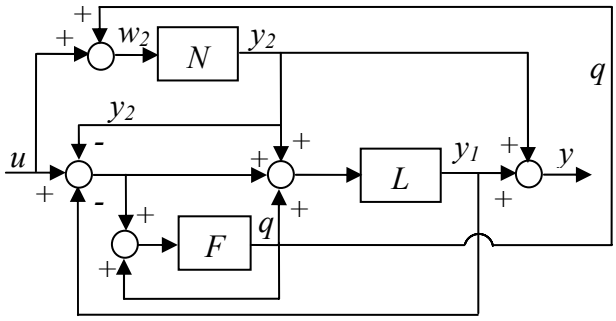

Figure 3.6: Block diagram of the unpartitioned augmented system with isolated nonlinear dynamics

Step 3: The nonlinear dynamics N is removed from the loop in Figure 3.6 to obtain the linear system in Figure 3.7. Since this linear system without the additional loop is internally stable, the

TF matrix from (u, q) to (y_1, $m+q$) is obtained with no unstable pole/zero cancellations. Figure 3.7 is hence equivalent to the feedback structure in Figure 3.8. Since the individual TFs in Figure 3.8 are stable, if

$$\frac{G_F(s)}{1+G_L(s)} \neq 1, \qquad \forall s \in \mathbb{C}_0^+ \cup \{\infty\}, \tag{3.5}$$

then the internal stability of the whole system is guaranteed [30]. Since $\left|G_F(s)/\left(1+G_L(s)\right)\right| \to 0$ as $|s| \to \infty$, using the maximum modulus principle [31], Eq. (3.5) holds if $\sup_{\tau \in \mathbb{R}} \left|G_F(j\tau)/\left(1+G_L(j\tau)\right)\right| < 1$. Since $G_F(\pm j\omega_r) = 1$ and $\left|1/\left(1+G_L(\pm j\omega_r)\right)\right| = |1-g_l| < 1$ from earlier discussion, there is a $\delta > 0$ such that $\left|G_F(j\tau)/\left(1+G_L(j\tau)\right)\right| < 1$ for all $\tau \in S$ where S is the set $(-\omega_r - \delta, -\omega_r + \delta) \cup (\omega_r - \delta, \omega_r + \delta)$. Note that $\sup_{\tau \in \mathbb{R}} \left|G_F(j\tau)\right| \leq 1$ and since $1/(1+G_L)$ is stable, $\sup_{\tau \in \mathbb{R}} \left|1/\left(1+G_L(j\tau)\right)\right|$ is finite. Since for any $\tau \notin S$, $G_F(j\tau)$ goes to zero uniformly as ζ goes to zero it follows that $\exists \zeta^* : \forall \zeta \in (0, \zeta^*]$, $\sup_{\tau \in \mathbb{R}} \left|G_F(j\tau)/\left(1+G_L(j\tau)\right)\right| < 1$. Hence Eq. (3.5) is satisfied and the internal stability of the system in Figure 3.8, and therefore of that in Figure 3.7 is guaranteed.

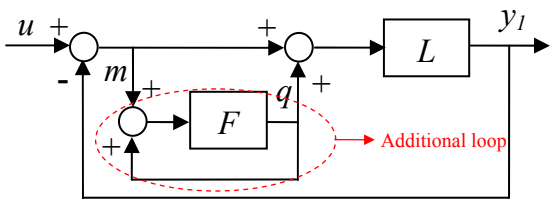

Figure 3.7: Block diagram of linear dynamics of augmented system

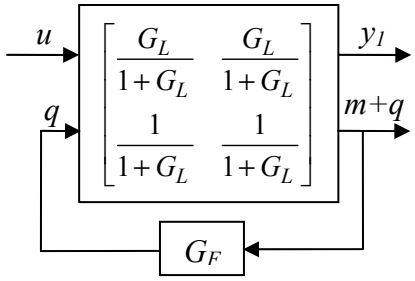

Figure 3.8: TF representation of linear dynamics of augmented system

Step 4: Noting that Figure 3.6 is an interconnection of the system in Figure 3.8 and the nonlinear system *N*, the system in Figure 3.6 can be represented as a feedback interconnection of two stable systems, one linear and the other nonlinear, as shown in Figure 3.9. The stability of this interconnection assuming $\|u\|_{L^\infty} < C_u$ and $\|x_0\|_{\mathbb{R}^n} < C_0$ (see *F1*) follows if y_2 remains bounded. Let $q = q_1 + q_2 + G_F/(1+G_L-G_F)u$ where $q_1 = -G_F(1+G_L)/(1+G_L-G_F)y_2$ and q_2 represents the contribution of the initial conditions of all the linear systems to q. Establishing the BIBO stability of system in Figure 3.9 is equivalent to establishing the BIBO stability of system in Figure 3.10 with $(1+G_L)/(1+G_L-G_F)u + q_2$ as the input and y_2 as the output.

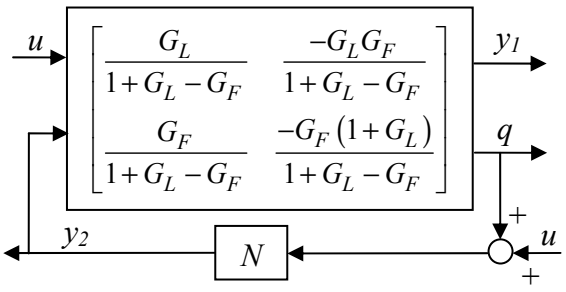

Figure 3.9: Feedback interconnection of the nonlinear system with the linear dynamics

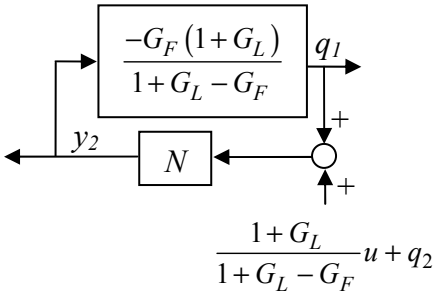

Figure 3.10: Feedback loop of the relevant dynamics in Figure 3.9

As $\zeta \to 0$, 2 poles of $1/(1+G_L-G_F)$ tend towards the imaginary axis and therefore for the nonlinearity *N* not to destabilize the loop in Figure 3.10, it seems that as $\zeta \to 0$, ε must also go to zero. But as shown in Lemma 3 (in Section 3.3), as $\zeta \to 0$, the residue at the poles tending to the imaginary axis tends to zero sufficiently fast. Hence given $\|u\|_{L^\infty} < C_u$ and $\|x_0\|_{\mathbb{R}^n} < C_0$, $\exists c_1, c_2$ independent of $\zeta \in (0, \zeta^*]$ such that $\|(1+G_L)/(1+G_L-G_F)u + q_2\|_{L^\infty} < c_1$ and the BIBO gain of $-G_F(1+G_L)/(1+G_L-G_F)$ is less than c_2. This enables obtaining an upper bound on ε

independent of $\zeta \in (0, \zeta^*]$, such that the nonlinearity does not destabilize the loop in Figure 3.10, as follows. Let ε be sufficiently small, so that for $C_N(C_0, 2c_1)$ defined as in Eq. (3.4), $\varepsilon c_2 C(C_0, 2c_1)(C_0 + 2c_1) < c_1$. Since the initial condition for the linear system is accounted for by q_2, $q_1(t=0) = 0$. Let t_m be the first time instant such that $|q_1(t = t_m)| = c_1$. Then, a contradiction is obtained since, from Eq. (3.4)

$$\begin{aligned} &\left\| y_2([0, t_m]) \right\|_{L^\infty} \le \varepsilon C_N(C_0, 2c_1)(C_0 + 2c_1) \\ \Rightarrow\ &\left\| q_1([0, t_m]) \right\|_{L^\infty} \le c_2 \left\| y_2([0, t_m]) \right\|_{L^\infty} \le \varepsilon c_2 C_N(C_0, 2c_1)(C_0 + 2c_1) < c_1. \end{aligned} \tag{3.6}$$

Hence, $\|q_1(t)\|_{L^\infty} < c_1$. Eq. (3.6) is valid since the bound $C_N(C_0, 2c_1)$ for the nonlinear system holds if the input is bounded by $2c_1$, which is true for $t \in [0, t_m]$. But noting that $\|q_1(t)\|_{L^\infty} < c_1$, Eq. (3.6) holds for $t_m = \infty$, i.e. $\|y_2(t)\|_{L^\infty} \le \varepsilon C_N(C_0, 2c_1)(C_0 + 2c_1) \le \varepsilon C_1 u + \varepsilon C_2$ for some C_1, $C_2 > 0$. The last inequality follows from the definition of c_1. This implies the BIBO stability of system in Figure 3.10 and hence of that in Figure 3.2.

Step 5: Figure 3.2 is again a perturbed stable linear system with the linear system having a BIBO gain bounded independently of $\zeta \in (0, \zeta^*]$ (step 4). Hence, for small ε (independent of ζ), when *u* is a sinusoid of frequency ω, the steady state value of *y*, y_{ss}, is periodic with period $2\pi/\omega$. But if y_{ss} contains harmonic at frequency ω_r, then the output *q* of the additional loop in Figure 3.2 which has a pole at $\pm j\omega_r$ will grow unbounded, contradicting the BIBO stability that was established. From Figure 3.9 which is equivalent to the augmented system of Figure 3.2, using Remark 2 it is seen that when *u* is a sinusoid of frequency ω, the effect of *F* on y_{ss} is small and hence *y* tracks *u* akin to the unaugmented loop and may contain some small amplitude harmonics. But, y_{ss} will not contain the harmonic at frequency ω_r. □

When the loop gain at ω_r does not satisfy Eq. (3.2), increasing the controller gain could resolve this problem and guarantee stability of the unpartitioned augmented loop. Increasing the controller gain can lead, however, to the unaugmented closed loop stability loss. In this scenario, when controller gains are fixed and Eq. (3.2) is not satisfied, a modified feedback structure that provides added flexibility in guaranteeing the stability of the corresponding augmented loop, while addressing the disturbance rejection problem, would be required. Such a structure containing a partitioning of the feedback path with a stable filter Γ (Figure 3.11) is introduced in Theorem 2, which generalizes Theorem 1. The partitioning does not change the given closed loop system. Stability of the augmented loop corresponding to this structure (Figure 3.12) is guaranteed by an appropriate choice of the partitioning filter as long as the closed-loop gain at ω_r is non-zero.

Theorem 2: Consider the feedback system shown in Figure 3.11, referred to as the partitioned unaugmented system where P, K, u and y are as in Theorem 1 and Γ *is a stable filter to be chosen. Assume that when* $\Gamma = 0$ *this system is described by the perturbed linear Eq. (3.1). Let assumptions F1 and F2 hold. Let* g_{nl}*, as defined in F3, be non-zero and choose* Γ *such that* $\Gamma(j\omega_r) = -(1-g_{nl})/g_{nl}$ *and* $\Gamma(j\omega) = 0$ *. Consider the feedback system in Figure 3.12, referred to as the partitioned augmented system, where the TF of* F *is given by Eq. (3.3). If in addition to the above assumptions* ε *is small, then,* $\exists \zeta^*$ *such that for all* $\zeta \in (0, \zeta^*]$*, the partitioned augmented system tracks the input sinusoid of frequency* ω *akin to the unaugmented system and possibly contains small magnitude higher harmonics of* ω *generated by the nonlinear perturbation, but the harmonic at frequency* ω_r *is asymptotically eliminated from its output .*

Proof: Using the proof technique of Theorem 1 (the details are omitted), with L as defined before, the condition for the stability of the partitioned augmented loop instead of Eq. (3.5), takes the form

$$G_F(s)\left(1-\frac{G_L(s)}{1+G_L(s)}+\Gamma(s)\frac{G_L(s)}{1+G_L(s)}\right)\neq 1,\quad \forall s\in\bar{\mathbb{C}}^+\cup\{\infty\}. \tag{3.7}$$

The latter holds if

$$\left|\left(1-\frac{G_L(j\tau)}{1+G_L(j\tau)}+\Gamma(j\tau)\frac{G_L(j\tau)}{1+G_L(j\tau)}\right)\right|<\frac{1}{|G_F(j\tau)|},\ \forall \tau\in\mathbb{R}\cup\{\infty\}, \tag{3.8}$$

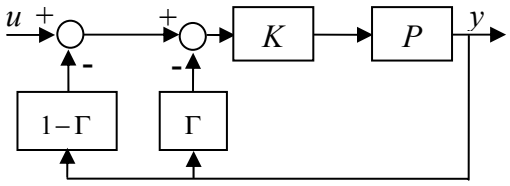

Figure 3.11: Block diagram of partitioned unaugmented system with stabilizing feedback

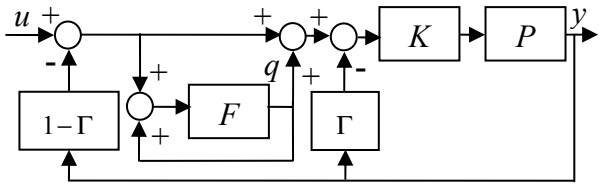

Figure 3.12: Block diagram of partitioned augmented system

which in turn follows, for ε sufficiently small, from the choice $\Gamma(j\omega_r)=-(1-g_{nl})/g_{nl}$ and properties of F, as in Theorem 1. The condition $\Gamma(j\omega)=0$ is needed to ensure that the augmented loop tracks the reference sinusoid at frequency ω akin to the unaugmented loop. □

3.3 Bounds on the gains of some linear and nonlinear systems

In this section, two lemmas used in the proof of Theorem 1 are presented. The first lemma shows that the nonlinear system N in Theorem 1 is BIBO stable and computes its gain.

Lemma 2: *With notations as in Theorem 1, if* $\|u\|_{L^\infty} < C_u$, $\|x_0\|_{\mathbb{R}^n} < C_0$ *and* ε *is sufficiently small, then the output of the nonlinear system N with states* n_1 *and* n_2 *is bounded by a constant that depends only on* C_u, C_0 *and is proportional to* ε.

Proof: From Lemma 1 it follows that if ε is sufficiently small, n_1 and n_2 remain in a bounded domain. Let L_0 be Lipschitz constant for the nonlinearity $g(x)$ for this domain (Lemma 1). Note that L_0 is a function of C_0 and C_u. Then,

$$\sup_{t\geq 0}\|n_1(t)-n_2(t)\|_{\mathbb{R}^n} = \sup_{t\geq 0}\left\|\int_0^t e^{A(t-\tau)}\varepsilon g\left(n_1(\tau)\right)d\tau\right\|_{\mathbb{R}^n}$$

$$= \sup_{t\geq 0}\left\|\int_0^t e^{A(t-\tau)}\varepsilon\left(g\left(n_1(\tau)\right)-g\left(n_2(\tau)\right)+g\left(n_2(\tau)\right)\right)d\tau\right\|_{\mathbb{R}^n}$$

$$\leq \sup_{t\geq 0}\int_0^t\left\|e^{A(t-\tau)}\right\|_{\mathcal{L}\left(\mathbb{R}^n\right)}\varepsilon\left(\left\|g\left(n_1(\tau)\right)-g\left(n_2(\tau)\right)\right\|_{\mathbb{R}^n}+\left\|g\left(n_2(\tau)\right)\right\|_{\mathbb{R}^n}\right)d\tau$$

$$\leq \sup_{t\geq 0}\int_0^t\left\|e^{A(t-\tau)}\right\|_{\mathcal{L}\left(\mathbb{R}^n\right)}\varepsilon L_0\left(\left\|n_1(\tau)-n_2(\tau)\right\|_{\mathbb{R}^n}+\left\|n_2(\tau)\right\|_{\mathbb{R}^n}\right)d\tau$$

$$\leq \sup_{t\geq 0}\left(\varepsilon L_0 M\left\|n_1(t)-n_2(t)\right\|_{\mathbb{R}^n}+\varepsilon L_0 M\left\|n_2(t)\right\|_{\mathbb{R}^n}\right)\Big/ a,$$

So, for ε such that $\varepsilon LM < a$,

$$\sup_{t\geq 0}\|n_1(t)-n_2(t)\|_{\mathbb{R}^n} \leq \sup_{t\geq 0}\|n_2(t)\|_{\mathbb{R}^n}\,\varepsilon LM\Big/(a-\varepsilon LM)$$

$$\leq \sup_{t\geq 0}\left(\left\|e^{At}x_0\right\|_{\mathbb{R}^n}+\left\|\int_0^t e^{A(t-\tau)}Bu(\tau)\,d\tau\right\|_{\mathbb{R}^n}\right)\varepsilon LM/(a-\varepsilon LM)$$

$$\leq \varepsilon C(C_0,C_u)(C_0+C_u)$$

for some $C(C_0,C_u)>0$. Hence for some $C_N(C_0,C_u)>0$, $\|y_2(t)\|_{L^\infty} \leq \varepsilon C_N(C_0,C_u)(C_0+C_u)$. □

Lemma 3 establishes bounds, independent of the control parameter $\zeta \in (0, \zeta^*]$, for the output of some linear plants. These bounds were used in Step 4 in the proof of Theorem 1.

Lemma 3: With notation as in Theorem 1, $\|u\|_{L^\infty} < C_u$ *and* $\|x_0\|_{\mathbb{R}^n} < C_0$, $\exists c_1, c_2$ *independent of* $\zeta \in (0, \zeta^*]$ *such that* $\left\|(1+G_L)/(1+G_L-G_F)u + q_2\right\|_{L^\infty} < c_1$, $\left\|G_F(1+G_L)/(1+G_L-G_F)\right\|_{op} < c_2$ *where the operator norm is the BIBO gain for the linear system. Note that* F *is a function of* ζ.

Proof: The BIBO gain of a linear system is the L_1-norm of its impulse response. Hence to show the existence of an uniform in ζ bound for the BIBO gain, the L_1-norm of the impulse response of the TF will be shown to be bounded uniformly in ζ. With $X(s)/Y(s) = 1/(1+G_L)$, let

$$H = \frac{G_F(1+G_L)}{(1+G_L-G_F)} = \frac{2\zeta\omega_r s Y}{\left(s^2+\omega_r^2\right)Y + 2\zeta\omega_r s(Y-X)}.$$

As $\zeta \to 0$, all but two of the poles of H tend to the zeros of Y, which are independent of ζ. Moreover the residues at these poles of H can be bounded independently of ζ. Hence the contribution of these poles to the impulse response and its L_1-norm and hence to $\|H\|_{op}$ can be bounded independently of ζ. Two of the poles of H will tend to $\pm j\omega_r$; let they be $p(\zeta)$ and its complex conjugate. Let δ, $\alpha > 0$ satisfy $\delta < \omega_r \alpha/4$ and $\forall s \in D_1$, $\left|X(s)/Y(s)\right| < 1-\alpha$, where $D_1 = \left\{s \in \mathbb{C} : \left|\mathrm{Re}(s - j\omega_r)\right| < \delta, \left|\mathrm{Im}(s - j\omega_r)\right| < \delta\right\}$. Such α, δ exist by Eq. (3.2). By continuous dependence of zeros of polynomials on the coefficients, $\exists \hat{\zeta} : \forall \zeta < \hat{\zeta}$, $p(\zeta) \in D_1$. By continuity of the TF, $\exists \beta > 0$ and $|\lambda| < \alpha\zeta\omega_r^2$ such that $\forall s \in D_2$, $\mathrm{Im}\left(s^2 + 2\zeta\omega_r s + \omega_r^2\right) = 2\zeta\omega_r^2 + \lambda$ where $D_2 = \left\{s \in \mathbb{C} : \left|\mathrm{Re}(s - j\omega_r)\right| < \beta\zeta, \left|\mathrm{Im}(s - j\omega_r)\right| < \delta\right\}$. Hence $\left(s^2 + 2\zeta\omega_r s + \omega_r^2\right) + 2\zeta\omega_r^2 (X/Y)$ cannot be

zero in D_2 and therefore, $p(\zeta) \in D_1$ but $p(\zeta) \notin D_2$. Hence, from the stability of the TF, $\mathrm{Re}\left(p(\zeta)\right) < -\beta e$ and residue of this pole in H is proportional to ζ. Therefore the contribution of this pole (and its conjugate) to the impulse response of H will be an exponent decaying faster than $e^{-\beta\zeta t}$ which when integrated and multiplied by the residue proportional to ζ can be bounded uniformly in ζ. Hence $\|H\|_{op}$ can be bounded uniformly in ζ, $\forall \zeta < \hat{\zeta}$. This, along with the fact that $\|H\|_{op}$ is a continuous function of $\zeta \in (0, \zeta^*]$ since H is stable and its impulse response depends continuously on the parameters, implies that $\|H\|_{op}$ can be bounded uniformly in ζ for $\zeta \in (0, \zeta^*]$ by c_2. Similar argument can be made for existence of the bound c_1. □

In this chapter the problem of rejecting an internally generated sinusoid from the output of a stable perturbed linear finite dimensional system is addressed by developing a closed loop augmentation procedure that depends minimally on the knowledge of the system dynamics. This procedure will be generalized in Chapters 4 and 5 to address rejection of a sinusoidal disturbance form perturbed infinite dimensional systems. In Chapter 4 rejection of finite number of sinusoids is discussed and in Chapters 4 and 7, results from simulations and experiments where two sinusoids are eliminated are presented.

CHAPTER 4

ROBUST TRACKING OF PERIODIC REFERENCES BY UNCERTAIN LINEAR INFINITE DIMENSIONAL PLANTS

In Chapter 2, the problem statement for controller design was formulated to address the rejection of sinusoids from the output of nonlinearly perturbed infinite dimensional plants. As a first step in addressing this problem, a non-model based control scheme was developed in Chapter 3 for nonlinearly perturbed finite dimensional plants. In this chapter, this control scheme is shown to be applicable to exponentially stable plants belonging to a class of linear infinite dimensional systems called Regular Linear Systems (RLS) for tracking, or equivalently rejecting, a finite number of sinusoids. Perturbations will be introduced into plants belonging to the class of RLS to obtain a class of nonlinearly perturbed infinite dimensional systems in Chapter 5. The proposed control scheme will then be shown to be applicable to plants in this class, thereby completely addressing the problem statement.

The class of RLS is a large subset of abstract linear systems, the most general linear class, and contains many physical models and PDEs. The plants in this class are primarily described in the time domain, but have been characterized extensively in the frequency domain as well [32], [33]. The control scheme proposed in Chapter 3, and to be extended to plants in an infinite dimensional class, uses the frequency domain characterization of the plant. But the testbed model, which must be related to this class so as to rigorously establish the applicability of the control scheme to the testbed, is in the time domain. Hence the class of RLS is well suited to the present work.

Background on the class of RLS is presented next. The non-model based control scheme in Theorem 2 of Chapter 3 is then shown to be applicable to exponentially stable plants in this class to track a single sinusoid. A discussion on obtaining desired robustness margins and on tuning the control parameters is included. The control scheme is then extended to address tracking of a finite number of sinusoids by a stable RLS. Finally the scheme is demonstrated in simulations on a delay system.

4.1 Background on regular linear systems

The following definitions and background on RLS can be found in [32]-[34] and references therein and are reproduced here to enhance the clarity of presentation. Let U, X and Y be Hilbert spaces and $\Omega = L^2([0,\infty),U)$ and $\Gamma = L^2([0,\infty),Y)$ be input and output spaces, respectively. An abstract linear system on Ω, X and Γ is a quadruple $\Sigma = (\mathbb{T},\Phi,\mathbb{L},\mathbb{F})$ where $\mathbb{T} = (\mathbb{T}_t)_{t\geq 0}$ is a C_0-semigroup on X, $\Phi = (\Phi_t)_{t\geq 0}$, $\mathbb{L} = (\mathbb{L}_t)_{t\geq 0}$, $\mathbb{F} = (\mathbb{F}_t)_{t\geq 0}$ are families of bounded linear operators from Ω to X (input to state), X to Γ (initial state to output) and Ω to Γ (input to output), respectively. The operators Φ, $\mathbb{L}$ and $\mathbb{F}$ can be extended naturally to the Fréchet space of inputs $\tilde{\Omega} = L^2_{loc}([0,\infty),U)$ and outputs $\tilde{\Gamma} = L^2_{loc}([0,\infty),Y)$, with the extensions denoted by Φ_∞, $\mathbb{L}_\infty$ and $\mathbb{F}_\infty$, respectively.

Let A be the infinitesimal generator of $\mathbb{T}$. The Hilbert spaces X_1 and X_{-1} are defined as follows: X_1 is $D(A)$ with the norm $\|x\|_{X_1} = \|(\beta I - A)x\|_X$, where $\beta \in \rho(A)$ is fixed and X_{-1} is the completion of X with respect to the norm $\|x\|_{X_{-1}} = \|(\beta I - A)^{-1} x\|_X$. The semigroup $\mathbb{T}$ can be extended to a semigroup on X_{-1} isomorphic to $\mathbb{T}$ and will be denoted by the same symbol. For

any abstract linear system, there exists an unique $B \in \mathcal{L}(U, X_{-1})$ called the control operator such that $\Phi_t u = \int_0^t \mathbb{T}_{t-\tau} B u(\tau) d\tau$, for all inputs $u \in \tilde{\Omega}$ and all $t \geq 0$. Then, for any initial state x_0 the state x of Σ at time $t \geq 0$ is expressed as

$$x(t) = \mathbb{T}_t x_0 + \Phi_t u = \mathbb{T}_t x_0 + \int_0^t \mathbb{T}_{t-\tau} B u(\tau) d\tau . \tag{4.1}$$

The state $x : [0, \infty) \to X$, as defined, is a continuous function. In general, $\hat{B} \in \mathcal{L}(U, X_{-1})$ is called a $\mathbb{T}$-admissible control operator if the map $\int_0^t \mathbb{T}_{t-\tau} \hat{B} u(\tau) d\tau \in \mathcal{L}(\Omega, X)$ for each $t \geq 0$. Associated with every abstract linear system is an unique $C \in \mathcal{L}(X_1, Y)$ called the observation operator such that $\forall x \in X_1$, $(\mathbb{L}_\infty x)(t) = C\mathbb{T}_t x$. $\mathbb{L}_\infty$ is completely determined by this equation due to the density of X_1 in X. The Λ-extension of C is defined by

$$C_\Lambda \bar{x} = \lim_{\lambda \to \infty} C\lambda(\lambda I - A)^{-1} \bar{x} , \tag{4.2}$$

with λ real and for all $\bar{x}$ in the domain

$$D(C_\Lambda) = \{\bar{x} \in X : \textit{the limit in Eq. 4.2 exists}\} .$$

The input-output operator of any abstract linear system can be described by a TF which is an operator valued analytic function defined and bounded on some right half complex plane. Let ***G*** denote the TF of Σ. ***G*** is called regular if the following limit exists $\forall v \in U$,

$$Dv = \lim_{\lambda \to \infty} G(\lambda) v, \ \lambda \textit{ real} .$$

Then $D \in \mathcal{L}(U, Y)$ is called the feedthrough operator of ***G***. In this case, the state $x(t)$ given in Eq. (4.1) and the output of Σ, $y = \mathbb{L}_\infty x_0 + \mathbb{F}_\infty u$, where x_0 is the initial state and $u \in \tilde{\Omega}$ is the input, satisfy pointwise almost everywhere (a.e.) in time, the equation

$$y(t) = C_\Lambda x(t) + Du(t). \tag{4.3}$$

If $\boldsymbol{G}$ is regular, then Σ is called a RLS. (A,B,C,D) as introduced are the generating operators (GOs) of Σ. A RLS Σ is called exponentially stable if the associated semigroup $\mathbb{T}$ satisfies $\|\mathbb{T}_t\|_{\mathcal{L}(X)} \le Me^{-at}$, $\forall t \ge 0$, for some $M \ge 1$ and $a > 0$.

In the rest of this chapter, an exponentially stable RLS $\Sigma_P = (\mathbb{T}, \Phi, \mathbb{L}, \mathbb{F})$, with GOs (A_P, B_P, C_P, D_P) and TF $G_P(s)$ satisfying $G_P(-j\tau) = \bar{G}_P(j\tau)$ $\forall \tau \in \mathbb{R}$, is considered.

4.2 Controller for tracking sinusoidal reference

Consider the exponentially stable RLS Σ_P with $U = Y = \mathbb{R}$ and TF $G_P(s)$. This section addresses the following tracking problem:

Given the regular linear system Σ_P, design a controller to ensure that the output y_p of Σ_P tracks a reference sinusoid u, such that $|y_p(t) - u(t)| \in L^2_\alpha([0,\infty), \mathbb{R})$ for some $\alpha < 0$.

Although a SISO plant is considered, extension to MIMO plants, where for each output an input to be tracked is identified, can be accomplished by choosing an appropriate set of internal model based filters on the basis of the principles expounded in the SISO case.

The feedback loop in the control scheme in Theorem 2 of Chapter 3 is modified to address the tracking problem. Understanding the role of the different filters in that scheme, a less intuitive but simplified equivalent feedback loop can be obtained by cascading the given stable, infinite-dimensional in general, system with a stable finite dimensional partitioning filter, adding positive and negative feedback paths that cancel one another, and forming an extended loop through a path containing an internal model based filter. The stability of the loop thus formed and asymptotic tracking of a periodic reference are guaranteed by choosing the filters

appropriately. The partitioning filter can be chosen to obtain desired quantitative robustness margins and the small gain, also present in the approaches in [11]-[16], in the internal model filter can then be chosen to guarantee stability and tuned to improve performance. This design for desired robustness margins and the intuition for tuning the small gain, valuable in practice and not addressed in [11]-[16], is enabled by the precise understanding of the role of the filters along with the graphical verification of the closed loop stability using gain plots afforded by the proposed approach. The tradeoff lies in the current approach requiring higher order controllers compared to those in [11]-[16].

Lemma 4 considers an interconnection, referred to as the unaugmented system, of the given linear system Σ_P with a stable partitioning filter. The stability of the augmented system, obtained via augmenting the unaugmented system with a simple internal model based filter, and the implied tracking of a sinusoidal reference under appropriate choice of the filters are established in Theorem 3.

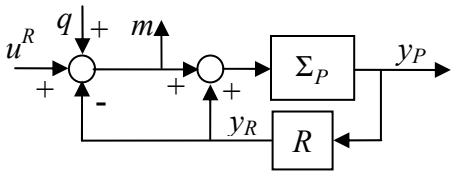

Figure 4.1: Unaugmented system obtained via interconnection of Σ_P and R

Lemma 4: Consider an interconnection of the given RLS Σ_P and R shown in Figure 4.1, referred to as the unaugmented system, where R is the strictly proper stable finite dimensional SISO linear system

$$\dot{x}_R = A_R x_R + B_R u_R,$$
$$y_R = C_R x_R.$$

Let $G_P(s)$ and $G_R(s)$ be the TFs of Σ_P and R, respectively. Let u^R+q be the input and y_P and m be the outputs of interest where the signal u^R is defined as the output of the stable system R with input u and zero initial conditions. Then the unaugmented system is an exponentially stable RLS and the Laplace transforms for y_P and m are given by

$$\begin{aligned}\hat{y}_P(s) &= G_P(s)\left(\hat{q}(s)+\hat{u}^R(s)\right),\\ \hat{m}(s) &= \left(1-G_P(s)G_R(s)\right)\left(\hat{q}(s)+\hat{u}^R(s)\right),\end{aligned} \tag{4.4}$$

which are valid $\forall s\in\mathbb{C}_\alpha$ (for some $\alpha\in\mathbb{R}$) on which the right hand side of the equations are well defined. Hence, the input-output representation of the unaugmented system is as shown in Figure 4.2.

Proof: Although the unaugmented system consists of positive and negative feedback loops, these cancel one another. Therefore the unaugmented system is simply a cascade interconnection of two exponentially stable RLS, Σ_P and R, and hence is an exponentially stable RLS with TFs from u^R+q to y_P and y_R being $G_P(s)$ and $G_R(s)G_P(s)$, respectively [33]. Since $m(t)=\left(q(t)+u^R(t)\right)-y_R(t)$, Eq. (4.4) follows. □

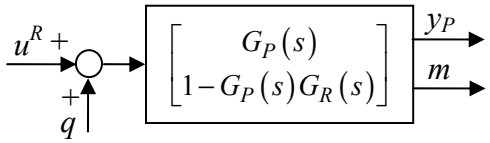

Figure 4.2: Input-output representation of the unaugmented system

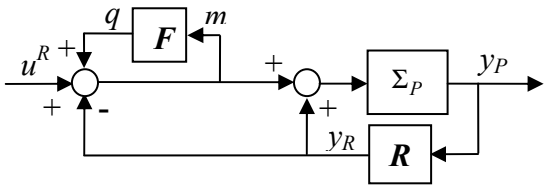

Figure 4.3: Augmented system

Let $(A_{UA}, B_{UA}, C_{UA}, D_{UA})$ be the GOs of the unaugmented system with input u^R+q and outputs y_P and m, and let $G_{UAm}(s) = 1 - G_P(s)G_R(s)$. The following theorem presents the controller design to ensure the tracking of a single sinusoid.

Theorem 3: Consider the unaugmented system shown in Figure 4.1 where Σ_P, R and u^R are as in Lemma 4. Let R be chosen such that

$$\left|\left(1 - G_P(j\omega)G_R(j\omega)\right)\right| < 1, \tag{4.5}$$

where ω is the frequency of u, the reference sinusoid to be tracked. Next consider the system shown in Figure 4.3, referred to as the augmented system. Let F be the linear stable SISO system with TF

$$G_F(s) = \frac{2\zeta\omega s}{s^2 + 2\zeta\omega s + \omega^2}, \tag{4.6}$$

where $0 < \zeta \ll 1$ is a parameter to be chosen. Then, for all sufficiently small ζ, the augmented system is an exponentially stable RLS and y_P tracks u asymptotically, i.e. $\left(y_p(t) - u(t)\right) \in L^2_\gamma\left([0,\infty), \mathbb{R}\right)$ with $\gamma < 0$.

Proof: From Lemma 4, the augmented system in Figure 4.3 is equivalent to the feedback interconnection of two exponentially stable RLS, the unaugmented system and $[0, F]$, as shown

in Figure 4.4. For this feedback system to be well posed, $1-[0\ G_F]\times[G_P\ G_{UAm}]^T = 1-G_{UAm}G_F(s)$ must be invertible on $\mathbb{C}_\alpha$ for some α. Note that the feedthrough operator D_F for $[0, F]$ is $[0,0]$ and hence $1-D_F D_{UA}$ is invertible. Moreover, since $G_P, G_{UAm}, G_F \in H^\infty$, if $(1-G_{UAm}G_F)^{-1} \in H^\infty$, then the augmented system is an exponentially stable RLS from Proposition 4.6 in [33].

From Lemma 4, A_{UA} is exponentially stable and hence $G_{UAm} \in H^\infty_{\beta_1}$ for some $\beta_1 < 0$. Let $\sup_{s\in\mathbb{C}_{\beta_1}} |G_{UAm}(s)| = M$. Note that all the TFs considered are continuous on the imaginary axis. From Eq. (4.5), $\exists \delta,\ \varepsilon > 0$ and the set $I = [\omega-\delta, \omega+\delta]\cup[-\omega-\delta, -\omega+\delta]$ such that $\forall \tau \in I$, $|G_{UAm}(j\tau)| < 1-\varepsilon$. Since $|G_F(j\tau)| \le 1 \ \ \forall \tau \in \mathbb{R}$ and for sufficiently small ζ, $|G_F(j\tau)| < (1-\varepsilon)/M$ $\forall \tau \in \mathbb{R} - I$, it follows that $|G_{UAm}G_F(j\tau)| < 1-\varepsilon$, $\forall \tau \in \mathbb{R}$. As $|s| \to \infty$ with $s \in \mathbb{C}_0^+$, $|G_{UAm}G_F(s)| \to 0$ uniformly. Since $G_{UAm}G_F(s)$ is analytic on $\mathbb{C}_0^+$, by the maximum modulus principle [31], $|G_{UAm}G_F(s)| < 1-\varepsilon$ and consequently $|1-G_{UAm}G_F(s)| > \varepsilon \ \ \forall s \in \mathbb{C}_0^+$. This implies that $(1-G_{UAm}G_F)^{-1} \in H^\infty$. Therefore the augmented system is an exponentially stable RLS. Hence the TFs from u^R to y_P and m, $H_p = G_P(1-G_{UAm}G_F)^{-1}$ and $H_m = G_{UAm}(1-G_{UAm}G_F)^{-1}$, respectively, belong to $H^\infty_{\beta_2}$ for some $\beta_2 < 0$.

Assume all initial conditions are zero. Let $u = A_0 \sin(\omega t)$. Then $\hat{u}(s) = A_0\omega / (s^2+\omega^2)$ and $\hat{u}^R(s) = G_R\hat{u}(s)$. For the error $e(t) = y_p(t) - u(t)$,

$$\hat{e}(s) = \hat{y}_P(s) - \hat{u}(s) = \left(G_P G_R (1-G_{UAm}G_F)^{-1} - 1\right)\hat{u}(s)$$

$$= A_0\omega(G_F - 1)G_{UAm}(1-G_{UAm}G_F)^{-1}(s^2+\omega^2)^{-1}.$$

Now, $G_F(s)-1$ can be written as $G_Q(s)\left(s^2+\omega^2\right)\big/(s+1)$ where $G_Q(s)$ is a rational, stable, proper TF corresponding to an exponentially stable RLS Q. Hence

$$\hat{e}(s) = A_0\omega G_Q G_{UAm}\left(1-G_{UAm}G_F\right)^{-1}(s+1)^{-1}$$

$$= \left[0 \; A_0\omega G_Q\right]\left[H_P \; H_m\right]^T(s+1)^{-1}.$$

Considering $e(t)$ to be the response of the cascade interconnection of the two exponentially stable RLS, the augmented system and $\left[0 \; A_0\omega Q\right]$, to the input e^{-t}, $e(t)\in L^\infty_{\alpha_1}\left([0,\infty),\mathbb{R}\right)$ for some $\alpha_1<0$ [32]. Now let $z(t)$ be the contribution of all the initial conditions to y_P. Then the total error $\bar{e}(t)=e(t)+z(t)$. Since the augmented system is an exponentially stable RLS $z(t)\in L^\infty_{\alpha_2}\left([0,\infty),\mathbb{R}\right)$ for some $\alpha_2<0$ [32]. Hence the error $\bar{e}(t)\in L^\infty_{\gamma}\left([0,\infty),\mathbb{R}\right)$ for some $\gamma<0$. □

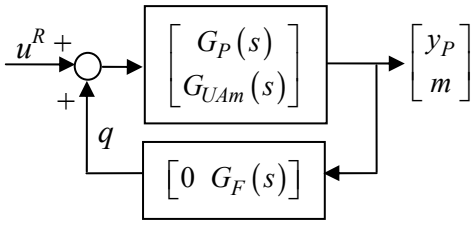

Figure 4.4: Input-output representation of the augmented system

4.3 Filter design for robustness and stability

The filter R in the tracking controller in Theorem 3 can be chosen so as to obtain guaranteed robustness to variations in the plant gain at the frequency of interest and the parameter ζ in the filter F can then be chosen to guarantee stability. In the following analysis, the perturbed plant is $\Sigma_{P,D}=\Sigma_P+\Sigma_D$, where the perturbation Σ_D is an exponentially stable RLS. Let the TF of $\Sigma_{P,D}$

be $G_{P^D} = G_P + \Delta_P$. Assume that $\Delta_P(-j\tau) = \bar{\Delta}_P(j\tau) \quad \forall \tau \in \mathbb{R}$. The robustness properties of the controller depend on the choice of the filter *R*. For this analysis let *R* be chosen so as to satisfy

$$\left|1 - G_P(j\omega) G_R(j\omega)\right| = 0 \tag{4.7}$$

where ω is the frequency of the sinusoid to be tracked. From the proof of Theorem 3, stability of the augmented system is guaranteed if $\left|G_{UAm}(j\tau) G_F(j\tau)\right| < 1, \ \forall \tau \in \mathbb{R}$, which in turn guarantees asymptotic tracking. This is achieved using Eq. (4.5) and by choosing $0 < \zeta \ll 1$ in Eq. (4.6). For the perturbed plant, stability of augmented system and asymptotic tracking is guaranteed if $\forall \tau \in \mathbb{R}$,

$$\left|\left(1 - \left(G_P(j\tau) + \Delta_P(j\tau)\right) G_R(j\tau)\right)\right| < \frac{1}{\left|G_F(j\tau)\right|}, \tag{4.8}$$

From Eq. (4.6), $\forall \tau$ away from $\pm\omega$, i.e. $\tau \notin (\pm\omega - \rho, \pm\omega + \rho)$ for some small ρ (proportional to ζ), $\left|G_F(j\tau)\right|$ is small (again proportional to ζ) and therefore large perturbation $\left|\Delta_P(j\tau)\right|$ at these values of τ will not invalidate the inequality Eq. (4.8) and hence will not cause instability.

For $\tau = \omega$ (or $-\omega$), $G_F(j\omega) = 1$ and hence for stability

$$\left|1 - \left(G_P(j\omega) + \Delta_P(j\omega)\right) G_R(j\omega)\right| < 1.$$

From Eq. (4.7), this is equivalent to $\left|\Delta_P(j\omega) / G_P(j\omega)\right| < 1$. Note that this inequality is optimal in the sense that when $\Delta_P(j\omega) = -G_P(j\omega)$, $\left|\Delta_P(j\omega) / G_P(j\omega)\right| = 1$ and $G_{P^D}(j\omega) = 0$. In this case asymptotic tracking of sinusoid at frequency ω can not be guaranteed by any internal model based feedback technique since G_{P^D} may have multiple zeros at $\pm j\omega$. Let J be the interval $(\omega - \rho, \omega + \rho)$. Note that, since ρ is proportional to $\zeta \ll 1$, it is reasonable to assume that on J, $G_R(j\tau)$ and $G_P(j\tau)$ do not vary significantly while $\left|G_F(j\tau)\right|$ reduces rapidly, by design. Hence

from Eq. (4.7), for η_1 small and $\eta_2 \approx 1$, $\left|1 - G_P(j\tau)G_R(j\tau)\right| < \eta_1$ and $\left(\left|G_R(j\tau)\right| / \left|G_R(j\omega)\right|\right) < \eta_2$, $\forall \tau \in J$. In this case it can be shown that if $\left|\Delta_P(j\tau)/G_P(j\omega)\right| < (1-\eta_1)/\eta_2 \approx 1$, the inequality Eq. (4.8) is not violated and hence the perturbation does not cause instability of the augmented system. The above argument can be repeated on the interval $(-\omega-\rho, -\omega+\rho)$.

Hence estimates for the admissible magnitude of $\left|\Delta_P(j\tau)\right|$ $\forall \tau \in \mathbb{R}$ have been computed. For τ away from $\pm\omega$, $\left|\Delta_P(j\tau)\right|$ can be large and for τ near ω, $\left|\Delta_P(j\tau)\right|$ must be less than $\left|G_P(j\omega)\right|$. In practice, $G_{P^D}(j\omega)$ can be monitored to recognize scenarios in which stability is at risk. Graphically this robustness condition states that as long as the perturbed gain at the frequency of interest ω stays in a disc of radius $\left|G_P(j\omega)\right|$ centered at $G_P(j\omega)$ in the complex plane, the closed loop will be stable. If a larger robustness margin is desired, it can be obtained by choosing $\alpha > 1$ and letting *R* satisfy

$$\left|1 - \alpha G_P(j\omega)G_R(j\omega)\right| = 0.$$

In this case closed loop will be stable provided the gain remains in the disc of radius $\alpha\left|G_P(j\omega)\right|$ centered at $\alpha G_P(j\omega)$. Larger the α, larger is the disc in the complex plane in which the perturbed gain can stay without loss of stability.

The design for robustness requires that ζ be small. The permissible values of ζ guaranteeing stability can be obtained as follows. In practice, the frequency response of the plant in an interval around the frequency of interest is available. Once the filter *R* is fixed for desired robustness, then the graph of $\left|1 - G_P(j\tau)G_R(j\tau)\right|$ can be obtained. From this graph, the maximum permissible value for the damping ratio ζ in *F* to guarantee stability can be computed by first ascertaining the decay/growth rates of $\left|G_P(j\tau)\right|$ and $\left|G_R(j\tau)\right|$ for τ near ω and then choosing ζ

to ensure that $|G_F(j\tau)|$ decays faster than $|1-G_P(j\tau)G_R(j\tau)|$ in this range. The various decay rates and their relative values can be visually estimated and compared using the gain plots. For closed loop stability, the plot of $|G_F(j\tau)||1-G_P(j\tau)G_R(j\tau)|$ must have magnitude less than one. Once the maximum permissible ζ is found, it can then be tuned to optimize transients. Typically, a larger value of ζ is desired since it increases the influence of the filter *F* and thereby quickens the rejection of the disturbance. In the mold oscillation system ζ and *R* were fixed based on the above discussion and the stability of the closed loop was graphically verified for each of the different plant gain data collected over a month.

4.4 Rejection of multiple sinusoids

The control scheme in Theorem 3 can be directly extended to addresses the tracking of periodic signal with a finite number of sinusoids. This extension is presented next as Theorem 4.

Theorem 4: Let Σ_P, *unaugmented system, augmented system and* u^R *be as in Theorem 3 and let R be a stable finite dimensional strictly proper SISO system satisfying*

$$|1-G_P(j\omega_i)G_R(j\omega_i)|<1, \quad \forall i=1...n, \tag{4.9}$$

where ω_i *are the frequencies of the sinusoids in u, the reference signal to be tracked. Let F be a linear stable system with TF* $G_F(s)$ *satisfying the following:*

i) $1-G_F(s)$ *has zeros at* $\pm j\omega_i$, $\forall i=1...n$,

ii) $|G_F(j\tau)|\le 1+\delta_2$, $\forall \tau\in\mathbb{R}$ *and* $|G_F(j\tau)|$ *decays in the intervals* $(\pm\omega_i-\delta_1,\pm\omega_i+\delta_1)$ *such that for* $\tau\notin(\pm\omega_i-\delta_1,\pm\omega_i+\delta_1)$, $|G_F(j\tau)|<\delta_2$ $\forall i=1...n.$

Then, for all sufficiently small values of δ_1 *and* δ_2*, the augmented system is an exponentially stable RLS and* y_P *tracks u asymptotically, i.e.* $e(t) \in L^2_\gamma([0,\infty),\mathbb{R})$ *for some* $\gamma < 0$*. Here* $(\pm\omega - x, \pm\omega + y) = (-\omega - x, -\omega + y) \cup (+\omega - x, +\omega + y)$.

Proof: The proof is analogous to that of Theorem 3. The stability of the augmented loop is established by showing that the positive feedback interconnection of G_F and $1 - G_P G_R$ is a stable RLS. The details are omitted. □

For example the filters

$$G_F(s) = \frac{\prod_{i=1}^{n}\left(s^2 + 2\zeta_i\omega_i s + \omega_i^2\right) - \prod_{i=1}^{n}\left(s^2 + \omega_i^2\right)}{\prod_{i=1}^{n}\left(s^2 + 2\zeta_i\omega_i s + \omega_i^2\right)} \quad \text{and} \quad G_R(s) = \sum_{i=1}^{n}\frac{X_i^1 s + X_i^2}{\left(s^2 + \omega_i s + \omega_i^2\right)}$$

with sufficiently small value of ζ_i's and appropriate values for X_i^1's and X_i^2's, so as to satisfy the gain condition Eq. (4.9), can be used to implement the control scheme in Theorem 4.

4.4.1 Delay system

The control scheme in Theorem 4 is applied to an exponentially stable RLS having the TF representation

$$G_P(s) = \frac{e^{-0.5s}}{s+1}, \tag{4.10}$$

to track the reference signal $u(t) = 2\sin(5t+4) + 3\sin(10t)$.

The TFs

$$G_R = \frac{-45.94s + 244.57}{s^2 + 5s + 25} + \frac{149.57s + 85.76}{s^2 + 10s + 100},$$

and $$G_F = \frac{0.5s}{s^2 + 0.5s + 25} + \frac{s}{s^2 + s + 100},$$

satisfy the assumptions in Theorem 4 since for $\omega_1 = 5$ and $\omega_2 = 10$

$$\left|1 - G_P(j\omega_i)G_R(j\omega_i)\right| = 0, \qquad i = 1,2, \tag{4.11}$$

and G_F satisfies $G_F(5j) = G_F(10j) = 1$ and decays to a sufficiently lower value fast enough. Consequently, as shown in Figure 4.5, the magnitude of the frequency response of $G_F(1 - G_P G_R)$ is always less than one implying the stability of the augmented system. The output and the tracking error obtained by using these filters and applying the controller of Theorem 4 to plant in Eq. (4.10) are shown in Figure 4.6. As seen, the controller ensures asymptotic tracking of u by the plant output.

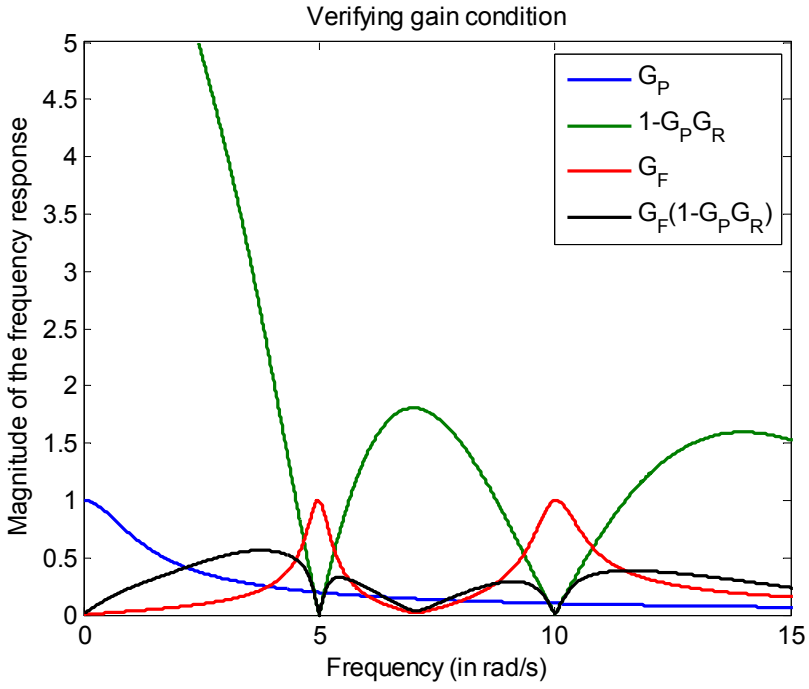

Figure 4.5: Verifying the gain condition for augmented system stability

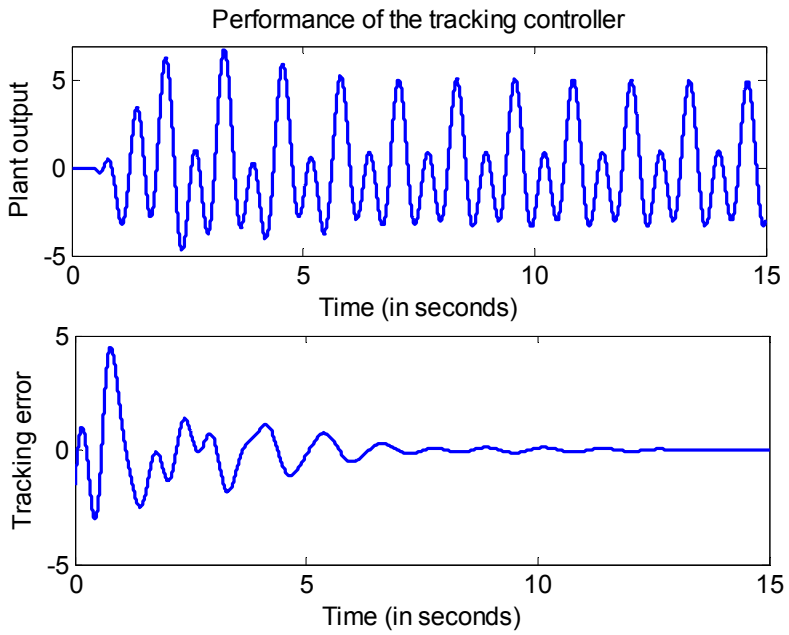

Figure 4.6: Output of the plant in Eq. (4.10) and tracking error using Theorem 4

CHAPTER 5

REJECTION OF SINUSOIDAL DISTURBANCES FROM UNCERTAIN NONLINEARLY PERTURBED INFINITE DIMENSIONAL PLANTS

The problem statement for controller synthesis formulated in Chapter 2 to ensure the rejection of periodic disturbances from the testbed of the mold oscillation system, characterized as a nonlinearly perturbed infinite dimensional system, is completely addressed in this chapter. A new class of systems - nonlinearly perturbed regular linear system (NPRLS) - that directly matches the phenomenology of the application of interest is considered. The definition of this new system class is given and a detailed characterization of its stability and response to periodic excitation is presented. Such a characterization, and its further generalization to interconnected systems, has been developed for finite dimensional systems in [29]. The results developed in this work are a first step towards obtaining such generalizations for infinite dimensional systems.

The robust control scheme presented in Chapter 4 for tracking of bandlimited periodic signals by regular linear systems (RLS) is applied to plants in the class of NPRLS and conditions for closed loop stability and rejection of internally generated unwanted harmonics from the output are rigorously ascertained. This is accomplished by first considering the closed loop without the nonlinear perturbation and then analyzing the effect of the perturbation on stability and performance using the aforementioned characterization of NPRLS. Establishing the existence of a non-zero upper bound on the magnitude of the nonlinearity independent of the tunable small parameter in the controller, under which the closed loop is guaranteed to be stable, is essential and is addressed via an involved lemma.

5.1 Nonlinearly perturbed regular linear systems (NPRLS)

Consider, an exponentially stable RLS $\Sigma_P = (\mathbb{T}, \Phi, \mathbb{L}, \mathbb{F})$, with GOs (A_P, B_P, C_P, D_P) and TF $G_P(s)$ as introduced in Section 4.1. The NPRLS, $\Sigma_{P,N}$, corresponding to this RLS Σ_P, is defined as being represented by the differential equation

$$\begin{aligned} \dot{x}_P &= A_P x_P + B_P u + \varepsilon g(x_P), \qquad x_P(0) = x_0, \\ y_P &= C_{P,\Lambda} x_P + D_P u, \end{aligned} \tag{5.1}$$

where $C_{P,\Lambda}$ is the Λ-extension of C_P, $\varepsilon > 0$ is a small constant, g is a nonlinear term, and the following assumptions hold:

Assumption 1: $\mathbb{T}$, the C_0-semigroup on X generated by A_P, is exponentially stable and satisfies $\|\mathbb{T}_t\|_{\mathcal{L}(X)} < Me^{-at}$ with $a > 0$ and $M \geq 1$.

Assumption 2: $g(x): X \to X$ satisfies the Lipschitz condition that, for any bounded domain $D \subset X$, $\exists L(D)$: $\|g(x) - g(y)\|_X < L(D)\|x - y\|_X$, $\forall\ x, y \in D$ and $g(0) = 0$.

Assumption 3: $(A_P, I_X, C_P, 0)$ are the GOs of an RLS $\left(\mathbb{T}, \Phi^g, \mathbb{L}, \mathbb{F}^g\right)$ with state space X and input and output taking values in X and Y respectively. I_X is the identity operator on X.

Under Assumptions 1-2, Lemma 8 shows that for a given $u \in L^\infty([0,\infty), U)$ and $x_0 \in X$, $\exists \bar{\varepsilon}: \forall \varepsilon < \bar{\varepsilon}$, the state equation in Eq. (5.1) has a unique continuous solution, bounded in X, and satisfying a variation of parameters formula. The existence proof is along the lines of the proof in chapter 6 of [35] and is sketched here since, though $B_P \in \mathcal{L}(U, X_{-1})$ it may not belong to $\mathcal{L}(U, X)$. Assumption 3 enables treating the nonlinearity as an input and renders the output equation in Eq. (5.1) meaningful. This is used in Lemma 9.

5.2 Stability and response of NPRLS under periodic excitation

This section contains a series of lemmas that characterize the response of NPRLS to periodic excitation. Consider Σ_P and its GOs as defined in Section 5.1. Since $\mathbb{T}$ is exponentially stable (Assumption 1), $\Phi_t : \Omega \to X$ is continuous for all t and $\|\Phi_t(u)\|_X \le \tilde{N}\|u\|_{L^2[0,t]}$, $\forall u \in \tilde{\Omega}$ [36]. But dealing with bounded input u, a bound on $\Phi_t(u)$ depending on $\|u\|_{U,\infty}$ is desired and is given by the following lemma.

Lemma 5: If $u \in L^\infty([0,\infty),U)$, *then* $\|\Phi_t u\|_X \le \bar{N}\|u\|_{U,\infty}$ *for some fixed* $\bar{N} > 0$ *independent of* t.

Proof: Consider the exponentially stable C_0-semigroup $\tilde{\mathbb{T}}_t = \mathbb{T}_t e^{bt}$ generated by $A_P + bI$ with $0 < b < a$. Fix any $t \ge 0$ and $v \in \Omega$. Then,

$$\tilde{\Phi}_t v = \int_0^t \tilde{\mathbb{T}}_{t-\tau} B_P v(\tau)\, d\tau = \int_0^t \mathbb{T}_{t-\tau} B_P \left(e^{b(t-\tau)} v(\tau)\right) d\tau = \int_0^t \mathbb{T}_{t-\tau} B_P \tilde{v}(\tau)\, d\tau = \Phi_t \tilde{v},$$

where $\tilde{v}(\tau) = e^{b(t-\tau)} v(\tau) \in L^2([0,t],U)$.

$\tilde{\Phi}_t \in \mathcal{L}(\Omega, X)$, since $\|\tilde{\Phi}_t v\|_X = \|\Phi_t \tilde{v}\|_X \le \tilde{N}\|\tilde{v}\|_{L^2[0,t]} \le \tilde{N} e^{bt}\|v\|_{L^2[0,t]}$ for any $v \in \Omega$. Since this holds for all t, B_P is a $\tilde{\mathbb{T}}$-admissible control operator and $(\tilde{\mathbb{T}}, \tilde{\Phi})$ is an abstract linear control system [36] where $\tilde{\Phi} = (\tilde{\Phi}_t)_{t \ge 0}$. Moreover, since $\tilde{\mathbb{T}}$ is exponentially stable, $\tilde{\Phi}$ is uniformly bounded with $\|\tilde{\Phi}_t\|_{\mathcal{L}(\Omega,X)} \le \tilde{\tilde{N}}$. Therefore,

$$\|\Phi_t u\|_X = \left\|\tilde{\Phi}_t\left(e^{-b(t-\tau)} u(\tau)\right)\right\|_X \le \tilde{\tilde{N}}\left\|e^{-b(t-\tau)} u\right\|_{L^2[0,t]} \le \tilde{\tilde{N}}\|u\|_{U,\infty}\left\|e^{-b(t-\tau)}\right\|_{L^2[0,t]} \le \bar{N}\|u\|_{U,\infty}$$

and the lemma is proven. □

Lemma 6: Let $u:[0,\infty)\to U$ *and* $v:[0,\infty)\to X$ *be continuous T-periodic functions. Then under Assumption 1,* $w_u(t)=\int_0^t \mathbb{T}_{t-\tau}B_P u(\tau)\,d\tau$ *and* $w_v(t)=\int_0^t \mathbb{T}_{t-\tau}v(\tau)\,d\tau$ *converge in* $\|\bullet\|_X$*, asymptotically, to continuous T-periodic functions. The rate of convergence depends on* $\|u\|_{U,\infty}$ *and* $\|v\|_{X,\infty}$ *but not on the particular functions.*

Proof: Since $B_P\in\mathcal{L}(U,X_{-1})$, the integration for w_u is in X_{-1}. That $w_u(t)\in X$, $\forall t$, and the continuity of w_u in X follows from the properties of RLS. Using Lemma 5 and a change of variables, it follows that for $n>m$, $p=n-m$ and $\forall s\in[0,T]$

$$\left\|\int_0^{nT+s}\mathbb{T}_{nT+s-\tau}B_P u(\tau)\,d\tau-\int_0^{mT+s}\mathbb{T}_{mT+s-\tau}B_P u(\tau)\,d\tau\right\|_X$$

$$=\left\|\int_0^{pT}\mathbb{T}_{nT+s-\tau}B_P u(\tau)\,d\tau\right\|_X=\left\|\mathbb{T}_{mT+s}\int_0^{pT}\mathbb{T}_{pT-\tau}B_P u(\tau)\,d\tau\right\|_X$$

$$=\left\|\mathbb{T}_{mT+s}\Phi_{pT}u\right\|_X\le Me^{-aTm}\bar{N}\|u\|_{U,\infty}.$$

Hence the sequence of continuous functions f_n defined as $f_n(s)=w_u(nT+s)$, $\forall s\in[0,T]$, is Cauchy in the supremum norm. Hence $f_n(s)$ converges to a function $f(s)$ uniformly $\forall s\in[0,T]$, which implies that $w_u(t)$ converges to a continuous *T*-periodic function asymptotically. A similar argument establishes the result for w_v. The claim about the rate of convergence follows from the proof. □

Lemma 7 formalizes a fact used to prove Lemma 8, which concludes that the state of the periodically excited NPRLS in Eq. (5.1) is periodic, asymptotically, with the same period. Lemma 8 was stated without proof in the finite dimensional context in Lemma 1 of Chapter 3.

Lemma 7: Let L *be the Lipschitz constant for* $g(x)$ *on* $D = B_c(0,d) \subset X$ *(Assumption 2). Let the continuous functions* $v, w : [0,\infty) \to D$ *satisfy* $\|w(t) - v(t)\|_X < C$, $\forall t > \bar{t}$. *Let* $x(t) = \int_0^t \mathbb{T}_{t-\tau} \varepsilon \left(g(w(\tau)) - g(v(\tau)) \right) d\tau$. *Then for any* $\mu > 0$, $\exists \bar{\bar{t}} > \bar{t}$: $\forall t > \bar{\bar{t}}$, $\|x(t)\|_X < \mu + (M\varepsilon LC)/a$.

Proof: Given $\mu > 0$, find $\bar{\bar{t}} > \bar{t}$: $e^{-a\left(\bar{\bar{t}} - \bar{t}\right)} < \mu a / (2d\varepsilon LM)$. Then, it follows easily that $\forall t > \bar{\bar{t}}$, $\|x(t)\|_X < \mu + (M\varepsilon LC)/a$. □

Lemma 8: Consider the RLS Σ_P, *the corresponding NPRLS* $\Sigma_{P,N}$ *given in Eq. (5.1) and the associated nonlinear integral map* $q = \mathbb{I}(p)$ *defined* $\forall t \in [0,\infty)$ *as*:

$$q(t) = p(t) - \mathbb{T}_t x_0 - \int_0^t \mathbb{T}_{t-\tau} B_P u(\tau) d\tau - \varepsilon \int_0^t \mathbb{T}_{t-\tau} g\left(p(\tau)\right) d\tau .$$

Let $\|x_0\|_X < C_0$ *and* $u : [0,\infty) \to U$ *be a continuous T-periodic function. Let Assumptions 1-2 hold. Then, since* Σ_P *is exponentially stable,* $\|\Phi_t u\|_X \le \tilde{N} \|u\|_{L^2[0,t)}$ *and from Lemma 5* $\|\Phi_t u\|_X \le \bar{N} \|u\|_{U,\infty}$, *for some* $\tilde{N}, \bar{N} > 0$ *and* $\forall t$. *Hence the map* $\mathbb{I}$ *is well defined from* $C_B([0,\infty), X)$ *to itself. Assume that* ε *is small enough so that for some* $0 < \alpha < 1$ *and* $D_0 = \left\{ x \in X : \|x\|_X \le \left(C_0 + \left(MC_0 + \bar{N} \|u\|_\infty \right) \right) / (1-\alpha) = d_0 \right\}$, $(\varepsilon M L_0)/a < \alpha$. *Here* L_0 *is the Lipschitz constant of* $g(x)$ *for the domain* D_0. *Then,* $\exists x_P, \hat{x}_P \in C_B([0,\infty), X)$ *with* $\mathbb{I}(x_P) = 0$ *and* $\hat{x}_P$ *a T-periodic function such that for any given* $\lambda > 0$, $\exists\, \hat{t} > 0$: $\left\| x_P[\hat{t},\infty) - \hat{x}_P[\hat{t},\infty) \right\|_{X,\infty} < \lambda$.

Proof: Step 1 of the proof establishes the existence of an unique solution to $\mathbb{I}(p)=0$, which would then be the variation of parameters solution to the state equation in Eq. (5.1). Step 2 proves asymptotic convergence of this solution to a *T*-periodic function.

Step 1: The initial condition satisfies $\|x_0\|_X < C_0 < d_0$. Let $\tilde{L}$ be the Lipschitz constant *of* $g(x)$ for $B_c(0,2Md_0) \subset X$ (Assumption 2). Let $\sigma > 0$ satisfy $\varepsilon M\tilde{L}\sigma < 1$ and $\tilde{N}\|u\|_{L^2[0,\sigma]} + 2\varepsilon M^2 d_0 \tilde{L}\sigma < Md_0$. Then the function H maps the complete metric space $C\left([0,\sigma], B_c(0,2Md_0)\right)$ to itself and is a contraction where $H(t)$ is defined as: $(Hp)(t) = \mathbb{T}_t x_0 + \int_0^t \mathbb{T}_{t-\tau}\left(B_P u(\tau) + \varepsilon g\left(p(\tau)\right)\right)d\tau, \quad \forall t \in [0,\sigma]$. This follows from the inequalities

$$\sup_{t\in[0,\sigma]} \left\|H(t)\right\|_X \le Md_0 + \tilde{N}\|u\|_{L^2[0,\sigma]} + 2\varepsilon M^2 d_0 \tilde{L}\sigma < 2Md_0,$$

$$\sup_{t\in[0,\sigma]} \left\|(Hx)(t) - (Hy)(t)\right\|_X = \sup_{t\in[0,\sigma]} \left\| \varepsilon \int_0^t \mathbb{T}_{t-\tau}\left(g\left(x(\tau)\right) - g\left(y(\tau)\right)\right)d\tau \right\|_X$$

$$\le \varepsilon M\tilde{L}\sigma \sup_{t\in[0,\sigma]} \left\|x(t) - y(t)\right\|_X$$

$$< \sup_{t\in[0,\sigma]} \left\|x(t) - y(t)\right\|_X.$$

By contraction mapping principle, there exists a unique fixed point $x_P(t) \in C\left([0,\sigma], B_c(0,2Md_0)\right)$ such that

$$x_P(t) = \mathbb{T}_t x_0 + \int_0^t \mathbb{T}_{t-\tau}\left(B_P u(\tau) + \varepsilon g\left(x_P(\tau)\right)\right)d\tau, \ \forall t \in [0,\sigma].$$

Since the choice of σ is fixed for a given d_0, showing that $\left\|x_P(\sigma)\right\|_X < d_0$ enables the application of the preceding argument with $x_P(\sigma)$ replacing x_0, implying the unique

continuation of $x_P(t)$ on to the interval $[\sigma, 2\sigma]$. Consequently, showing $x_P(t) \in B(0, d_0)$ $\forall t \in [0,\infty)$, will establish it as the unique continuous function defined on the interval $[0,\infty)$ satisfying $\forall t \in [0,\infty)$,

$$x_P(t) = \mathbb{T}_t x_0 + \int_0^t \mathbb{T}_{t-\tau} B_P u(\tau) d\tau + \int_0^t \mathbb{T}_{t-\tau} \varepsilon g\left(x_P(\tau)\right) d\tau \tag{5.2}$$

and equivalently, $x_P(t)$ will be the unique function in $C_B\left([0,\infty), X\right)$ satisfying $\mathbb{I}(x_P) = 0$.

To show that $x_P(t)$ never leaves $B(0, d_0)$, assume that $t_f > 0$ is the first time instant when $\left\|x_P(t_f)\right\|_X = d_0$. Then

$$\left\|x_P(t_f)\right\|_X < MC_0 + \bar{N}\|u\|_{U,\infty} + \varepsilon \left\|g \circ x_P\left(\left[0, t_f\right]\right)\right\|_{X,\infty} M/a,$$

$$\Rightarrow \left\|x_P(t_f)\right\|_X < MC_0 + \bar{N}\|u\|_{U,\infty} + \varepsilon L_0 \left\|x_P(t_f)\right\|_X M/a,$$

$$\Rightarrow \left\|x_P(t_f)\right\|_X < \left(MC_0 + \bar{N}\|u\|_{U,\infty}\right) \Big/ (1 - \varepsilon L_0 M/a) < \left(MC_0 + \bar{N}\|u\|_{U,\infty}\right) \Big/ (1-\alpha) < d_0.$$

This is a contradiction and hence the equation $\mathbb{I}(p) = 0$, has a unique solution $x_P(t) \in C_B\left([0,\infty), X\right)$ which satisfies Eq. (5.2).

Step 2: Next, it is shown that $x_P(t)$ tends to a T-periodic function, $\hat{x}_P(t)$, asymptotically. The proof uses Assumption 2 to successively construct T-periodic approximations for $\hat{x}_P(t)$. Let $\int_0^t \mathbb{T}_{t-\tau} B_P u(\tau) d\tau$ and $\int_0^t \mathbb{T}_{t-\tau} \varepsilon g\left(v_0(\tau)\right) d\tau$ converge asymptotically to T-periodic functions $v_0(t)$ and $v_1(t)$, respectively (Lemma 6). For $k > 1$, let v_k be the T-periodic function to which $\int_0^t \mathbb{T}_{t-\tau} \varepsilon g\left(v_0(\tau) + v_{k-1}(\tau)\right) d\tau$ converges asymptotically. The following norm inequalities hold:

$\|v_0\|_{X,\infty} \le \bar{N}\|u\|_\infty < d_0$ and $\|v_0 + v_k\|_{X,\infty} \le \bar{N}\|u\|_\infty \sum_{i=0}^{k} \alpha^i < d_0$ implying that $v_0(t)$ and $v_0(t) + v_k(t)$ belong to D_0 - a fact used repeatedly for majorizing the nonlinearity. The sequence of T-periodic functions $\{v_0 + v_k\}$ is shown to be Cauchy in $C_B([0,\infty), X)$ and its limit $\hat{x}_P$ is the function to which $x_P(t)$ converges asymptotically. To prove $\{v_0 + v_k\}$ is Cauchy, it is shown below that for a given $\delta > 0$, $\exists N$ such that $\forall r, s > N$, $\|(v_0 + v_r) - (v_0 + v_s)\|_{X,\infty} < \delta$. Since $\{v_0 + v_k\}$ is in D_0 $\forall k \ge 1$, it follows from the remark on the rate of convergence in Lemma 6 that $\exists t_0 : \forall t > t_0$ and $\forall k \ge 1$,

$$C_0 M e^{-at} + \left\| \int_0^t \mathbb{T}_{t-\tau} B_P u(\tau) d\tau - v_0(t) \right\|_X < \alpha(1-\alpha)\delta/8,$$

$$\left\| \int_0^t \mathbb{T}_{t-\tau} \varepsilon g(v_0(\tau)) d\tau - v_1(t) \right\|_X < \alpha(1-\alpha)\delta/8 \text{ and}$$

$$\left\| \int_0^t \mathbb{T}_{t-\tau} \varepsilon g(v_0(\tau) + v_k(\tau)) d\tau - v_{k+1}(t) \right\|_X < \alpha(1-\alpha)\delta/8.$$

Since $x_P(t) = \mathbb{T}_t x_0 + \int_0^t \mathbb{T}_{t-\tau}\left(B_P u(\tau) + \varepsilon g(x_P(\tau))\right) d\tau \in D_0$, it follows that $\forall\ t > t_0$,

$$x_P(t) - v_0(t) = \mathbb{T}_t x_0 + \int_0^t \mathbb{T}_{t-\tau} B_P u(\tau) d\tau - v_0(t) + \int_0^t \mathbb{T}_{t-\tau} \varepsilon g(x_P(\tau)) d\tau,,$$

$$\Rightarrow \|x_P(t) - v_0(t)\|_X < C_0 M e^{-at} + \left\| \int_0^t \mathbb{T}_{t-\tau} B_P u(\tau) d\tau - v_0(t) \right\|_X + (M\varepsilon L_0/a) d_0,$$

$$\Rightarrow \|x_P(t) - v_0(t)\|_X < \alpha(1-\alpha)\delta/2 + \alpha d_0. \tag{5.3}$$

Using Eq. (5.3) and choosing $\mu = \alpha(1-\alpha)\delta/4$ in Lemma 7, $\forall t > t_0 + t_1$, where $e^{-at_1} < \mu a/(2M\varepsilon L_0 d_0)$,

$$x_P(t) - v_0(t) - v_1(t) = \mathbb{T}_t x_0 + \int_0^t \mathbb{T}_{t-\tau} B_P u(\tau)\, d\tau - v_0(t) + \int_0^t \mathbb{T}_{t-\tau} \varepsilon g\left(v_0(\tau)\right) d\tau - v_1(t)$$

$$+ \int_0^t \mathbb{T}_{t-\tau} \varepsilon \left(g\left(x_P(\tau)\right) - g\left(v_0(\tau)\right)\right) d\tau,$$

$$\left\| x_P(t) - v_0(t) - v_1(t) \right\|_X < C_0 M e^{-at} + \left\| \int_0^t \mathbb{T}_{t-\tau} B_P u(\tau)\, d\tau - v_0(t) \right\|_X + \left\| \int_0^t \mathbb{T}_{t-\tau} \varepsilon g\left(v_0(\tau)\right) d\tau - v_1(t) \right\|_X$$

$$+ \mu + \left(M\varepsilon L_0 / a\right)\left(\alpha(1-\alpha)\delta/2 + \alpha d_0\right),$$

$$\left\| x_P(t) - v_0(t) - v_1(t) \right\|_X < \alpha(1-\alpha)\delta/2 + \alpha^2(1-\alpha)\delta/2 + \alpha^2 d_0.$$

Now, for $k = j > 1$ for $t > t_0 + jt_1$ assume that

$$\left\| x_P(t) - v_0(t) - v_j(t) \right\|_X < \sum_{i=1}^{j+1} \alpha^i (1-\alpha)\delta/2 + \alpha^{j+1} d_0.$$

Then, for $k = j+1$ and $t > t_0 + (j+1)t_1$ and $\mu = \alpha(1-\alpha)\delta/4$ in Lemma 7,

$$x_P(t) - v_0(t) - v_{j+1}(t) = \mathbb{T}_t x_0 + \int_0^t \mathbb{T}_{t-\tau} B_P u(\tau)\, d\tau - v_0(t) + \int_0^t \mathbb{T}_{t-\tau} \varepsilon g\left(v_0(\tau) + v_j(\tau)\right) d\tau - v_{j+1}(t)$$

$$+ \int_0^t \mathbb{T}_{t-\tau} \varepsilon \left(g\left(x_P(\tau)\right) - g\left(v_0(\tau) + v_j(\tau)\right)\right) d\tau,$$

$$\left\| x_P(t) - v_0(t) - v_{j+1}(t) \right\|_X < C_0 M e^{-at} + \left\| \int_0^t \mathbb{T}_{t-\tau} B_P u(\tau)\, d\tau - v_0(t) \right\|_X$$

$$+ \left\| \int_0^t \mathbb{T}_{t-\tau} \varepsilon g\left(v_0(\tau) + v_j(\tau)\right) d\tau - v_{j+1}(t) \right\|_X$$

$$+ \mu + \left(M\varepsilon L_0 / a\right)\left(\sum_{i=1}^{j+1} \alpha^i (1-\alpha)\delta/2 + \alpha^{j+1} d_0 \right),$$

$$\Rightarrow \left\| x_P(t) - v_0(t) - v_{j+1}(t) \right\|_X < \sum_{i=1}^{j+2} \alpha^i (1-\alpha)\delta/2 + \alpha^{j+2} d_0 .$$

Hence, by induction, given $\delta > 0$, for any $l > 0$ and $t > t_0 + lt_1$, noting $\alpha < 1$,

$$\left\| x_P(t) - v_0(t) - v_l(t) \right\|_X < \sum_{i=1}^{l+1} \alpha^i (1-\alpha)\delta/2 + \alpha^{l+1} d_0 < \alpha\delta/2 + \alpha^{l+1} d_0 . \tag{5.4}$$

Let N be such that $\alpha^N d_0 < (1-\alpha)\delta/2$. Then for $\forall r > s > N$ and for $t > t_0 + rt_1$,

$$\begin{aligned}
&\left\| \left(v_0(t) + v_r(t)\right) - \left(v_0(t) + v_s(t)\right) \right\|_X \\
&= \left\| \left(x_P(t) - v_0(t) - v_r(t)\right) - \left(x_P(t) - v_0(t) - v_s(t)\right) \right\|_X \\
&\le \left\| \left(x_P(t) - v_0(t) - v_r(t)\right) \right\|_X + \left\| \left(x_P(t) - v_0(t) - v_s(t)\right) \right\|_X \\
&\le \alpha\delta + \left(\alpha^{r+1} + \alpha^{s+1}\right) d_0 < \delta .
\end{aligned}$$

Since all v_i's are *T*-periodic functions, it is easy to see that

$$\left\| \left(v_0(t) + v_r(t)\right) - \left(v_0(t) + v_s(t)\right) \right\|_X < \delta, \ \forall t \ge 0, \forall r, s > N .$$

Let this Cauchy sequence of *T*-periodic functions $\{v_0 + v_k\}$ converge to $\hat{x}_P$ in $C_B\left([0,\infty) \to X\right)$. It is easy to check that $\hat{x}_P$ is also *T*-periodic. Now given $\lambda > 0$, let J and k be such that $\alpha^J d_0 < (1-\alpha)\lambda/2$, $k > J$ and $\left\| \hat{x}_P(t) - v_0(t) - v_k(t) \right\|_{X,\infty} < \lambda/2$. Deriving Eq. (5.4) with λ instead of δ, it follows that $\forall t > \hat{t}$ with $\hat{t}$ sufficiently large

$$\begin{aligned}
\left\| x_P(t) - \hat{x}_P(t) \right\|_X &< \left\| x_P(t) - v_0(t) - v_k(t) \right\|_X + \left\| \hat{x}_P(t) - v_0(t) - v_k(t) \right\|_X \\
&\le \alpha\lambda/2 + \alpha^{k+1} d_0 + \lambda/2 < \lambda
\end{aligned}$$

$$\Rightarrow \left\| x_P\left[\hat{t},\infty\right) - \hat{x}_P\left[\hat{t},\infty\right) \right\|_{X,\infty} < \lambda . \ \square$$

Remark 3: From Lemma 8, for a T-periodic sinusoidal excitation and ε small, Eq. (5.1) has a unique continuous state $x_P(t)$ satisfying Eq. (5.2) such that $\lim_{t\to\infty}\left\|\hat{x}_P(t)-x_P(t)\right\|_X=0$, where $\hat{x}_P(t)$ is a T-periodic function. Furthermore, a careful study of the proof reveals that for a fixed $0<\delta<1$, a $\bar{t}$ can be found such that $\forall t>n^2\bar{t}$, $\left\|\hat{x}_P(t)-x_P(t)\right\|_X<\delta^n$ for every integer $n>0$. Hence it follows that $\hat{x}_P(t)-x_P(t)\in L^2\left((0,\infty],X\right)$.

If $C_P\in\mathcal{L}(X,Y)$ in Eq. (5.1), it follows from Lemma 8 that $y_P(t)$ is continuous and tends to a *T*-periodic function asymptotically. But when $C_P\in\mathcal{L}(X_1,Y)$, as is the case for a general RLS, Lemma 9 clarifies the behavior of $y_P(t)$.

Lemma 9: Let the assumptions in Lemma 8 hold. Then the output $y_P(t)$ of Eq. (5.1) can be written as $y_{l,P}(t)+y_{nl,P}(t)+y_{0,P}(t)$ where $y_{l,P}$ and $y_{l,P}+y_{nl,P}$ are the T-periodic components of the output in the absence and presence of the nonlinearity, respectively and $y_{0,P}\in L^2\left((0,\infty],Y\right)$.

Proof: From Remark 3 and Assumptions 1-3, since $x_P(t)$ is known and bounded, the NPRLS Eq. (5.1) can be regarded as a RLS with 2 inputs, u and $\varepsilon g(x_P)$. Let *n* satisfy $\left\|\mathbb{T}(nT)\right\|_{\mathcal{L}(X)}<1$. Consider the system

$$\begin{aligned}&\dot{\bar{x}}_P=A_P\bar{x}_P+B_Pu+\varepsilon g(\hat{x}_P),\qquad \bar{x}_P(0)=\left(I-\mathbb{T}(nT)\right)^{-1}\left(\Phi_{nT}u+\Phi_{nT}^{g}\varepsilon g(\hat{x}_P)\right),\\&\bar{y}_P=C_{P,\Lambda}\bar{x}_P+D_Pu.\end{aligned}\tag{5.5}$$

Since the inputs to this system are *T*-periodic, with the chosen initial conditions (as in finite dimensions), $\bar{x}_P$ is a *T*-periodic continuous function. From the output equation, which is valid a.e. in time it follows that $\bar{y}_P$ is periodic a.e. and by linearity can be written as $\bar{y}_P = y_{l,P} + y_{nl,P}$ to distinguish the contribution of the 2 inputs: u and $\varepsilon g(\hat{x}_P)$. Equations (5.1) and (5.5) differ in the initial conditions and the second input. But the difference in the second input is in $L^2((0,\infty],X)$ since $\|g(\hat{x}_P)-g(x_P)\|_X \le L_0\|\hat{x}_P - x_P\|_X$. (use Remark 3, $\|\hat{x}_P\|_{X,\infty} \le d_0$, $\|x_P\|_{X,\infty} \le d_0$). From the properties of exponentially stable RLS the difference in the outputs in Eqs. (5.1) and (5.5), $y_{0,P} = y_P - \bar{y}_P$, must satisfy $y_{0,P} \in L^2((0,\infty],Y)$. Clearly, the L^2-norm over one period for $\varepsilon g(\hat{x}_P)$ and consequently for $y_{nl,P}$ is proportional to ε. □

5.3 Rejection of sinusoid from NPRLS

In the present section, the input and output take values in $\mathbb{R}$, i.e. $U = Y = \mathbb{R}$. For all TFs $G(s)$ and $\forall \tau \in \mathbb{R}$, it is assumed that $G(-j\tau)$ is the complex conjugate of $G(j\tau)$. In Lemmas 8 and 9, if u is a sinusoid of period *T*, then using the theory of TFs for RLS [32], $y_{l,P}$, the *T*-periodic component of the output in the absence of the nonlinearity, can be shown to be a sinusoid. In Theorem 5 the controller designed in Theorem 3 of Chapter 4, to ensure tracking of a reference sinusoid by RLS, is applied to the NPRLS in Eq. (5.1) to address the problem statement in Chapter 2. Theorem 5 is a generalization of Theorem 2 to infinite dimensional systems.

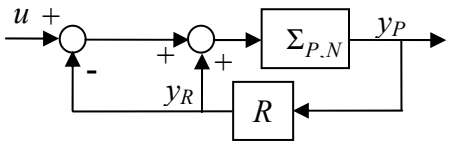

Figure 5.1: Unaugmented system

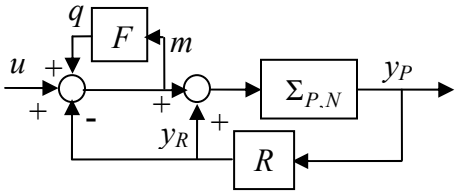

Figure 5.2: Augmented system

Theorem 5: Consider the RLS Σ_P *and the NPRLS* $\Sigma_{P,N}$ *in Eq. (5.1) satisfying Assumptions 1-3. The unaugmented system shown in Figure 5.1 is a cascade interconnection (the feedbacks cancel out) of* $\Sigma_{P,N}$ *and a stable s-dimensional SISO filter R:*

$$\dot{x}_R = A_R x_R + B_R u_R,$$
$$y_R = C_R x_R.$$

Also assume the following:

I1. The input u to $\Sigma_{P,N}$ *is a sinusoid of frequency* $\omega = 2\pi/T$ *and amplitude* C_u. *Let the initial condition* x_0 *satisfy* $\|x_0\|_X < C_0$. *By Lemma 9, for sufficiently small* ε, *the output* y_P *of Eq. (5.1) is a sum of a* L^2*-function and a T-periodic function.*

I2. Consistent with the problem statement, assume that $\Sigma_{P,N}$ *tracks the input sinusoid of frequency* ω *satisfactorily, but its output* y_P *contains small amplitude higher harmonics of* ω, *including* ω_r, *due to nonlinear effects.*

I3. If the input u to $\Sigma_{P,N}$ is u_{ω_r}, a small amplitude sinusoid of frequency ω_r, the periodic component of the output y_P contains a sinusoid at ω_r (Lemma 9); let it be $S_{y_P,\omega_r}(t)$. Let the complex gain from u_{ω_r} to S_{y_P,ω_r}, $G_{P,N}(j\omega_r)$, be bounded away from zero.

Choose R so that its strictly proper TF, G_R, satisfies $\left|1-G_{P,N}(j\omega_r)G_R(j\omega_r)\right|<1$. In the augmented system (Figure 5.2), F is the linear stable SISO system with TF

$$G_F(s)=\frac{2\zeta\omega_r s}{s^2+2\zeta\omega_r s+\omega_r^2}, \tag{5.6}$$

with $0<\zeta\ll 1$, a parameter to be chosen. Let the GOs of F be $(A_F(\zeta),\zeta B_F,C_F,0)$ where $A_F(\zeta)$ is a linear function of ζ, and B_F and C_F are independent of ζ. Then, for small ε, $\exists\zeta^*:\forall\zeta\in(0,\zeta^*]$ the augmented system in Figure 5.2 with $\Sigma_{P,N}$ replaced by Σ_P is an exponentially stable RLS. Assuming that $(A_P,B_P,I,0)$ are the GOs of an RLS, $\exists\bar{\varepsilon}$ such that if $\varepsilon<\bar{\varepsilon}$ the augmented system in Figure 5.2, now with $\Sigma_{P,N}$, is stable for each $\zeta\in(0,\zeta^*]$ and tracks the input sinusoid of frequency ω akin to the unaugmented system and possibly contains small magnitude higher harmonics of ω generated by the nonlinear perturbation, but the harmonic at frequency ω_r is eliminated from its output.

Proof: Let $G_P(j\omega_r)$ be the TF gain of Σ_P at ω_r. From Lemma 9 $\left|G_P(j\omega_r)-G_{P,N}(j\omega_r)\right|$ is small for small ε, and hence $\left|1-G_P(j\omega_r)G_R(j\omega_r)\right|<1$. From Theorem 3 it follows that $\exists\zeta^*:\forall\zeta\in(0,\zeta^*]$, the augmented system in Figure 5.2 with $\Sigma_{P,N}$ replaced by Σ_P, denoted as $\Sigma_P^c(\zeta)$, is an exponentially stable RLS; the superscript *c* indicates 'closed loop'. The state space and GOs for $\Sigma_P^c(\zeta)$ are $X^c=X\times\mathbb{R}^s\times\mathbb{R}^2$ and $\left(A_P^c(\zeta),B_P^c(\zeta),C_P^c,D_P^c\right)$ respectively, with input u and output y_P where:

$$A_P^c = \begin{bmatrix} A_P & 0 & B_P C_F \\ B_R C_{P,\Lambda} & A_R & B_R D_P C_F \\ 0 & -\zeta B_F C_R & A_F(\zeta) + \zeta B_F C_F \end{bmatrix}, \; B_P^c = \begin{bmatrix} B_P \\ B_R D_P \\ \zeta B_F \end{bmatrix},$$

$$C_P^c = \begin{bmatrix} C_{P,\Lambda} & 0 & D_P C_F \end{bmatrix}, \quad D_P^c = \begin{bmatrix} D_P \end{bmatrix}.$$

Let A_P^c, generate the exponentially stable semigroup $\mathbb{T}^c(\zeta)$. Denote the augmented system in Figure 5.2 (now, with $\Sigma_{P,N}$) by $\Sigma_{P,N}^c$. Its differential equation representation is:

$$\begin{aligned} \dot{x} &= A_P^c x + B_P^c u + \varepsilon g^c(x), \quad x(0) = \hat{x}_0, \\ y_P^c &= C_{P,\Lambda}^c x + D_P^c u, \end{aligned} \tag{5.7}$$

where $x = [x_P, x_R, x_F]^T$, $\hat{x}_0 = [x_0, 0, 0]^T$, $C_{P,\Lambda}^c$ is the λ-extension of C_P^c and $g^c(x) = [g(x_P), 0, 0]^T$. From Lemmas 8 and 9, for each $\zeta \in (0, \zeta^*]$, $\exists \varepsilon(\zeta) : \forall \varepsilon < \varepsilon(\zeta)$, the NPRLS $\Sigma_{P,N}^c$ is stable and has a unique output that can be written as $y_P^c = y_{l,P}^c + y_{nl,P}^c + y_{0,P}^c$ where $y_{l,P}^c$, a sinusoid of frequency ω, and $y_{l,P}^c + y_{nl,P}^c$, a T-periodic function, are periodic components of the output of $\Sigma_{P,N}^c$ in the absence and presence of the nonlinearity, respectively and $y_{0,P}^c \in L^2([0,\infty), \mathbb{R})$. The L^2-norm over a period for $y_{nl,P}^c$ is small (proportional to ε). Comparing the TFs, from u to y_P, of $\Sigma_P(\zeta)$ and $\Sigma_P^c(\zeta)$ and noting that the gain of F at all frequencies away from ω_r (like ω) is small (proportional to ζ), it can be shown that $y_{l,P}^c - y_{l,P}$ is small, implying that the augmented system tracks the input sinusoid of frequency ω akin to the unaugmented system. The loop containing F in Figure 5.2 can be replaced by 1/(1-F), which has poles at $\pm j\omega_r$, with output $m = u - C_R x_R + C_F x_F$ and input $u - y_R$. Hence the presence of the harmonic at ω_r in $y_{nl,P}^c$ and so in y_R would lead to m becoming unbounded. Since this contradicts the fact that the states of the

stable NPRLS $\Sigma_{P,N}^{c}$ are bounded, $y_{nl,P}^{c}$ must have no harmonic at ω_r. The existence of a $\bar{\varepsilon}$ independent of ζ such that the augmented loop is stable for each $\zeta \in (0, \zeta^*]$ follows from Lemma 8 if both the effect of the initial condition and the integral $\int_0^t \mathbb{T}_{t-\tau}^{c} \varepsilon \left[g(x_P), 0, 0 \right]^T d\tau$ can be bounded independent of ζ. The latter is established in Lemma 10 in Section 5.4. The former can be established analogously. □

Theorem 5 addresses the rejection of a single sinusoid from the output of a NPRLS. Theorem 6 extends Theorem 5 to address the rejection of *n*-sinusoids. It is stated next without proof.

Theorem 6: Consider the RLS Σ_P, NPRLS $\Sigma_{P,N}$, ω, unaugmented system and R as in Theorem 5. Assume that I1 and I2 hold. For $i = 1,...,n$, let ω_i be an integer multiple of ω with S_{y_P,ω_i}, defined as in I3, bounded away from zero. Let

$$G_R(s) = \sum_{i=1}^{n} \frac{x_{2i-1} s + x_{2i}}{s^2 + \omega_i s + \omega_i^2}. \tag{5.8}$$

Choose x_j's for $j = 1,...,2n$ to satisfy $\left| 1 - G_{P,N}(j\omega_i) G_R(j\omega_i) \right| = 0$ for $i = 1,...,n$. In the augmented system (Figure 5.2), F is the linear stable SISO system with TF

$$G_F(s) = \frac{\prod_{i=1}^{n} \left(s^2 + 2\zeta_i \omega_i s + \omega_i^2 \right) - \prod_{i=1}^{n} \left(s^2 + \omega_i^2 \right)}{\prod_{i=1}^{n} \left(s^2 + 2\zeta_i \omega_i s + \omega_i^2 \right)}$$

with $0 < \zeta_i \ll 1$ for $i = 1,...,n$. There exists $\bar{\varepsilon}$ and ζ^* such that if $\varepsilon < \bar{\varepsilon}$ and $\zeta_i \in (0, \zeta^*]$ for $i = 1,...,n$, the augmented system in Figure 5.2 is stable and tracks the input sinusoid of frequency ω akin to the unaugmented system and possibly contains small magnitude higher harmonics of

ω generated by the nonlinear perturbation, but the harmonics at frequency ω_i, $i=1,...,n$, are eliminated from its output. □

5.4 Interaction between the control parameter and the nonlinearity

Lemma 10 proves the claim used in Theorem 5 that the response of the closed loop system to the nonlinearity treated as an exogenous input, can be bounded by a constant independent of the control parameter ζ.

Lemma 10: For $\zeta \in (0, \zeta^*]$ the exponentially stable closed loop semigroup, $\mathbb{T}_t^c(\zeta)$, in Theorem 5 is such that $\left\| \int_0^t \mathbb{T}_{t-\tau}^c(\zeta) \varepsilon \left[g(x_P), 0, 0 \right]^T d\tau \right\|_X < M^c$ where M^c depends on x_P but is independent of ζ.

Proof: Obtaining a bound for $\int_0^t \mathbb{T}_{t-\tau}^c \varepsilon \left[g(x_P), 0, 0 \right]^T d\tau$ is equivalent to obtaining a bound for $\int_0^t \mathbb{T}_{t-\tau}^c \left[v, 0, 0 \right]^T d\tau$ independent of the control parameter $\zeta \in (0, \zeta^*]$. This is completed in two steps by first considering the case when ζ is not near zero and then considering the case when ζ is near zero.

Step 1: The exponential stability of $\mathbb{T}_t^c(\zeta)$ ensures the existence of $M(\zeta) = 2 \sup_{t \geq 0} \left\| \mathbb{T}_t^c(\zeta) \right\|_{\mathcal{L}(X^c)}$ and $a(\zeta)$, the largest positive number such that $\left\| \mathbb{T}_t^c(\zeta) \right\|_{\mathcal{L}(X^c)} \leq M(\zeta) e^{-a(\zeta)t}$. For any $\zeta_1, \zeta_2 \in (0, \zeta^*]$, $A_P^c(\zeta_2) - A_P^c(\zeta_1) = (\zeta_2 - \zeta_1) A^\Delta$, where A^Δ is a bounded linear operator on X^c.

Hence from perturbation theory of C_0-semigroups [35], it follows that $M(\zeta)$ and $a(\zeta)$ are continuous positive functions of $\zeta \in (0, \zeta^*]$. Hence on any compact interval $[\zeta', \zeta^*]$, $\int_0^t \mathbb{T}_{t-\tau}^c [v,0,0]^T \, d\tau$ can be bounded by a constant independent of ζ. If a bound for $\int_0^t \mathbb{T}_{t-\tau}^c [v,0,0]^T \, d\tau$ can be found for ζ near zero, then the lemma is proven. This bound is found in step 2, next.

Step 2: In the given NPRLS $\Sigma_{P,N}$ in Eq. (5.1), using Assumption 3, the nonlinearity can be treated as an input, v. It follows that the extended system $\Sigma_{P,ext}$:

$$\begin{aligned} \dot{x}_P &= A_P x_P + B_P u + v, \qquad x_P(0) = x_0, \\ y_P &= C_{P,\Lambda} x_P + D_P u, \\ y &= x_P. \end{aligned}$$

is an exponentially stable RLS with two inputs and two outputs. Let the TF representation for $\Sigma_{P,ext}$ be given by the matrix

$$G_P = \begin{bmatrix} G_{11} & G_{12} \\ G_{21} & G_{22} \end{bmatrix}.$$

Consider the unaugmented in Figure 5.1 and the augmented system Figure 5.2, but with $\Sigma_{P,N}$ replaced by the RLS $\Sigma_{P,ext}$. The input-output representation corresponding to these systems is shown in Figure 5.3.

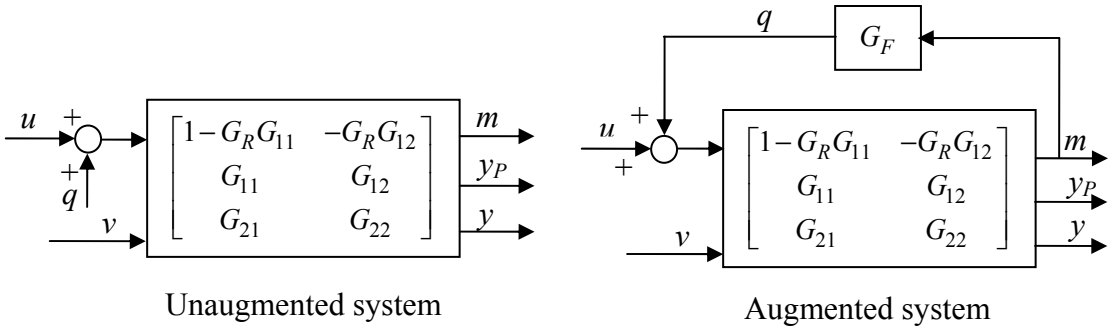

Figure 5.3: Input-output representation of the unaugmented and augmented systems with $\Sigma_{P,ext}$

Considering the inputs u and v and the outputs y_P and y the block diagram for the augmented system in Figure 5.3 can be simplified to obtain the input-output representation shown in Figure 5.4.

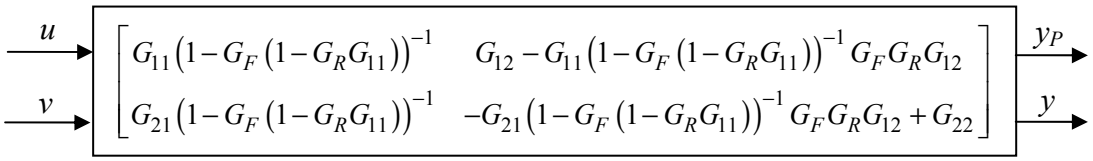

Figure 5.4: Simplified input-output representation of the augmented system with $\Sigma_{P,ext}$

If a bound for $\left[x_P(t), x_R(t), x_F(t)\right]^T = \int_0^t \mathbb{T}_{t-\tau}^c \left[v, 0, 0\right]^T d\tau$ can be found for ζ near zero, then the lemma is proven. A bound for $x_P(t)$ is provided below. Bounds for $x_R(t)$ and $x_F(t)$ can be obtained similarly. From the input-output representation of the augmented system, finding a bound for $x_P(t)$ for ζ near zero is equivalent to showing that for sufficiently small ζ the linear system corresponding to the TF $\left(-G_{21}\left(1-G_F\left(1-G_RG_{11}\right)\right)^{-1}G_FG_RG_{12}+G_{22}\right)$ is BIBO stable with BIBO gain independent of ζ. This is accomplished in the rest of the proof. It is assumed that

$\left|1-G_R(j\omega_r)G_{11}(j\omega_r)\right|=0$, although Theorem 5 requires $\left|1-G_R(j\omega_r)G_{11}(j\omega_r)\right|<1$. This simplifies the presentation of the arguments, which can be applied in the absence of this assumption as well. Since $\left(1-G_F\left(1-G_RG_{11}\right)\right)^{-1}$ is a scalar function it commutes with other scalar functions and it follows that

$$-G_{21}\left(1-G_F\left(1-G_RG_{11}\right)\right)^{-1}G_FG_RG_{12}+G_{22}=-\left(1-G_F\left(1-G_RG_{11}\right)\right)^{-1}G_{21}G_FG_RG_{12}+G_{22}. \qquad (5.9)$$

Note that an exponentially stable RLS with bounded output operator is BIBO stable. Since the output operators of G_{21} and G_{22} is identity and the output operator of $G_FG_RG_{12}$ is the same as the output operator of G_FG_R which is bounded, all these systems are BIBO stable. Hence $G_{21}G_FG_RG_{12}$ is a BIBO stable system with BIBO gain independent of ζ, for small ζ. This property will next be shown to hold for $\left(1-G_F\left(1-G_RG_{11}\right)\right)^{-1}$. G_{11} is a scalar analytic function on some right half complex plane. Let $1-G_RG_{11}=G$. Then

$$\left(1-G_F\left(1-G_RG_{11}\right)\right)^{-1}=1+\frac{2\zeta\omega_r sG}{\left(s^2+2\zeta\omega_r s+\omega_r^2-2\zeta\omega_r sG\right)}.$$

$\left(s^2+\omega_r^2\right)$ has two zeros at $\pm j\omega_r$. For a fixed $\delta>0$, on the boundary of vertical strip of width 2δ centered about the imaginary axis $\left|s^2+\omega_r^2\right|>\left|2\zeta\omega_r s(1-G)\right|$ for sufficiently small ζ. Hence using Rouché's theorem $\left(s^2+2\zeta\omega_r s+\omega_r^2-2\zeta\omega_r sG\right)$ also has only two zeros, β and $\bar{\beta}$, in this vertical strip; furthermore again from Rouché's theorem these zeros converge to $\pm j\omega_r$ as $\zeta\to 0$. From the stability of $2\zeta\omega_r sG\Big/\left(s^2+2\zeta\omega_r s+\omega_r^2-2\zeta\omega_r sG\right)$ established in Theorem 5, β and $\bar{\beta}$ are in the left half complex plane and are the only zeros of $\left(s^2+2\zeta\omega_r s+\omega_r^2-2\zeta\omega_r sG\right)$ in a right half plane strictly containing the imaginary axis.

Consider the domain $D_1 = \{s \in \mathbb{C}: |\mathrm{Re}(s - j\omega_r)| < \gamma\zeta, |\mathrm{Im}(s - j\omega_r)| < \lambda\}$ where γ and λ are chosen to satisfy $\gamma\lambda < \omega_r^2/8$, $\gamma < \omega_r/16$, $\lambda < \omega_r/16$ and for $s \in D_1$, $G(s) < 1/16$. This is possible since $G(\pm j\omega_r) = 0$. Then for $s = j\omega_r + \alpha \in D_1$ and ζ sufficiently small, $|s^2 + 2\zeta\omega_r s + \omega_r^2|$ = $|(j\omega_r + \alpha)^2 + 2\zeta\omega_r(j\omega_r + \alpha) + \omega_r^2|$ = $|\alpha(2j\omega_r + \alpha + 2\zeta\omega_r) + j2\zeta\omega_r^2|$ $> \zeta\omega_r^2$. Also $|2\zeta\omega_r sG|$ = $|2\zeta\omega_r(j\omega_r + \alpha)G|$ $< \zeta\omega_r^2/2$. Hence $(s^2 + 2\zeta\omega_r s + \omega_r^2 - 2\zeta\omega_r sG)$ does not have any zero in D_1. But for ζ sufficiently small, $(s^2 + 2\zeta\omega_r s + \omega_r^2 - 2\zeta\omega_r sG)$ has a zero in $D_2 = \{s \in \mathbb{C}: |\mathrm{Re}(s - j\omega_r)| < \lambda, |\mathrm{Im}(s - j\omega_r)| < \lambda\}$. This establishes that the rate of convergence of β and $\bar{\beta}$ to $\pm j\omega_r$ is either proportional to ζ or slower.

Let r be the residue of $sG/(s^2 + 2\zeta\omega_r s + \omega_r^2 - 2\zeta\omega_r sG)$ at β. Then r $= \beta G(\beta)/(2\beta + 2\zeta\omega_r - 2\zeta\omega_r G(\beta) - 2\zeta\omega_r \beta G'(\beta))$. Since $\beta \to j\omega_r$, as $\zeta \to 0$, it follows that r is uniformly bounded for small ζ. Hence,

$$\frac{2\zeta\omega_r sG(s)}{(s^2 + 2\zeta\omega_r s + \omega_r^2 - 2\zeta\omega_r sG)} = 2\zeta\omega_r\left(\frac{r}{s-\beta} + \frac{\bar{r}}{s-\bar{\beta}}\right) + H(s),$$

where $H(s)$ is a scalar valued analytic function bounded on a right half plane which is independent of ζ, strictly including the imaginary axis. Now the system $2\zeta\omega_r\left(\frac{r}{s-\beta} + \frac{\bar{r}}{s-\bar{\beta}}\right)$ is a stable finite dimensional system with BIBO gain independent of ζ since $\beta \in D_2$ and $\beta \notin D_1$. Next $H(s)$ is shown to be a BIBO system. For some $\rho > 0$, on a fixed vertical line *L* which is to the left of the imaginary axis by ρ, the functions $2\zeta\omega_r sG/(s^2 + 2\zeta\omega_r s + \omega_r^2 - 2\zeta\omega_r sG)$ and

$2\zeta\omega_r\left(\frac{r}{s-\beta}+\frac{\overline{r}}{s-\overline{\beta}}\right)$ are in L^2 and as $\zeta\to 0$, the L^2 norm of these functions on L goes to zero. Hence the same must hold for $H(s)$ on L. In addition $H(s)$ is analytic to the right of L for ρ small. Let $H(s)$ correspond to the function $h(t)$. Then $e^{\rho t}h(t)$ corresponds to $H(s-\rho)$. But restricted to the imaginary axis, $H(s-\rho)$ is in L^2 with norm uniformly bounded in ζ and hence the same holds for $e^{\rho t}h(t)$. The BIBO gain of $H(s)$ can be bounded as follows:

$$\int_0^\infty |h(\tau)|\,d\tau=\int_0^\infty e^{-\rho\tau}\left|e^{\rho\tau}h(t-\tau)\right|d\tau\le\int_0^\infty\left|e^{\rho\tau}h(\tau)\right|^2 d\tau\int_0^\infty e^{-2\rho\tau}d\tau\le C\,.$$

The constant $C\to 0$ as $\zeta\to 0$. Hence it follows that $\left(1-G_F\left(1-G_RG_{11}\right)\right)^{-1}$ is BIBO stable with BIBO gain independent of ζ, for small ζ and that the same holds for the TF in Eq. (5.9) from the above arguments. Hence the lemma is proved. □

In this chapter a control scheme for rejecting an internally generated sinusoid from the output of a plant belonging to the class of NPRLS was presented. In Chapter 6 the testbed model will be classified as a NPRLS thereby justifying the application of the proposed scheme to the testbed to eliminate distortions in the mold displacement profile.

CHAPTER 6

CLASSIFICATION OF THE TESTBED MODEL AS A NONLINEARLY PERTURBED REGULAR LINEAR SYSTEM

The problem of eliminating distortions from the mold displacement profile of the testbed was formulated in Chapter 2, based on the testbed model, as periodic disturbance rejection from a nonlinearly perturbed infinite dimensional system. In Chapter 5 the class of nonlinearly perturbed regular linear systems (NPRLS) was introduced and a control scheme for rejecting sinusoids from plants belonging to this class was proposed. In the present chapter the testbed model, under reasonable assumptions, will be related to the NPRLS class, thereby justifying the application of the proposed control scheme to eliminate distortions from the displacement profile of mold in the testbed. Specifically, the state operator of the linearized testbed model will be shown to be the generator of a C_0-semigroup which guarantees the wellposendess of the linearized equations. The exponential stability of the semigroup is justified under reasonable assumptions. Making these assumptions rigorous is an open problem and is a subject for future research. Some analysis tools that can help in this regard are used in Appendix A to show that a beam model, closely related to the testbed model, is exponentially stable. Finally by verifying the assumptions on the input and output operators and on the nonlinearity, the testbed model is classified as a NPRLS.

6.1 Modified testbed model

A detailed model for the testbed was presented in Chapter 2. The main equations of the model, with relevant modifications, are presented next. The testbed consists of a long flexible structure hinged in the middle, carrying an end mass (mold) at one end and excited by an electro-hydraulic actuator at the other end (Figure 6.1). The flexible structure is treated as two beams, each of length *l*, attached at the hinge. Each beam is modeled using the Timoshenko equation which is a set of two coupled linear partial differential equations (PDEs). The coordinate along the length of the beams is x (hinge is at $x=0$) and the vertical and the angular displacements to the left and to the right of the hinge are denoted by (y_L,ψ_L) and (y_R,ψ_R), respectively. Thus, the model of the beam is given by the PDE system

$$m_b\frac{\partial^2 y_L}{\partial t^2}+\gamma_y\frac{\partial y_L}{\partial t}=\frac{\partial}{\partial x}\left(k'Ga_b\left(\frac{\partial y_L}{\partial x}-\psi_L\right)\right)-m_b g\,,$$

$$\frac{I}{a_b}m_b\frac{\partial^2 \psi_L}{\partial t^2}+\gamma_\psi\frac{\partial \psi_L}{\partial t}=\frac{\partial}{\partial x}\left(EI\frac{\partial \psi_L}{\partial x}\right)+k'Ga_b\left(\frac{\partial y_L}{\partial x}-\psi_L\right),$$

$$m_b\frac{\partial^2 y_R}{\partial t^2}+\gamma_y\frac{\partial y_R}{\partial t}=\frac{\partial}{\partial x}\left(k'Ga_b\left(\frac{\partial y_R}{\partial x}-\psi_R\right)\right)-m_b g\,,$$

$$\frac{I}{a_b}m_b\frac{\partial^2 \psi_R}{\partial t^2}+\gamma_\psi\frac{\partial \psi_R}{\partial t}=\frac{\partial}{\partial x}\left(EI\frac{\partial \psi_R}{\partial x}\right)+k'Ga_b\left(\frac{\partial y_R}{\partial x}-\psi_R\right).$$

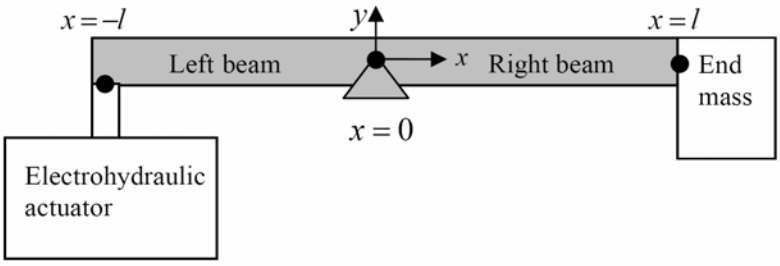

Figure 6.1: Simplified schematic of the testbed

The end mass (mold) dynamics is modeled using a linear ordinary differential equation (ODE). The actuator dynamics is assumed to be modeled by a system of nonlinearly perturbed stable linear ODEs owing to its stable predominantly linear response as discussed in Chapter 2. Furthermore, as discussed in Section 6.4, the nonlinearity can be justified to be a Lipschitz function. The actuator dynamics Eq. (6.1) and mold dynamics Eq. (6.2) are part of the boundary conditions of the beam. The boundary conditions are:

$$\begin{bmatrix} \dfrac{\partial y_L(-l)}{\partial t} \\ \dfrac{\partial^2 y_L(-l)}{\partial t^2} \\ \dfrac{\partial x_a}{\partial t} \end{bmatrix} = V \begin{bmatrix} y_L(-l) \\ \dfrac{\partial y_L(-l)}{\partial t} \\ x_a \end{bmatrix} + \begin{bmatrix} 0 \\ \dfrac{k'Ga_b}{m_p}\left(\dfrac{\partial y_L(-l)}{\partial x} - \psi_L(-l)\right) - g \\ 0 \end{bmatrix} + Bu + \varepsilon N\left(y_L(-l), \frac{\partial y_L(-l)}{\partial t}, x_a\right), \tag{6.1}$$

$$k'Ga_b\left(\frac{\partial y_R(l)}{\partial x} - \psi_R(l)\right) + Mg + M\frac{\partial^2 y_R(l)}{\partial t^2} + \gamma_M \frac{\partial y_R(l)}{\partial t} = 0, \tag{6.2}$$

$$y_L(0) = y_R(0) = 0,\ \frac{\partial \psi_L(-l)}{\partial x} = \frac{\partial \psi_R(l)}{\partial x} = 0,\ \psi_L(0) = \psi_R(0),\ \frac{\partial \psi_L(0)}{\partial x} = \frac{\partial \psi_R(0)}{\partial x}.$$

In the equations x_a, V, N, ε, B and u stand for additional *d*-dimensional actuator states, a Hurwitz matrix, the Lipschitz nonlinear term, a small constant, input matrix and scalar input signal, respectively. The other parameters in the equations are as defined in Chapter 2.

For simplicity of notation, the derivative with respect to the space and time variables will henceforth be denoted with subscripts x and t, respectively. Also let $k'Ga_b/m_b = \alpha$, $Ea_b/m_b = \beta$, $k'Ga_b^2/m_b I = \alpha\alpha_1$, $k'Ga_b/M = \alpha\alpha_2$, $\gamma_y/m_b = d_1$, $k'Ga_b/m_p = \hat{\alpha}$, $\gamma_\psi a_b/m_b I = d_2$,

$\gamma_M / M = d_3$. Define the spaces $L_l^2 = L^2(-l,0)$, $L_r^2 = L^2(0,l)$, $H_l^n = H^n(-l,0)$, $H_r^n = H^n(0,l)$, $H_{l,0}^n = \{f : f \in H^n(-l,0), f(0) = 0\}$ and $H_{r,0}^n = \{f : f \in H^n(0,l), f(0) = 0\}$. Consider the space

$$Z = \left\{ \begin{array}{l} (a_1, a_2, a_3, f_1, f_2, f_3, f_4, f_5, f_6, f_7, f_8, a_4) \in \mathbb{R} \times \mathbb{R} \times \mathbb{R}^d \times H_{l,0}^1 \times L_l^2 \times H_l^1 \times L_l^2 \times H_{r,0}^1 \times L_r^2 \times H_r^1 \times L_r^2 \times \mathbb{R} \\ \text{with } \; a_1 = f_1(-l), f_3(0) = f_7(0) \end{array} \right\}.$$

Henceforth z_1 and z_2 will be generically used to represent elements of Z with their components being $(a_1, a_2, a_3, f_1, f_2, f_3, f_4, f_5, f_6, f_7, f_8, a_4)$ and $(b_1, b_2, b_3, g_1, g_2, g_3, g_4, g_5, g_6, g_7, g_8, b_4)$, respectively. The inner product on Z is defined as

$$\begin{aligned} \langle z_1, z_2 \rangle_Z = a_1 b_1 + \frac{\alpha}{\hat{\alpha}} a_2 b_2 + a_3^T b_3 + \alpha \int_{-l}^{0} f_{1,x} g_{1,x} \mathrm{dx} + \int_{-l}^{0} f_2 g_2 \mathrm{dx} + \int_{-l}^{0} f_3 g_3 \mathrm{dx} + \beta \int_{-l}^{0} f_{3,x} g_{3,x} \mathrm{dx} + \int_{-l}^{0} f_4 g_4 \mathrm{dx} \\ + \alpha \int_{0}^{l} f_{5,x} g_{5,x} \mathrm{dx} + \int_{0}^{l} f_6 g_6 \mathrm{dx} + \int_{0}^{l} f_7 g_7 \mathrm{dx} + \beta \int_{0}^{l} f_{7,x} g_{7,x} \mathrm{dx} + \int_{0}^{l} f_8 g_8 \mathrm{dx} + \frac{1}{\alpha_2} a_4 b_4. \end{aligned}$$

The inner product induces a norm on Z. The completion of Z with respect to this norm follows using the fact that the H^1-norm of a function on $(-l,0)$ dominates its infinity norm.

The linearization of the testbed model is obtained by dropping the nonlinear term N from the actuator dynamics, Eq. (6.1). The resulting evolution equation on Z is

$$z_t = Az + F \tag{6.3}$$

where $z = \left(y_l(-l), y_{l,t}(-l), x_a, y_l, y_{l,t}, \psi_l, \psi_{l,t}, y_r, y_{r,t}, \psi_r, \psi_{r,t}, y_{r,t}(l)\right)$, F stands for all the external forces and the operator A is as defined next. The domain of the operator A, $D(A)$, is given by

$$D(A) = \left\{ \begin{array}{l} z_1 \in \mathbb{R} \times \mathbb{R} \times \mathbb{R}^d \times H_{l,0}^2 \times H_{l,0}^1 \times H_l^2 \times H_l^1 \times H_{r,0}^2 \times H_{r,0}^1 \times H_r^2 \times H_r^1 \times \mathbb{R} \text{ and} \\ a_1 = f_1(-l), \, a_2 = f_2(-l), f_{3,x}(-l) = 0, f_3(0) = f_7(0), f_{3,x}(0) = f_{7,x}(0), \\ f_{7,x}(l) = 0, \, f_4(0) = f_8(0), a_4 = f_6(l). \end{array} \right\}$$

The density of $D(A)$ in Z follows from the usual arguments using infinitely differentiable functions and Sobolev embedding. If $z_1 \in D(A)$ and $z_2 = Az_1$ then,

$$g_1 = f_2,\ g_2 = \alpha f_{1,xx} - d_1 f_2 - \alpha f_{3,x},$$

$$g_3 = f_4,\ g_4 = \alpha\alpha_1 \left(f_{1,x} - f_3\right) + \beta f_{3,xx} - d_2 f_4,$$

$$g_5 = f_6,\ g_6 = \alpha f_{5,xx} - d_1 f_6 - \alpha f_{7,x},$$

$$g_7 = f_8,\ g_8 = \alpha\alpha_1 \left(f_{5,x} - f_7\right) + \beta f_{7,xx} - d_2 f_8,$$

$$\left[b_1, b_2, b_3\right]^T = V\left[a_1, a_2, a_3\right]^T + \left[0, \hat{\alpha}\left(f_{1,x}(-l) - f_3(-l)\right), 0\right]^T \text{ and}$$

$$b_4 = \alpha\alpha_2 \left(f_7(l) - f_{5,x}(l)\right) - d_3 a_4.$$

6.2 Wellposedness of the linearized testbed model

In this section, the state operator associated with the linearization of the testbed model is shown to be a bounded perturbation of an *m*-dissipative operator and hence the infinitesimal generator of a C_0-semigroup. Define the operator A_0 on Z with $D(A_0) = D(A)$ such that if $z_2 = A_0 z_1$ where $z_1 \in D(A)$, then the components of z_2 satisfy: $b_1 = a_2$, $b_2 = -a_1\hat{\alpha}/\alpha + \hat{\alpha} f_{1,x}(-l)$, $b_3 = 0$, $g_1 = f_2$, $g_2 = \alpha f_{1,xx}$, $g_3 = f_4$, $g_4 = \beta f_{3,xx} - f_3$, $g_5 = f_6$, $g_6 = \alpha f_{5,xx}$, $g_7 = f_8$, $g_8 = \beta f_{7,xx} - f_7$, and $b_4 = -\alpha\alpha_2 f_{5,x}(l)$.

Lemma 11: The operator A_0 is dissipative.

Proof: Let $z_1 \in D(A)$. Then using the definition of A_0,

$$\begin{aligned}\left\langle A_0 z_1, z_1 \right\rangle_Z = a_1 a_2 - a_1 a_2 + \alpha f_{1,x}(-l) a_2 + \alpha \int_{-l}^{0} f_{1,x} f_{2,x} \mathrm{dx} + \alpha \int_{-l}^{0} f_{1,xx} f_2 \mathrm{dx} - \int_{-l}^{0} f_3 f_4 \mathrm{dx} + \int_{-l}^{0} f_3 f_4 \mathrm{dx} \\ + \beta \int_{-l}^{0} f_{3,x} f_{4,x} \mathrm{dx} + \beta \int_{-l}^{0} f_{3,xx} f_4 \mathrm{dx} + \alpha \int_{0}^{l} f_{5,x} f_{6,x} \mathrm{dx} + \alpha \int_{0}^{l} f_{5,xx} f_6 \mathrm{dx} - \int_{0}^{l} f_7 f_8 \mathrm{dx} + \int_{0}^{l} f_7 f_8 \mathrm{dx} \\ + \beta \int_{0}^{l} f_{7,x} f_{8,x} \mathrm{dx} + \beta \int_{0}^{l} f_{7,xx} f_8 \mathrm{dx} - \alpha f_{5,x}(l) a_4 .\end{aligned}$$

Simplifying this expression via integration by parts and using the boundary conditions in the definition of $D(A)$, it follows that $\left\langle A_0 z_1, z_1 \right\rangle_Z = 0$. Hence A_0 is dissipative. □

Lemma 12: Fix $\lambda > 0$. For each $z_1 \in Z$, there exists $z_2 \in D(A)$ such that $\lambda z_2 - A_0 z_2 = z_1$.

Proof: Given the components f_3, f_4, f_7 and f_8 of z_1, the components g_3, g_4, g_7 and g_8 of z_2 must satisfy the equations:

$$\begin{aligned}&\lambda g_3(x) - g_4(x) = f_3(x), x \in (-l, 0), \\ &g_3(x) - \beta g_{3,xx}(x) + \lambda g_4(x) = f_4(x), x \in (-l, 0), \\ &\lambda g_7(x) - g_8(x) = f_7(x), x \in (0, l), \\ &g_7(x) - \beta g_{7,xx}(x) + \lambda g_8(x) = f_8(x), x \in (0, l), \\ &(g_3, g_4, g_7, g_8) \in H_l^2 \times H_l^1 \times H_r^2 \times H_r^1, g_4(0) = g_8(0), \\ &g_3(0) = g_7(0), g_{3,x}(0) = g_{7,x}(0), g_{3,x}(-l) = g_{7,x}(l) = 0.\end{aligned}$$

Finding the solution g_3, g_4, g_7 and g_8 to this set of equations is equivalent to finding p_1 and p_2 satisfying

$$\begin{aligned}&\lambda p_1(x) - p_2(x) = q_1(x), \ x \in (-l, l), \\ &p_1(x) - \beta p_{1,xx}(x) + \lambda p_2(x) = q_2(x), \ x \in (-l, l), \\ &p_1 \in H^2(-l, l), p_2 \in H^1(-l, l), p_{1,x}(l) = p_{1,x}(-l) = 0,\end{aligned} \tag{6.4}$$

where q_1 (or q_2) is the function on $(-l,l)$ obtained by concatenating functions f_3 and f_7 (or f_4, and f_8).

Let $\mu^2 = \left(\lambda^2+1\right)\big/\beta$. Eliminating p_2 in Eq. (6.4), p_1 must satisfy

$$p_{1,xx}(x) = \mu^2 p_1(x) - \left(\lambda q_1(x) + q_2(x)\right)\big/\beta,\ p_1 \in H^2(-l,l),\ p_{1,x}(l) = p_{1,x}(-l) = 0.$$

The solution to this ODE in terms of the free parameter C is

$$p_1(x) = C\cosh\left(\mu(x+l)\right) - \int_{-l}^{x} \frac{\sinh\left(\mu(x-s)\right)}{\mu}\frac{\lambda q_1(s) + q_2(s)}{\beta}\mathrm{ds}.$$

The derivative is given by the expression

$$p_{1,x} = C\mu\sinh\left(\mu(x+l)\right) - \int_{-l}^{x} \cosh\left(\mu(x-s)\right)\frac{\lambda q_1(s) + q_2(s)}{\beta}\mathrm{ds}.$$

Clearly $p_{1,x}(-l) = 0$. Using $p_{1,x}(l) = 0$, C is computed. From the expression for $p_{1,x}$, it follows that $p_1 \in H^2(-l,l)$. Using Eq. (6.4) $p_2 \in H^1(-l,l)$ can then be obtained. g_3, g_4, g_7 and g_8 are obtained as suitable restrictions of p_1 and p_2 to $(-l,0)$ and $(0,l)$.

Next, given the components f_1, f_2, a_1, a_2 and a_3 of z_1, consider the set of equations

$$\begin{aligned}
&\lambda g_1(x) - g_2(x) = f_1(x),\ \ x \in (-l,0),\\
&-\alpha g_{1,xx}(x) + \lambda g_2(x) = f_2(x), x \in (-l,0),\ \ g_1 \in H^2_{l,0},\ \ g_2 \in H^1_{l,0},\\
&\lambda b_1 - b_2 = a_1, -\hat{\alpha} g_{1,x}(-l) + \lambda g_2(-l) + \hat{\alpha} g_1(-l)\big/\alpha = a_2,\\
&\lambda b_3 = a_3,\ g_1(-l) = b_1, g_2(-l) = b_2.
\end{aligned}$$

By substitution g_1 satisfies $\lambda^2 g_1 - \alpha g_{1,xx} = \lambda f_1 + f_2$. With $\mu = \lambda/\sqrt{\alpha}$, g_1 is given in terms of the free parameters C_1 and C_2 by the expression

$$g_1(x) = C_1\cosh(\mu x) + \frac{C_2}{\mu}\sinh(\mu x) - \int_{-l}^{x} \frac{\sinh\left(\mu(x-s)\right)}{\alpha\mu}\left(\lambda f_1(s) + f_2(s)\right)\mathrm{ds}\,.$$

$g_1(0)=0$ gives C_1. Since $g_1, g_2, f_1 \in H^1(-l,0)$, they are continuous on the closed interval $[-l,0]$. Hence using $\lambda g_1(x)-g_2(x)=f_1(x)$, $g_2(-l)=\lambda g_1(-l)-f_1(-l)$ holds.

Combined with $-\hat{\alpha}g_{1,x}(-l)+\lambda g_2(-l)+\hat{\alpha}g_1(-l)/\alpha=a_2$, C_2 can be found. Let $g_2=\lambda g_1-f_1$. b_1, b_2 and b_3 can be computed directly. From the expression for $g_{1,x}$ it can be shown that $g_1 \in H^2_{l,0}$ and it implies that $g_2 \in H^1_{l,0}$.

Finally given the components f_5, f_6 and a_4 of z_1, consider the set of equations

$$\begin{aligned}
&\lambda g_5(x)-g_6(x)=f_5(x), \quad x\in(0,l),\\
&-\alpha g_{5,xx}(x)+\lambda g_6(x)=f_6(x), \quad x\in(0,l), \quad g_5\in H^2_{r,0}, \quad g_6\in H^1_{r,0},\\
&\alpha\alpha_2 g_{5,x}(l)+\lambda b_4=a_4, b_4=g_6(l).
\end{aligned}$$

As before with $\mu=\lambda/\sqrt{\alpha}$

$$g_5(x)=C\sinh(\mu x)-\int_0^x \frac{\sinh\left(\mu(x-s)\right)}{\alpha\mu}\left(\lambda f_5(s)+f_6(s)\right)\mathrm{ds}.$$

Clearly $g_5(0)=0$. Again using $g_6(l)=\lambda g_5(l)-f_5(l)$ and $\alpha\alpha_2 g_{5,x}(l)+\lambda g_6(l)=a_4$, C can be calculated. Letting $b_4=g_6(l)$, the solution to above set of equations is obtained. Again from the expression for $g_{5,x}$ it can be shown that $g_5 \in H^2_{r,0}$ and it implies that $g_6 \in H^1_{r,0}$.

Hence all the components of z_2 are obtained where z_2 satisfies, $\lambda z_2 - A_0 z_2 = z_1$. □

Theorem 7: A is the infinitesimal generator of a C_0-semigroup, $S(t)$, on Z.

Proof: As mentioned earlier, $D(A)$ is dense in Z. From Lemmas 11 and 12, A_0 is an *m*-dissipative operator. Therefore, by Lumer-Phillips theorem [35], A_0 is the infinitesimal generator of a C_0-semigroup on Z. Note that $A=A_0+\hat{A}$ where the operator $\hat{A}$ can be shown to be

bounded on Z using Sobolev embeddings. Since A_0 generates a C_0-semigroup on Z, so does A [35]. □

6.3 Exponential stability of the semigroup

Asymptotic stability of a single Timoshenko beam under boundary control and distributed control has been addressed in [37]-[42] and [42]-[45], respectively. Stabilization of a network of Timoshenko beams has been addressed in [46], [47]. These papers consider simple boundary conditions (except [38], [39]). Considering a single Timoshenko beam, [38] and [39] account for the presence of a pair of actuators (with constraints) and an end mass, respectively, at the boundary. In contrast to these works, the linearized testbed model in the present work is a network of two damped Timoshenko beams with dynamic boundary conditions given by the end mass dynamics and linearized actuator dynamics. It is unreasonable to expect that the exponential stability of the semigroup, $S(t)$, associated with the testbed model can be established without imposing constraints on the actuator equation. Next, an argument using reasonable assumptions is presented to justify the exponential stability of $S(t)$.

The linearized testbed model can be represented in a feedback form as shown in Figure 6.2. Let the following assumption hold:

Assumption 4: The beam equation with piston position as input and shear force as output is an exponentially stable RLS with TF $G_B(s)$.

Owing to the presence of damping, the exponential stability of the RLS is expected. A system of PDEs closely related to the beam equation is shown to be exponentially stable due to the presence of damping, in Appendix A. In application, the actuator is chosen to be more powerful

than the system it drives. Hence the stable strictly proper TF, $G_A(s)$, of the actuator model from the shear force to the piston position will satisfy $\left|G_A(j\tau)G_B(j\tau)\right|<1$, $\forall \tau \in \mathbb{R}$. This implies the exponential stability of the semigroup $S(t)$.

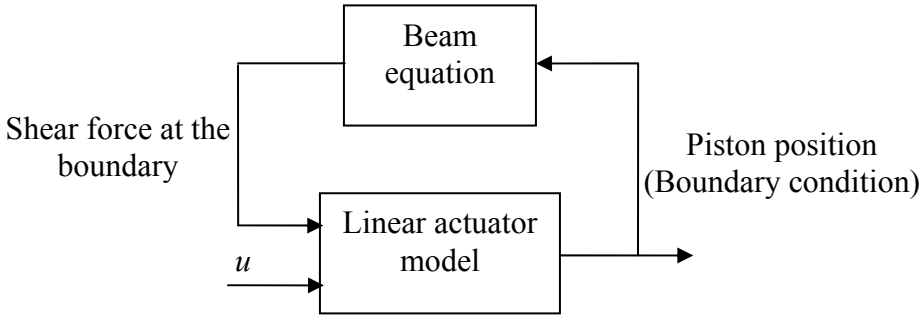

Figure 6.2: Interconnection of actuator and beam

6.4 Testbed model belongs to the class of NPRLS

The nonlinearly perturbed testbed model can be written as an evolution equation

$$\begin{aligned} z_t &= Az + B_c u + B_g g + \varepsilon N(z) \equiv Az + B_{in}\left[u, g\right]^T + \varepsilon N(z), \\ y_{out} &= C_{out} z = y_L(-l). \end{aligned} \tag{6.5}$$

Here B_c is the input operator. It is bounded since it is derived from the matrix B (see actuator model Eq. (6.1)). B_g is the linear map from gravity to the state space and from the PDE model it is also a bounded operator. Therefore the operator B_{in} is a bounded linear operator. The output y_{out} is the first state of z and therefore C_{out} is a bounded operator. From Section 6.3 A generates an exponentially stable semigroup.

Assumptions 1-3 in Section 5.1 will be verified next. Using Theorem 5.1 in [48] and Proposition 4.3 in [34] it follows that $(A, B_{in}, C_{out}, 0)$ are the generating operators of an

exponentially stable regular linear system (RLS) and therefore Assumption 1 is satisfied. The TF associated with this RLS $G(s) = C_{out}(sI_Z - A)^{-1} B_{in}$. It clearly satisfies $G(\bar{s}) = \bar{G}(s)$. Though the nonlinear term is written as $N(z)$, it is in fact a map from the finite dimensional space corresponding to $(y_L(-l), y_{L,t}(-l), x_a)$ to itself. Assuming turbulent flow, a simplified model was used in Chapter 2 for the orifice flow in terms of a non-Lipschitz at zero square root of the pressure drop function. But more complex Lipschitz functions [49]-[51] model the orifice flow better by correctly accounting for the laminar nature of the flow for small pressure drops. Hence it is reasonable to assume that the function $N(z)$, capturing the flow nonlinearities, is in fact Lipschitz. The complex flow equations are not used in the simulations since they equal the square root function when the pressure drop is not near zero, a typical feature in this application. Furthermore, when the input and gravity are absent the testbed is at equilibrium and $N(z=0)$ can be taken to be zero. Hence Assumption 2 is satisfied. Clearly $(A, I_Z, C_{out}, 0)$ are the generating operators of a RLS where I_Z is the identity map on Z. Hence Assumption 3 is satisfied. The requirement that ε be small is satisfied as discussed and seen from the predominant linearity of the testbed actuator response in Chapter 2. Since all the assumptions in Chapter 5 are satisfied, Eq. (6.5) is a NPRLS.

The control technique for the rejection of sinusoids from NPRLS presented in Theorem 5 and Theorem 6 considers a single input and does not account for the presence of the constant input, gravity. But this is not limiting since gravity can be ignored while applying the theorems and then it can be introduced as an input to the stable closed loop NPRLS. The stability of the resulting system is guaranteed provided the nonlinearity is small. Hence Theorem 5 and Theorem

6 can be applied to the testbed model and therefore to the testbed, and eventually to the mold oscillation system, to eliminate distortions from the mold profile. The details are presented in Chapter 7.

CHAPTER 7

RESULTS FROM SIMULATIONS AND EXPERIMENTS

The testbed model was classified as a nonlinearly perturbed regular linear system (NPRLS) in Chapter 6 and therefore the control schemes presented in Chapter 5 for the rejection of sinusoids from NPRLS can be applied to the testbed model, and to the physical testbed, to eliminate distortions from the mold displacement profiles. The results from these tests are presented in Section 7.1. In Section 7.2, under suitable justification, the control scheme is applied to the mold oscillation system excited at a fixed frequency, in the absence of steel, to eliminate unwanted harmonics. Typical signals generated by the controllers are presented in Section 7.3. Section 7.4 discusses the development of the codes and the selection of controller parameters that enable the implementation of the controller in production. Results from the controller test performed during production with molten steel are presented in Section 7.5.

7.1 Controller validation on testbed model and testbed

The computational model of the testbed and the physical testbed, both of which are stabilized via proportional feedback using gains of 0.6 and 2, respectively, exhibit distortion in the mold position profile (Figure 2.6 and Figure 2.9) when excited at 4.6 Hz. This distortion was hypothesized to be caused by the presence of a small amplitude harmonic at 9.2 Hz in the piston position signal. To eliminate this harmonic the control scheme in Theorem 5 is applied. Using a reference sinusoid of frequency 9.2 Hz, and amplitude of 0.05 mm for the model and 0.25 mm for the testbed, the gain $G_{P,N}\left(j2\pi\times 9.2\right)$ was computed. This gain satisfied the inequality

$\left|1-G_{P,N}\left(j2\pi\times 9.2\right)\right|<1$ in case of the model and the testbed. Hence the filter $R=1$ satisfies the condition $\left|1-G_{P,N}\left(j\omega_r\right)G_R\left(j\omega_r\right)\right|<1$ in Theorem 5. The filter F in Eq. (5.6) is introduced with $\omega_r=2\pi\times 9.2$ and $\zeta=0.1$. This ζ is small enough to guarantee the stability of the augmented loop corresponding to the model and the testbed. The results from the controller testing on these systems are presented next.

7.1.1 Testbed model

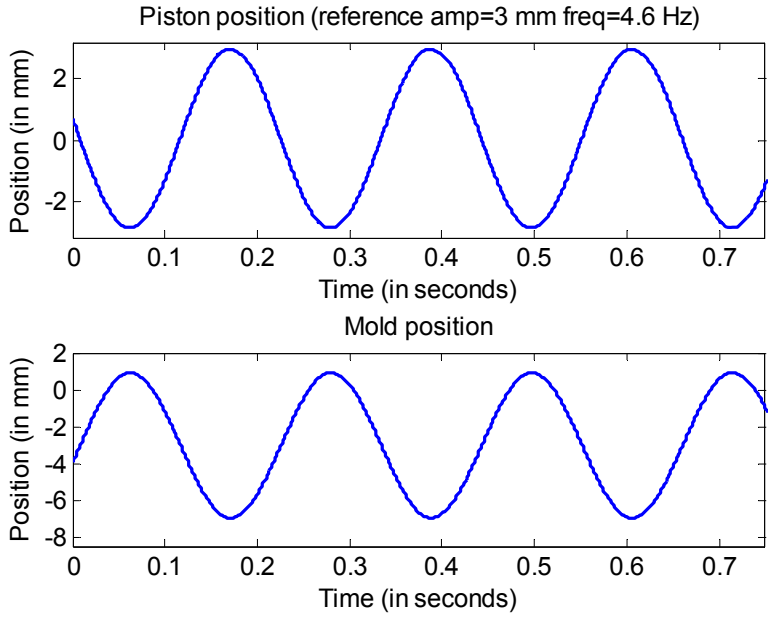

Figure 7.1: Simulation data from testbed model - piston and mold position with reference at 4.6 Hz obtained by applying the controller in Theorem 5

To test the control scheme a reference sinusoid of amplitude 3 mm and frequency 4.6 Hz is chosen as the input to the augmented loop corresponding to the testbed model. Comparing Figure 7.1 with Figure 2.9, the distortion in the mold position has been completely eliminated. Comparing Figure 7.2 and Figure 2.12 reveals that this is achieved by rejecting the sinusoid at

frequency 9.2 Hz contained in the piston position. It is also seen that the augmentation of the closed loop has minimal effect on the system response at frequencies away from 9.2 Hz and the tracking at 4.6 Hz is preserved, as stated in Theorem 5.

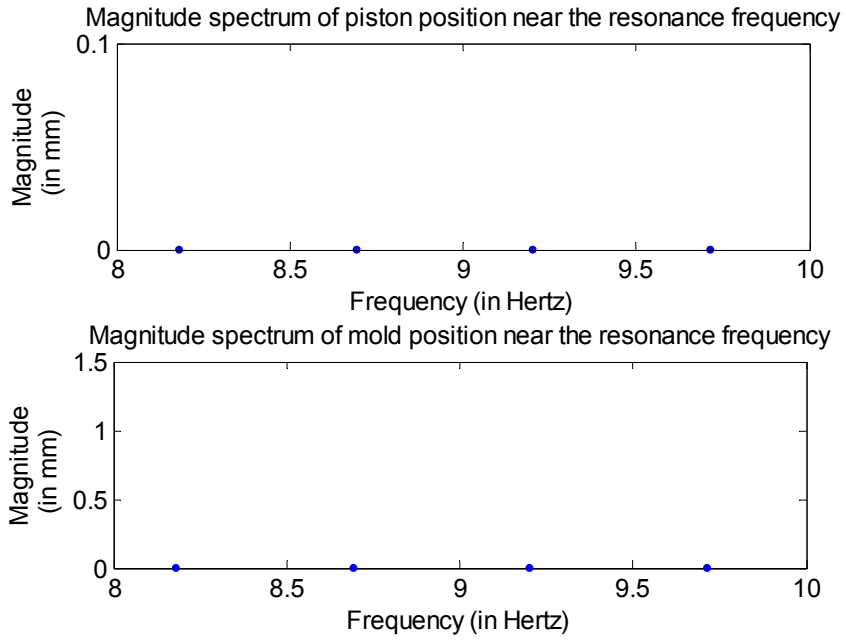

Figure 7.2: Simulation data from testbed model - magnitude spectra of the piston and mold position shown in Figure 7.1 near the beam resonance frequency (peak at 9.2 Hz is completely eliminated)

7.1.2 Testbed

A discrete version of the filter F in Eq. (5.6) is obtained by using the first order hold discretization with 1 millisecond sampling interval, which is adequate since the largest frequency of interest is 9.2 Hz. Data is recorded with the same sampling interval. A reference sinusoid of amplitude 3 mm and frequency 4.6 Hz is chosen as the input to the augmented loop corresponding to the testbed. Figure 7.3 shows the resulting piston and mold position profiles. The distortion in the mold position is significantly reduced compared to the unaugmented case shown in Figure 2.6. From Figure 7.4, it is seen that the peak at 9.2 Hz in the magnitude

spectrum of the piston position has been removed, causing a 70% reduction in the corresponding peak in the mold position, compared to Figure 2.11. The piston position profiles in Figure 7.3 and Figure 2.6 are similar, since the augmentation procedure has minimal influence on the response of the closed loop at frequencies away from 9.2 Hz. The residual peak at 9.2 Hz and the corresponding distortion in the mold position is believed to be caused by other nonlinearities affecting the system such as friction in the hinges.

The results from the testbed model and the testbed confirm the hypothesis that the major cause of distortions in the mold profiles in these systems is the small amplitude higher harmonics in the piston position signal. Next this hypothesis will be verified for the mold oscillation system.

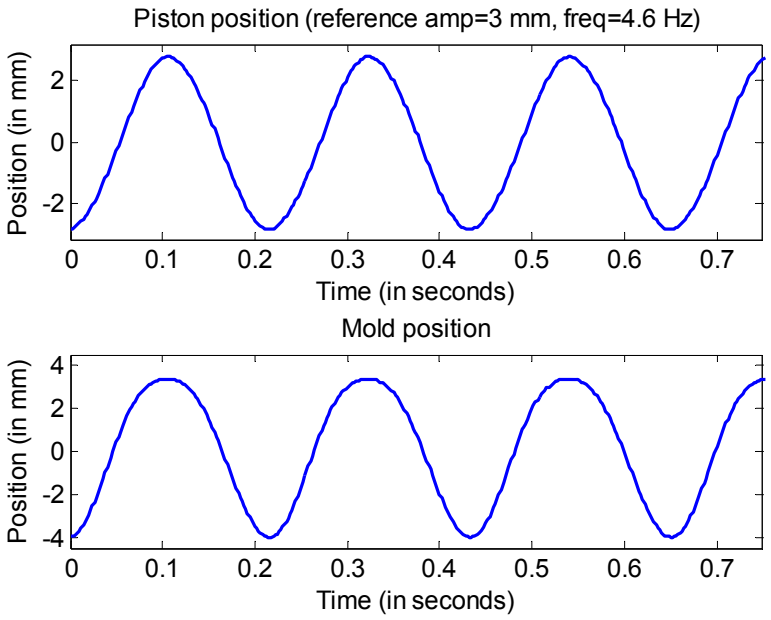

Figure 7.3: Experimental data from testbed - piston and mold position with reference at 4.6 Hz obtained by applying the controller in Theorem 5

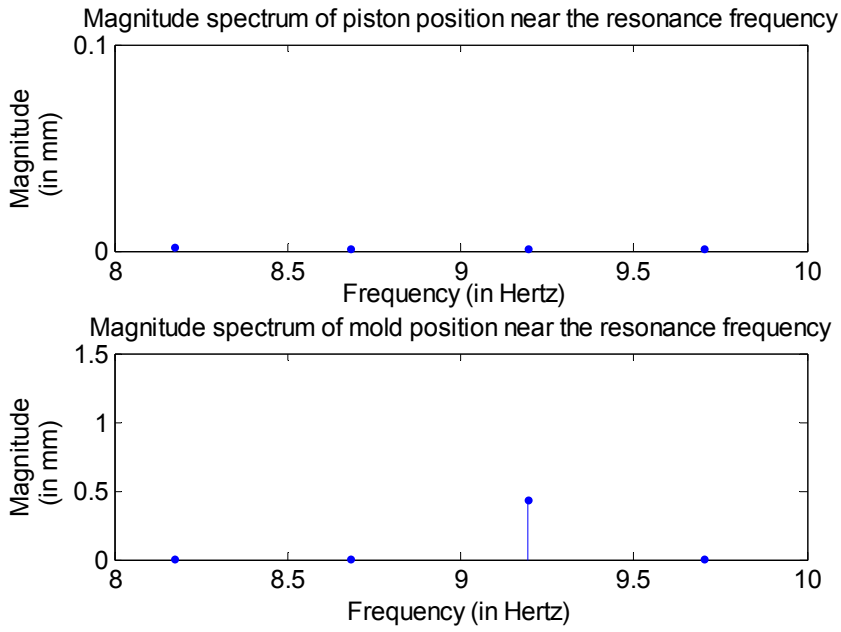

Figure 7.4: Experimental data from testbed - magnitude spectra of the piston and mold position shown in Figure 7.3 near the beam resonance frequency (magnitude at 9.2 Hz in mold position reduced by a factor of 3.25 compared to Figure 2.11)

7.2 Controller validation on the mold oscillation system

Owing to the satisfactory performance of the controller on the testbed model and the physical testbed, access to the mold oscillation system was granted. As seen in Figure 2.4, with a proportional controller gain of 0.7, when the reference input frequency is 4.4 Hz and amplitude is 3.5 mm the mold velocity profile exhibits significant distortion. To identify the cause of distortion, the magnitude spectra of the piston and mold position signals were computed as in the case of the testbed and are shown in Figure 7.5. The piston and mold spectra exhibit peaks at harmonics of 4.4 Hz with the peaks at the second and third harmonics being the most prominent. Using the magnitude and phase data of the first six harmonics in the mold position signal, the mold velocity signal is reconstructed (Figure 7.6). Harmonics higher than the sixth are not used since they seem to be influenced by the vibrations in the sensor mounting and are not reliable. The reconstructed mold velocity profile exhibits distortion similar to that in Figure 2.4.

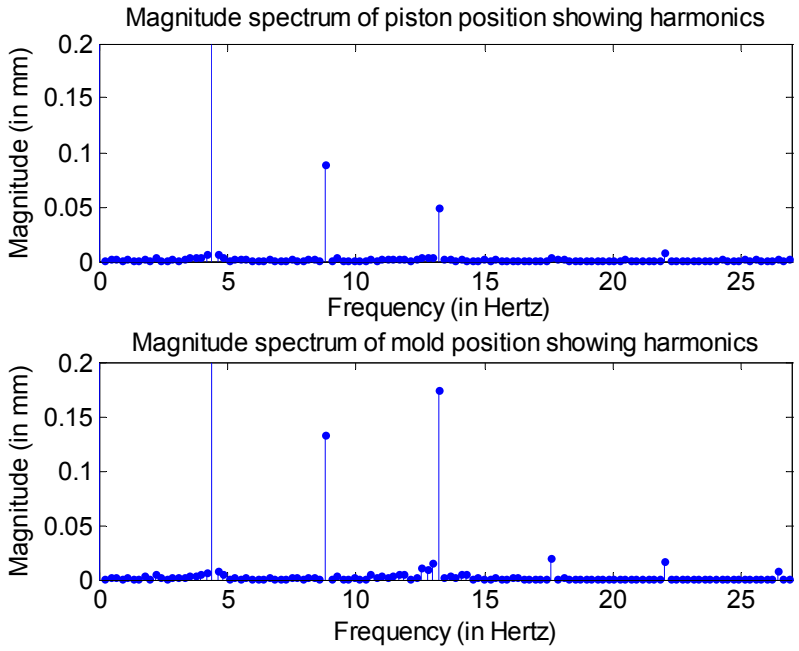

Figure 7.5: Experimental data from mold oscillation system - magnitude spectra of the piston and mold position showing the harmonics with reference at 4.4 Hz

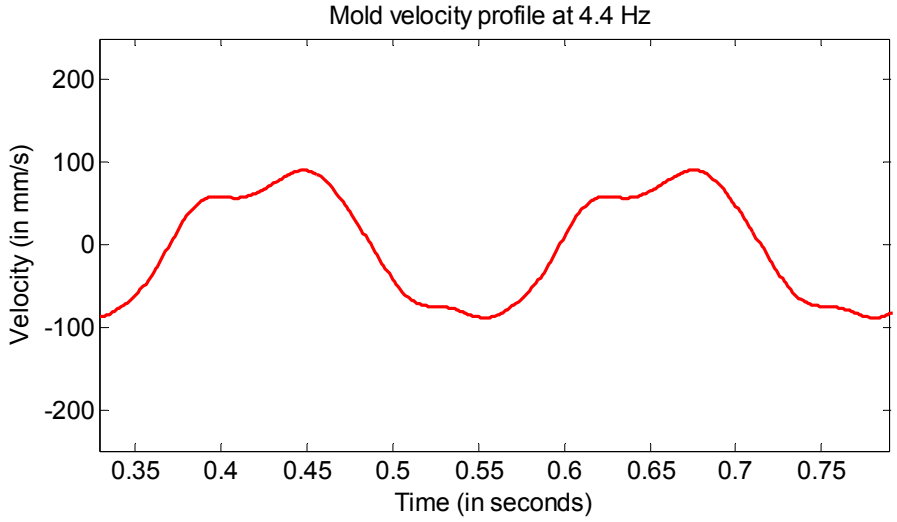

Figure 7.6: Experimental data from mold oscillation system – mold velocity profile at 4.4 Hz obtained by using the magnitude and phase data of the harmonics in the mold position signal

The input-output (reference-piston position) behavior of the mold oscillation system is predominantly linear. Considering the peaks at the second and third harmonic in Figure 7.5, the hypothesis formulated using the testbed that the small amplitude harmonics of the input frequency in the piston position signal generated by the nonlinear actuator dynamics are the source of distortion in the mold profiles, seems to be true for the mold oscillation system thereby making the problem statement in Chapter 2 relevant. The mold oscillation system differs from the testbed in being more rigid and complicated, thereby causing the distortions at the testbed to be more severe. But the structural similarities, in terms of a hinged flexible structure supporting an end mass and excited by an electro-hydraulic actuator, and the similar source of distortion suggest that the non-model based control scheme in Theorem 5 developed to address the distortion problem in the testbed can be applied to the mold oscillation system. In the mold oscillation system, two harmonics, second and third, must be eliminated as opposed to a single harmonic in the testbed and hence the controller in Theorem 6, instead of Theorem 5, is used with n=2.

The filters R and F in the augmented loop were chosen as specified in Theorem 6 with $\omega_1 = 2\pi \times 8.8$, $\omega_2 = 2\pi \times 13.2$ and $\zeta_1 = \zeta_2 = 0.02$. The filters were implemented by obtaining a discrete version using first order hold approximation with a sampling interval of 1 millisecond. A reference input of frequency 4.4 Hz and amplitude 3.5 mm was chosen for the augmented loop and the magnitude spectrum of the corresponding piston and mold position signals are shown in Figure 7.7. As expected, the peaks at 8.8 Hz and 13.2 Hz in the magnitude spectra of the piston position signal are completely eliminated, causing a significant reduction in the corresponding peaks for the mold position signal. This leads to the removal of the distortion in the mold velocity profile as shown, both in Figure 7.8 obtained from the position data and in Figure 7.9

which is the screenshot of the monitoring system at Nucor Steel. At 4.4 Hz, the third harmonic is the significant cause of distortion while at higher frequencies (above 5 Hz), the second harmonic starts contributing to the distortions.

The cause of distortion in the mold profiles of the mold oscillation system has therefore been correctly identified as the small amplitude harmonics in the piston position. Using the control schemes proposed in Chapter 5, the distortions have been eliminated. Results similar to those presented here for the reference frequency of 4.4 Hz have been obtained for other frequencies as well.

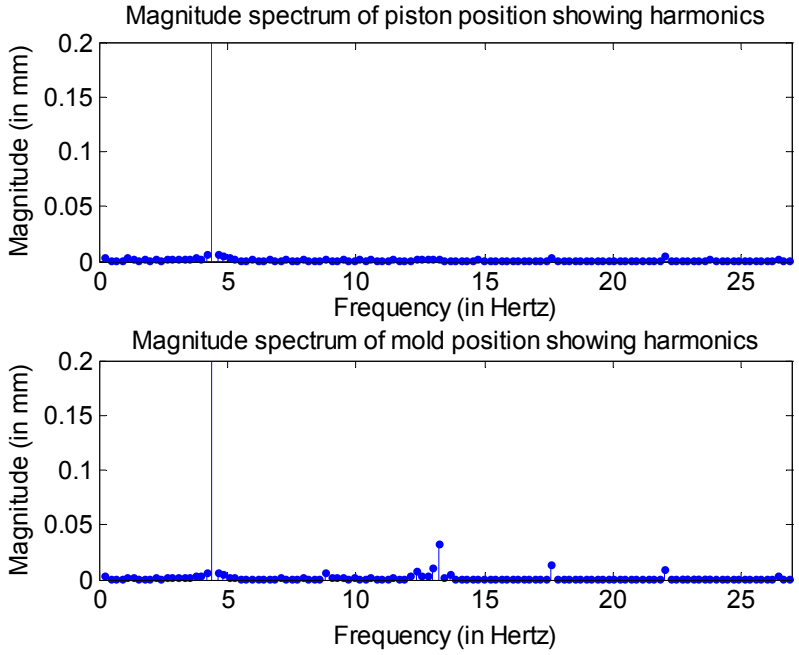

Figure 7.7: Experimental data from mold oscillation system - magnitude spectra of the piston and mold position showing the harmonics with reference at 4.4 Hz obtained by applying the controller in Theorem 6 (magnitude at 8.8 Hz and 13.2 Hz in mold position is significantly reduced compared to Figure 7.5)

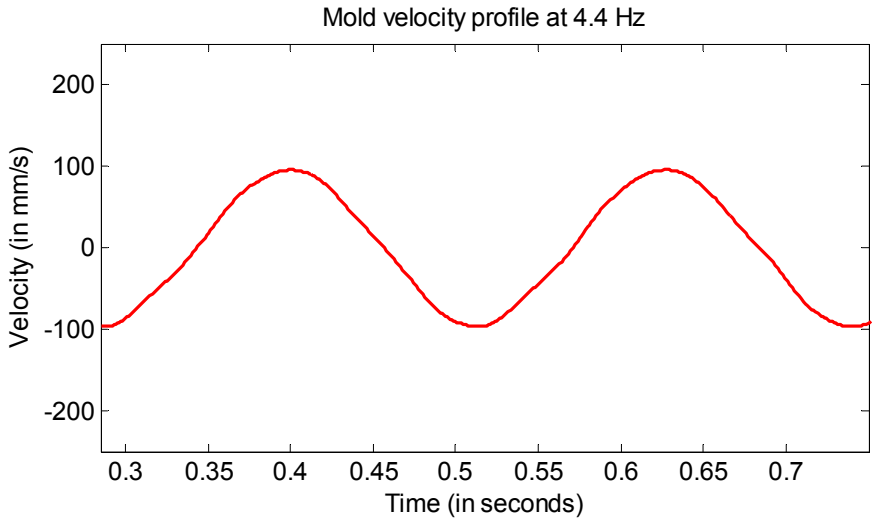

Figure 7.8: Experimental data from mold oscillation system – mold velocity profile at 4.4 Hz obtained by applying the controller in Theorem 6 (compared to Figure 7.6 the distortions are significantly lower)

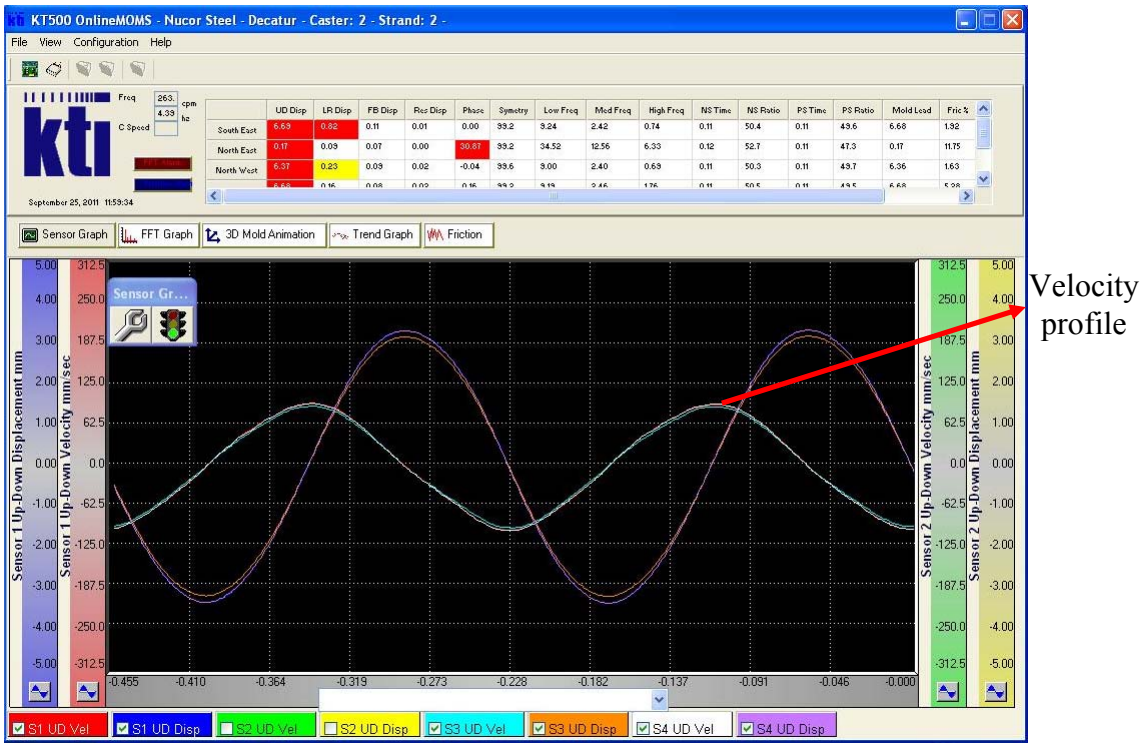

Figure 7.9: Screenshot of the mold displacement and velocity profiles obtained by applying the controller in Theorem 6 as displayed by the monitoring system at Nucor Steel

7.3 Typical control signals

Typical signals generated by the controllers used to eliminate the distortions in the mold profiles in the testbed model, the testbed and the mold oscillation system are presented in this section. In practice, the initial reference frequency is chosen to be zero so as to stabilize the system at the equilibrium position and then the frequency is changed smoothly resulting in a quasi steady state operation of the systems. So as to evaluate the controller response, as well as to obtain clearer graphical representations, the reference frequency is changed rapidly to collect the data presented in this section. All the control signals are smooth, present no unexpected oscillations or spikes and eventually converge to a periodic function.

7.3.1 Testbed model

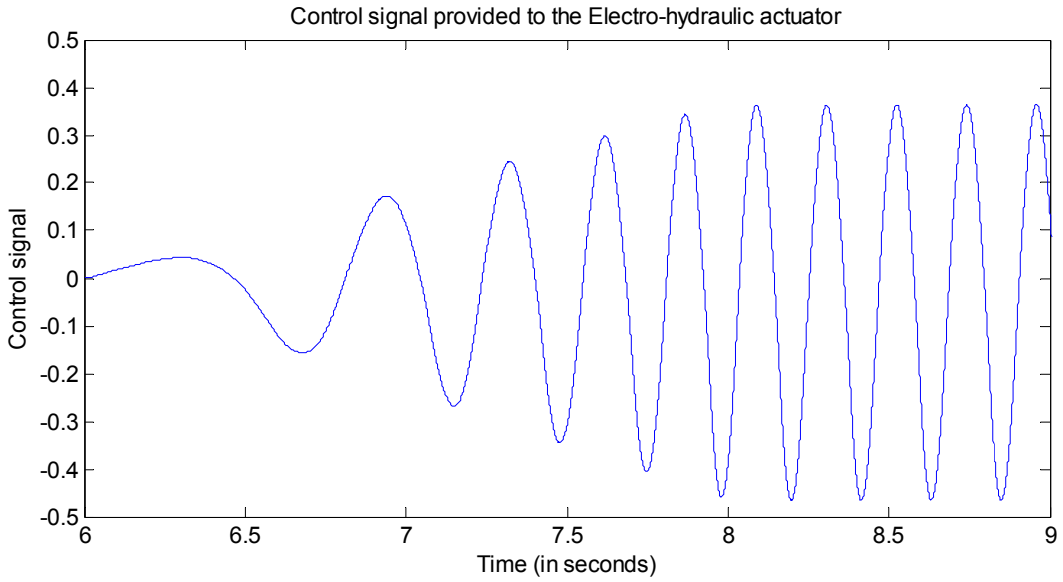

Figure 7.10: Typical control signal in the testbed model

The testbed model was simulated using the controller from Theorem 5 as described in Section 7.1.1. The frequency of the reference was ramped quickly from 0 Hz to 4.6 Hz. The resulting control signal, shown in Figure 7.10, is smooth and converges to a periodic function.

7.3.2 Testbed

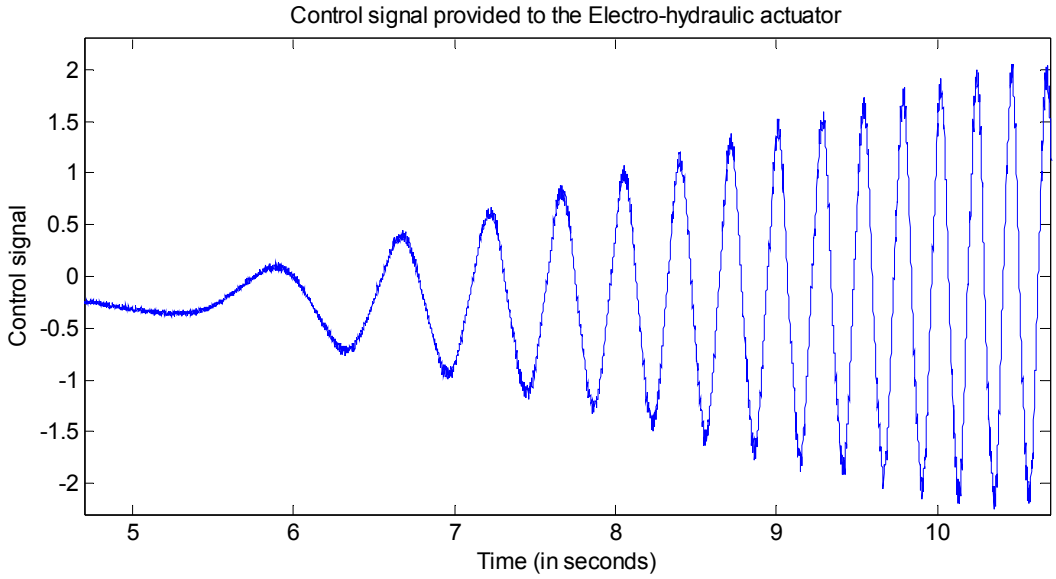

Figure 7.11: Typical control signal in the testbed

The controller from Theorem 5 was implemented on the testbed as described in Section 7.1.2. The frequency of the reference was increased from 0 Hz to 4.6 Hz and the corresponding control signal is shown in Figure 7.11. The control signal is smooth but for the presence of measurement noise. Note that the experiments in Section 7.1.2 and this section were conducted using identical controllers but on different days.

7.3.3 Mold oscillation system

As discussed in Section 7.2, the controller from Theorem 6 was implemented on the mold oscillation system to eliminate the distortion from the mold velocity profile. The frequency of the reference was increased from 0 Hz to 4.4 Hz and the resulting smooth control signal is shown in Figure 7.12. The experiments in Section 7.2 and this section were conducted using similar controllers but on different days.

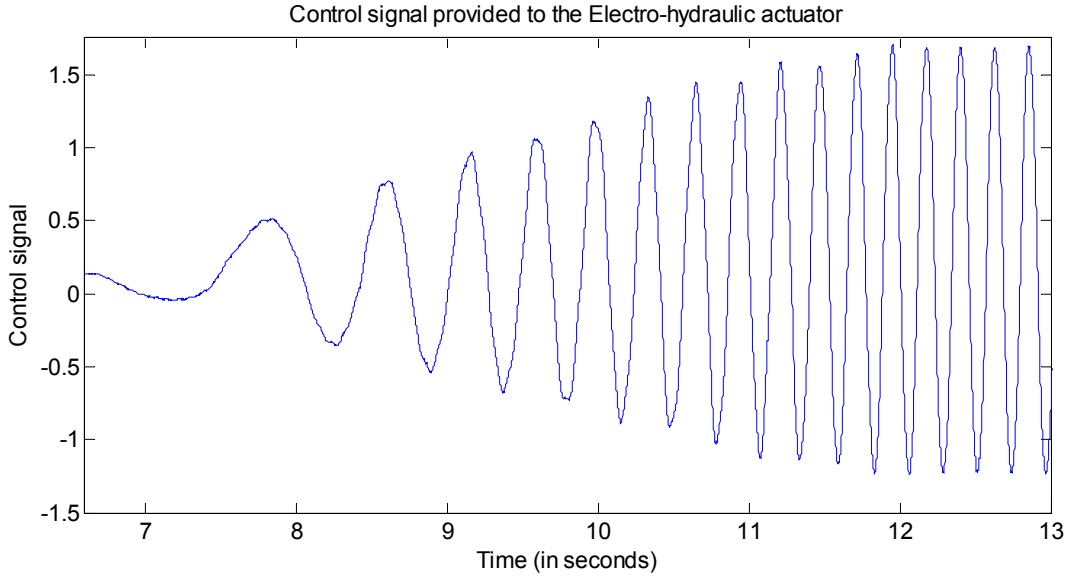

Figure 7.12: Typical control signal in the mold oscillation system

7.4 Code development and parameter selection

This section discusses the various practical aspects related to implementing the proposed control scheme in production. In particular, the details of the code that implements the controller by varying the filter coefficients as a function of excitation frequency and the selection of controller parameters on the basis of robustness requirements are discussed.

7.4.1 Details of the hardware and software

The piston and mold position signals were measured using Temposonics linear position sensor which has a resolution of less than 2 microns. The controller is implemented using hardware and software from National Instruments. The hardware comprises of the CompactRIO embedded chassis, which includes a real-time controller and a reconfigurable FPGA, and a set of input/output modules. The software used is LabVIEW. Codes developed in LabVIEW are executed both in the real-time controller and the FPGA which can communicate with one another. In the FPGA, codes can be executed at a faster rate than in the real-time controller. But typically the size of the code, in terms of the number of computations, which can be executed in the FPGA is smaller. Additionally compiling the codes in FPGA is very time consuming. Hence, in the present work, most of the calculations are performed in the real-time controller. The FPGA core which communicates with the sensors and actuators via input and output modules, respectively, implements a code that performs the following – i) collect the digital signal from the sensor, calculate the physical position, and transmit it to the real-time controller and ii) obtain the controller output signal from the real-time controller and transmit it to the actuator. There are two important codes implemented in the real-time controller. They are the identification code and the controller code. These codes are discussed next.

7.4.2 Automation of the code for production

In Section 7.2 it was shown that the control scheme presented in Chapter 5 can successfully eliminate distortions from the mold velocity profile at a given frequency of excitation. But during production, the oscillation frequency for the mold can be changed from one value to another. When this occurs, the coefficients for the filters R and F in Theorem 6 must change

automatically. Although during production the mold oscillation frequency will be in the range 3.5 Hz - 5.2 Hz, the frequency is in fact slowly ramped up from 0 Hz during start up and therefore the range of interest is 0 Hz - 5.2 Hz.

From experiments, the mold velocity profile exhibits almost no distortion in the frequency range 3.6 Hz - 3.85 Hz. In the range 3.85 Hz - 5.2 Hz, the distortions occur due to the presence of the third harmonic, and at times the second harmonic, in the piston position. The third harmonic frequency is near a structural resonance frequency. In this range the control scheme in Chapter 5 demonstrated in Section 7.2 can be used to eliminate the distortions in the mold profiles. In the range 0 Hz - 3.6 Hz, the frequencies between 3 Hz and 3.6 Hz are more crucial. Distortions in this range can possibly be addressed using the control scheme in Chapter 5 but now considering third and fourth harmonics. But instead an intuitive approach of adding the error between the mold and piston position to the actuator control signal is used. Hence

$$w = 0.7\Big(\big(u - x_p\big) + 0.35\big(x_p + x_m\big)\Big),$$

where w, u, x_p and x_m are the actuator control signal, reference sinusoid, piston position and mold position, respectively. The gain 0.35, was determined experimentally to guarantee stability of the mold oscillation system and also provide satisfactory performance in the frequency range 0 Hz - 3.6 Hz. This approach does not perform well in the frequency range 3.85 Hz - 5.2 Hz. Hence the more involved approach in Chapter 5 is used.

7.4.2.1 Identification code

To implement the control scheme from Chapter 5 in the range 3.85 Hz - 5.2 Hz, the plant gains in the frequency range 7.7 Hz - 10.4 Hz (second harmonic) and 11.55 Hz - 15.6 Hz (third harmonic) must be obtained. In the testbed, the plant gain could be obtained by directly choosing

a reference sinusoid with small amplitude at the desired frequency (9.2 Hz). But in the mold oscillation system, reference sinusoids of small amplitude (hundreds of microns) at certain frequencies (near beam resonance frequencies) lead to instability. It is believed that at small amplitudes of excitation, the nonlinear effects in the system such as play and friction in the hinges influences and dominates the actuator dynamics causing instability. Hence larger amplitudes of excitation are desired to suppress these effects; but references with large amplitude at the resonance frequency may damage the equipment. This difficulty is resolved by choosing the reference to be a sum of two sinusoids – one with large amplitude (thousands of microns) at a frequency which is a submultiple of the frequency of interest and the other with small amplitude (hundreds of microns) at the frequency of interest which could be near the resonance frequency. Using integration identities the magnitude and phase of the sinusoid at the frequency of interest in both the reference and the piston position are calculated and used to obtain the plant gain. For instance to obtain the plant gain at 12 Hz, the reference signal used is $3\sin(8\pi t)+0.3\sin(24\pi t)$ mm. The amplitudes of the sinusoids must be chosen judiciously. In this example, the amplitude at 12 Hz must be small so as not to damage the system by creating excessive oscillations. But at the same time if it is too small, the two sinusoids at 12 Hz in the piston position signal, one generated as a harmonic of the 4 Hz sinusoid and the other by the 12 Hz sinusoid in the reference, may be indistinguishable. These considerations lead to experimentally determining the appropriate amplitudes for the sinusoids at all the frequencies of interest.

A detailed identification code is developed to compute the plant gain at the frequencies of interest. For obtaining the plant gain between 7.7 Hz and 10.4 Hz, this code increases the frequency f incrementally from 3.85 Hz to 5.2 Hz in steps of 0.05 Hz. At each step the reference signal is chosen to be $3\sin(2\pi ft)+0.4\sin(4\pi ft)$ and the data collected over a specified

number of cycles is processed using integration identities to obtain the plant gain. The plant gain between 11.55 Hz – 15.6 Hz, is similarly obtained but with the reference signal being $3\sin(2\pi ft)+a\sin(6\pi ft)$, where $a=0.3$ for $f<4.55$ and $a=0.5$ for $f\geq 4.55$. The identification code computes all the plant gains sequentially and stores them in an array.

The identification code uses the plant gains and computes the constants x_1, x_2, x_3, x_4 in the filter *R* of Theorem 6 (with *n*=2) at each frequency of excitation, ω (in radians) as follows. Let the gains $G_{P,N}(2j\omega)=1/(a_1(\omega)+ja_2(\omega))$ and $G_{P,N}(3j\omega)=1/(a_3(\omega)+ja_4(\omega))$. Then using $\omega_1=2\omega$ and $\omega_2=3\omega$ in Eq. (5.8), Theorem 6 requires that

$$G_R(2j\omega)=a_1(\omega)+ja_2(\omega), \qquad G_R(3j\omega)=a_3(\omega)+ja_4(\omega).$$

$x_1(\omega)$, $x_2(\omega)$, $x_3(\omega)$, $x_4(\omega)$ can then be obtained by solving linear equations of the form

$$\begin{bmatrix} \frac{1}{2\omega} & 0 & \frac{12}{61\omega} & \frac{5}{61\omega^2} \\ 0 & -\frac{1}{4\omega^2} & \frac{10}{61\omega} & -\frac{6}{61\omega^2} \\ \frac{18}{61\omega} & -\frac{5}{61\omega^2} & \frac{1}{3\omega} & 0 \\ -\frac{15}{61\omega} & -\frac{6}{61\omega^2} & 0 & -\frac{1}{9\omega^2} \end{bmatrix} \begin{bmatrix} x_1(\omega) \\ x_2(\omega) \\ x_3(\omega) \\ x_4(\omega) \end{bmatrix} = \begin{bmatrix} a_1(\omega) \\ a_2(\omega) \\ a_3(\omega) \\ a_4(\omega) \end{bmatrix}.$$

These values are stored in a file to be accessed while implementing the controller.

7.4.2.2 Controller code

In the controller code, the stabilizing proportional control for the actuator is always implemented with a proportional gain of 0.7. In addition, if the frequency of excitation is between 0 Hz and 3.6 Hz the intuitive control using the mold position is activated and if it is between 3.85 Hz and 5.2 Hz the control scheme from Chapter 5 is used. The frequency range 3.6 Hz - 3.85 Hz, where

no additional control is required, acts as a buffer region where one of the additional controllers is turned off and the other one is turned on smoothly. Details regarding implementing the controller in Theorem 6 are discussed next.

Figure 7.13 shows the augmented loop in Theorem 6 with an additional input. The additional input is useful for obtaining the equivalent simplified block diagram, shown in Figure 7.14, which is implemented.

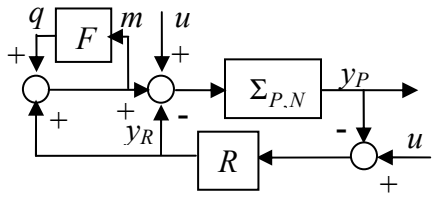

Figure 7.13: Augmented loop in Theorem 6 with an additional input

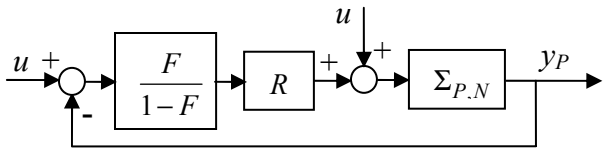

Figure 7.14: Simplified block diagram of augmented loop

From Theorem 6 with n=2, it follows after some simplification that

$$\frac{F}{1-F}=\underbrace{\frac{2\zeta_1\omega_1 s\left(1+2\zeta_2\omega_2 s\Big/\left(\omega_2^2-\omega_1^2\right)\right)}{\left(s^2+\omega_1^2\right)}}_{G_1}+\underbrace{\frac{2\zeta_2\omega_2 s\left(1+2\zeta_1\omega_1 s\Big/\left(\omega_1^2-\omega_2^2\right)\right)}{\left(s^2+\omega_2^2\right)}}_{G_2}.$$

A state space realization for G_1 is

$$A_1=\begin{bmatrix}0 & 1\\ -\omega_1^2 & 0\end{bmatrix},\ B_1=\begin{bmatrix}0\\ 1\end{bmatrix},\ C_1=\begin{bmatrix}-\omega_1^2\dfrac{2\zeta_1\omega_1 2\zeta_2\omega_2}{\left(\omega_2^2-\omega_1^2\right)} & 2\zeta_1\omega_1\end{bmatrix},\ D_1=\begin{bmatrix}\dfrac{2\zeta_1\omega_1 2\zeta_2\omega_2}{\left(\omega_2^2-\omega_1^2\right)}\end{bmatrix}, \qquad (7.1)$$

and for G_2 is

$$A_2 = \begin{bmatrix} 0 & 1 \\ -\omega_2^2 & 0 \end{bmatrix}, B_2 = \begin{bmatrix} 0 \\ 1 \end{bmatrix}, C_2 = \begin{bmatrix} -\omega_2^2 \frac{2\zeta_1\omega_1 2\zeta_2\omega_2}{\left(\omega_1^2 - \omega_2^2\right)} & 2\zeta_2\omega_2 \end{bmatrix}, D_2 = \begin{bmatrix} \frac{2\zeta_1\omega_1 2\zeta_2\omega_2}{\left(\omega_1^2 - \omega_2^2\right)} \end{bmatrix}. \quad (7.2)$$

Discrete time approximations for G_1 and G_2 are obtained using the first order hold equivalent [52] since it allows the derivation of explicit expressions for the matrices in the discrete state space as functions of ω_1 and ω_2. This makes implementing the filters G_1 and G_2, with coefficients being functions of ω_1 and ω_2, easy. Using a sampling interval of 0.001 seconds, the discrete time state space representation corresponding to Eq. (7.1) is

$$A_1^d = \begin{bmatrix} \cos\left(\frac{\omega_1}{1000}\right) & \sin\left(\frac{\omega_1}{1000}\right)\frac{1}{\omega_1} \\ -\omega_1 \sin\left(\frac{\omega_1}{1000}\right) & \cos\left(\frac{\omega_1}{1000}\right) \end{bmatrix}, B_1^d = \begin{bmatrix} \frac{2000}{\omega_1^3}\sin\left(\frac{\omega_1}{1000}\right)\left(1-\cos\left(\frac{\omega_1}{1000}\right)\right) \\ \frac{2000}{\omega_1^2}\cos\left(\frac{\omega_1}{1000}\right)\left(1-\cos\left(\frac{\omega_1}{1000}\right)\right) \end{bmatrix},$$

$$C_1^d = \begin{bmatrix} -\omega_1^2 \frac{2\zeta_1\omega_1 2\zeta_2\omega_2}{\left(\omega_2^2 - \omega_1^2\right)} & 2\zeta_1\omega_1 \end{bmatrix},$$

$$D_1^d = \begin{bmatrix} \frac{2\zeta_1\omega_1 2\zeta_2\omega_2}{\left(\omega_2^2 - \omega_1^2\right)} \end{bmatrix} + C_1^d \begin{bmatrix} \frac{1}{\omega_1^2} - \frac{1000}{\omega_1^3}\sin\left(\frac{\omega_1}{1000}\right), & \frac{1000}{\omega_1^2} - \frac{1000}{\omega_1^2}\cos\left(\frac{\omega_1}{1000}\right) \end{bmatrix}^T,$$

and the discrete time state space representation corresponding to Eq. (7.2) is

$$A_2^d = \begin{bmatrix} \cos\left(\frac{\omega_2}{1000}\right) & \sin\left(\frac{\omega_2}{1000}\right)\frac{1}{\omega_2} \\ -\omega_2 \sin\left(\frac{\omega_2}{1000}\right) & \cos\left(\frac{\omega_2}{1000}\right) \end{bmatrix}, B_2^d = \begin{bmatrix} \frac{2000}{\omega_2^3}\sin\left(\frac{\omega_2}{1000}\right)\left(1-\cos\left(\frac{\omega_2}{1000}\right)\right) \\ \frac{2000}{\omega_2^2}\cos\left(\frac{\omega_2}{1000}\right)\left(1-\cos\left(\frac{\omega_2}{1000}\right)\right) \end{bmatrix},$$

$$C_2^d = \begin{bmatrix} -\omega_2^2 \frac{2\zeta_1\omega_1 2\zeta_2\omega_2}{\left(\omega_1^2 - \omega_2^2\right)} & 2\zeta_2\omega_2 \end{bmatrix},$$

$$D_2^d = \begin{bmatrix} \frac{2\zeta_1\omega_1 2\zeta_2\omega_2}{\left(\omega_1^2 - \omega_2^2\right)} \end{bmatrix} + C_2^d \begin{bmatrix} \frac{1}{\omega_2^2} - \frac{1000}{\omega_2^3}\sin\left(\frac{\omega_2}{1000}\right), & \frac{1000}{\omega_2^2} - \frac{1000}{\omega_2^2}\cos\left(\frac{\omega_2}{1000}\right) \end{bmatrix}^T.$$

The filter R in Theorem 6 with n=2, has the TF representation

$$G_R(s) = \underbrace{\frac{x_1 s + x_2}{s^2 + \omega_1 s + \omega_1^2}}_{H_1} + \underbrace{\frac{x_3 s + x_4}{s^2 + \omega_2 s + \omega_2^2}}_{H_2},$$

where the constants x_1, x_2, x_3, x_4 are functions of the excitation frequency ω. The discrete time state space representation for H_1 and H_2 obtained using the first order hold equivalent are complicated functions of ω_1 and ω_2 that cannot be implemented easily. Hence H_1 and H_2 are represented as shown in the block diagram in Figure 7.15. Discrete time state space representation of each of the blocks in Figure 7.15 can then be obtained as simple explicit functions of ω_1 and ω_2 (as in the case of G_1 and G_2) which can be easily implemented.

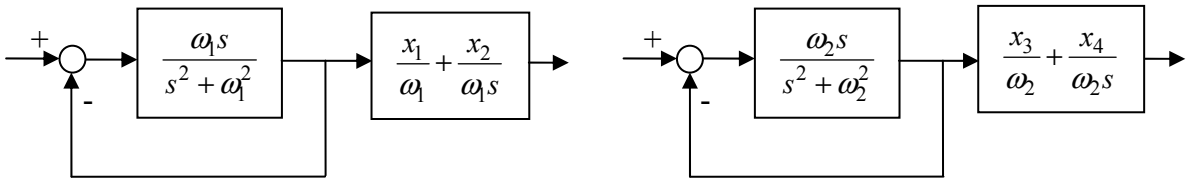

Figure 7.15: Equivalent representations of H_1 and H_2

The controller code accesses a lookup table with values $x_1(\omega)$, $x_2(\omega)$, $x_3(\omega)$, $x_4(\omega)$ obtained from the identification code. Hence, when the excitation frequency ω is changed, the coefficients of the filters in Figure 7.14 which are coded in as functions of ω, also change accordingly.

7.4.3 Robustness requirements

The identification code can be run on the mold oscillation system only once every two weeks when the production is stopped for maintenance. During the two week period, the plant gains can

change. Hence it is necessary to get an estimate of the variations in the plant gain to verify that the control scheme implemented using a fixed set of plant gains remains stable during whole two week period. Figure 7.16 and Figure 7.17 show the magnitude and phase, respectively, of the plant gains computed over a month in 2011. The trend exhibited by the plant gain in these plots is typical, i.e. the overall shape of the curves remains the same with some variations in the values.

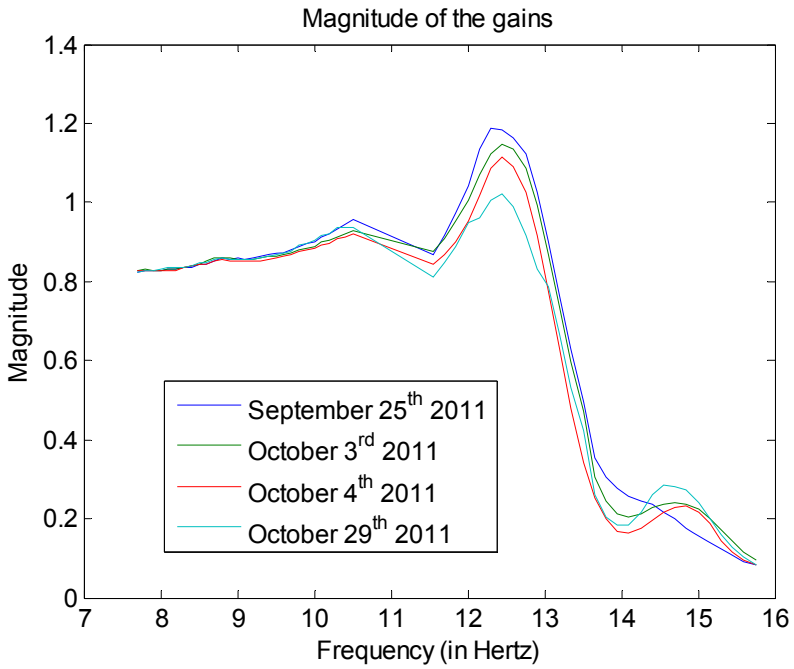

Figure 7.16: Magnitude of the plant gains computed using data collected over a one month period

In Theorem 6 the filter R is designed to satisfy $\left|1-G_{P,N}(j\omega_1)G_R(j\omega_1)\right|=0$ and $\left|1-G_{P,N}(j\omega_2)G_R(j\omega_2)\right|=0$. Since the plant is nonlinearly perturbed the estimate, that the augmented loop remains stable provided the plant gain does not vary by more than 100 %, derived in Section 4.3 for linear plants with R satisfying similar equalities continues to hold, approximately. The percentage variation in the plant gains between successive testing dates is

less than 50 %. Hence it follows that the controller in Theorem 6 is sufficiently robust to handle the variations in the plant gains. If robustness to more than 100 % variation in plant gain were desired, it can be obtained by choosing the filter *R* appropriately as discussed in Section 4.3.

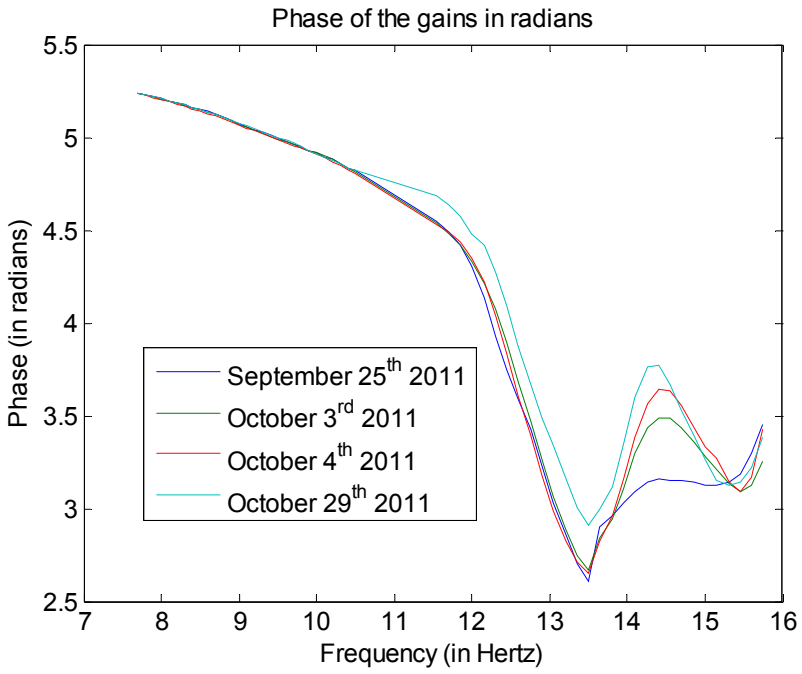

Figure 7.17: Phase of the plant gains computed using data collected over a one month period

In the robustness estimates derived in Section 4.3, it was assumed that the filter *F* decays sufficiently fast away from the frequencies of interest. The parameters ζ_1 and ζ_2 must be small to satisfy this requirement (along with the stability requirement). At the same time a large ζ_1 and ζ_2 tends to improve the transients by increasing the controller output. Hence for this application ζ_1 and ζ_2 are chosen to be 0.01 and 0.005, respectively to ensure that the filter *F* decays as fast as the plant gains in Figure 7.16. With these values, the controller developed using the data from September 25th guarantees closed loop stability on all four days for which data is presented in Figure 7.16.

7.5 Controller validation in production

The results for the mold oscillation system presented thus far are from experiments performed without steel in the mold. The development of the comprehensive control codes in LabVIEW, discussed in Section 7.4, facilitated the testing of the proposed control techniques during production. To this end, the LabVIEW codes were integrated with the Siemens system that controls the whole casting process and decides the amplitude and frequency of oscillation. The plant gains needed for the controller design cannot be estimated during production and are obtained in the absence of steel in the mold. To understand the effect of mold friction on the plant gain, the pressures in the actuator were monitored at low frequencies of oscillation (near 3 Hz). The variations in the pressures with and without steel are estimated to be small compared to the maximum pressure in the system. Also, using data in [53] the maximum frictional force is estimated to be much lesser than the mold weight. Hence it is reasonable to expect that the variations in the plant gain are within the robustness margins of the control scheme.

The control scheme was implemented in production. First the mold was excited at the standard operational parameters – frequency of 3.38 Hz and amplitude of 4.5 mm, using the simple controller that uses the mold position as a feedback. The oscillations marks obtained on the surface of the steel slab are shown in Figure 7.18.

Next the mold was excited at the new operational parameters – frequency of 4.33 Hz and amplitude of 3.5 mm, using the controller in Theorem 6. The mold oscillation system could not be operated at this frequency before owing to distortions in the mold velocity profiles. But with the proposed control scheme, the mold profiles are distortion free (Figure 7.19).

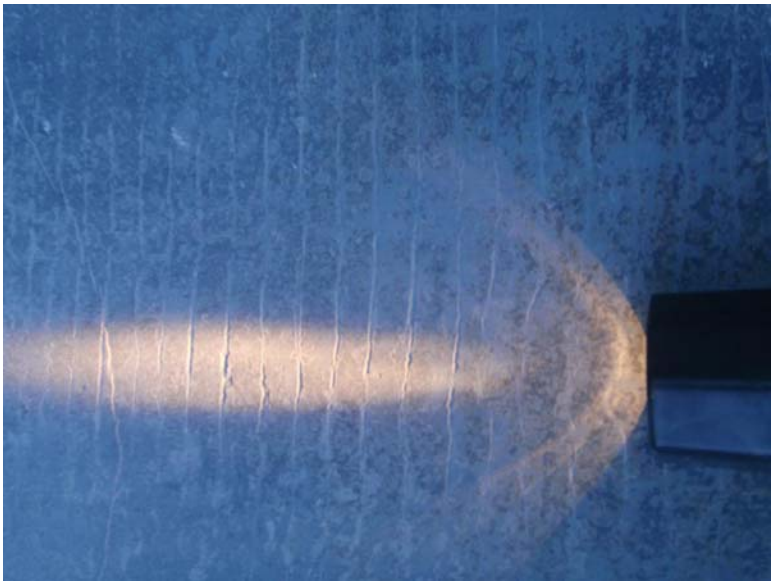

Figure 7.18: Oscillations marks on the surface of the steel using standard oscillation practice

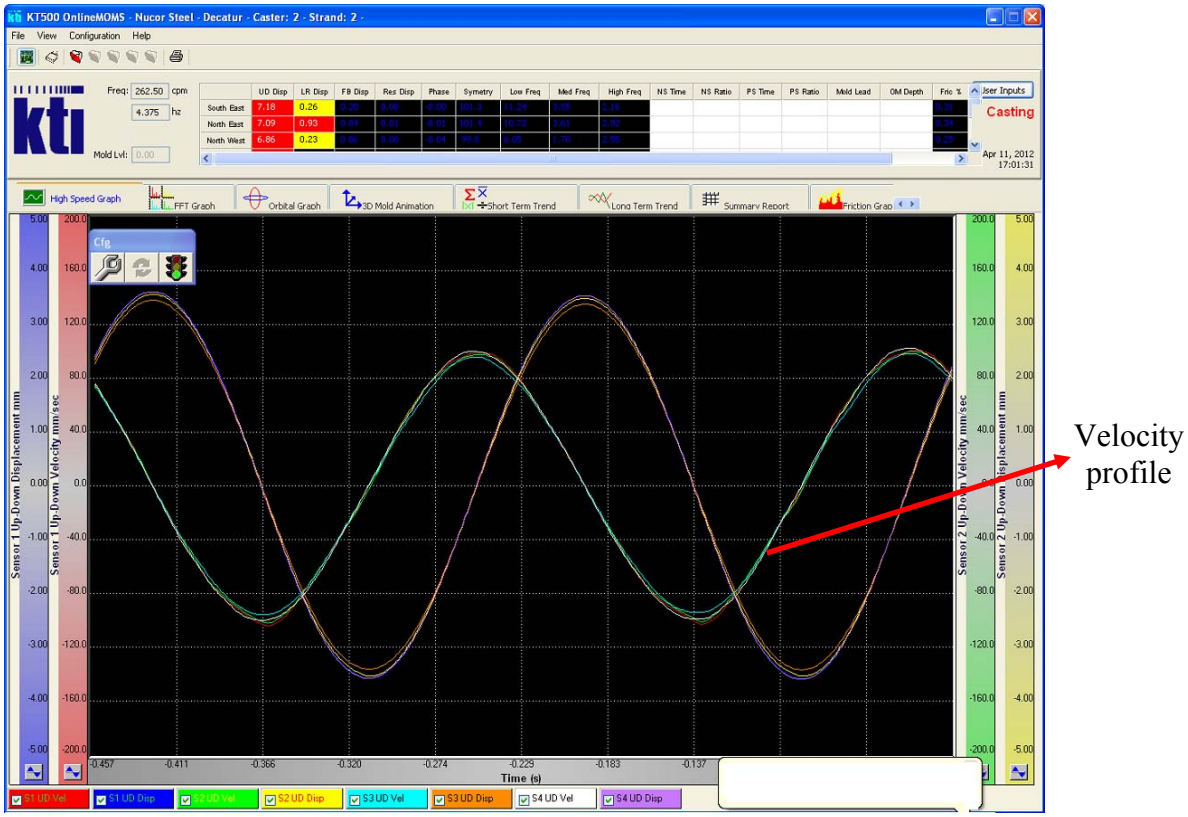

Figure 7.19: Screenshot of the mold displacement and velocity profiles displayed by the monitoring system at Nucor Steel during production

The oscillations marks obtained on the surface of the steel slab using the new operational parameters are shown in Figure 7.20. Compared to those in Figure 7.18, these marks are shallower thereby reducing the chances of formation of surface cracks. Apart from improving the surface quality of the steel grades already being produced, this will allow Nucor to explore the possibility of producing newer crack sensitive grades of steel and entering new markets.

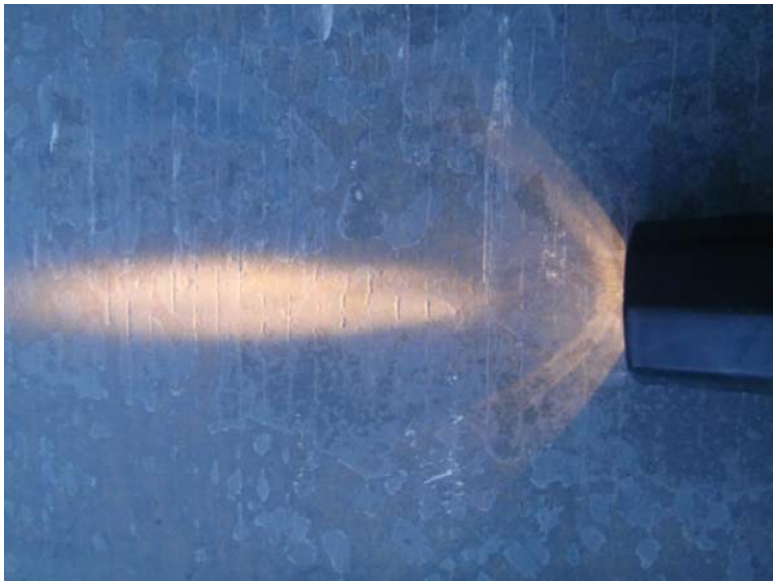

Figure 7.20: Oscillations marks on the surface of the steel using new oscillation practice enabled by the control scheme in Theorem 6

CHAPTER 8

CONCLUSIONS

A longstanding motion distortion problem in the mold oscillation system at Nucor Steel, Decatur was solved by developing a non-model based robust control scheme for the rejection of bandlimited periodic disturbances from the output of nonlinearly perturbed infinite dimensional systems. Solving this problem helps improve the surface quality of the steel slabs being produced which in turn facilitates the casting of new crack sensitive grades of steel. The proposed control scheme, implemented using hardware and software from National Instruments, is currently being integrated with the existing system to make it a permanent feature in the overall plant control architecture. A summary of the dissertation and suggestions for future work are presented next.

8.1 Summary

The distortion problem in the mold oscillation system was recreated on an industrial scale physical testbed which is similar, but not identical, to the mold oscillation system. A fundamentally based analytical model of the testbed, exhibiting comparable distortions, was developed. Using experimental results from the testbed and simulation of the model the source of distortion was identified to be the nonlinear characteristics of the electro-hydraulic actuator. The problem statement for eliminating the distortion was formulated as robust periodic disturbance rejection from uncertain nonlinearly perturbed infinite dimensional systems.

The problem statement was first addressed assuming finite dimensional dynamics by developing an internal model principle based control scheme that uses the plant gain at the

frequencies of interest alone. This scheme was then shown to be applicable to plants in the class of regular linear systems for tracking sinusoidal signals. An infinite dimensional class of systems, nonlinearly perturbed regular linear systems (NPRLS), matching the phenomenology of the application was introduced and characterized. The control scheme was shown to be applicable for rejecting sinusoids from the output of plants in this class, thereby completely addressing the problem statement.

The testbed model was shown to belong to the newly introduced class, thereby establishing the suitability of the proposed control scheme for rejecting sinusoids from the testbed model, the testbed and, owing to structural similarities, from the mold oscillation system. The efficacy of the control scheme was first demonstrated on all three systems and finally implemented in production resulting in improved surface quality of the steel slabs.

8.2 Future research directions

The control scheme proposed in this work is non-adaptive and depends completely on the robustness margins to ensure stability in the face of slowly varying plant gains. Developing adaptive versions of this scheme can help improve closed loop performance and extend its applicability to systems where the plant gains at the disturbance frequency are not readily available. When the nominal plant model is known, an approach for adaptively improving closed loop performance involves updating the stable filter corresponding to the Youla parametrization of the stabilizing controller [54]. Next, this approach is considered in the context of the control scheme proposed in this dissertation.

8.2.1 Youla parametrization of the proposed controller

Youla parametrization represents all the stabilizing controllers of a linear finite dimensional plant in terms of stable filters. This enables recasting the problem of optimizing the closed loop performance, either adaptively or otherwise, in terms of these filters [54]. The controller proposed in this dissertation for rejecting a single sinusoid also has a representation in terms of a stable filter, Q.

Given a stable finite dimensional SISO plant P any stabilizing controller K for this plant can be written in terms of a stable filter Q as

$$K = \frac{Q}{1 - PQ}. \tag{8.1}$$

For this controller to be independent of the plant model, a key feature of the control scheme in this dissertation, the filter Q must have the following structure –

$$Q = \frac{G_1}{PG_1 + G_2}, \tag{8.2}$$

where the filters G_1 and G_2 must be selected to satisfy the conditions:

(i) Q is stable

(ii) K has poles at $\pm j\omega_r$.

Condition (ii) ensures that the harmonic at frequency ω_r can be rejected by the controller. With Q as defined in Eq. (8.2), the controller K in Eq. (8.1) is given as G_1/G_2 and is independent of the plant model.

To obtain the controller developed in this dissertation, let

$$G_1 = \frac{2\zeta\omega_r s}{s^2 + \omega_r^2} R \text{ and } G_2 = 1.$$

Then condition (ii) is clearly satisfied. The filter R and constant ζ must be chosen to satisfy condition (i). Choose R to be a stable filter with $P(j\omega_r)R(j\omega_r)=1$. Then,

$$Q=\frac{2\zeta\omega_r sR}{s^2+\omega_r^2+2\zeta\omega_r sPR}=\frac{2\zeta\omega_r sR}{s^2+2\zeta\omega_r s+\omega_r^2+2\zeta\omega_r s(1-PR)}. \tag{8.3}$$

If $D=s^2+2\zeta\omega_r s+\omega_r^2+2\zeta\omega_r s(1-PR)$ has no zeros in $\mathbb{C}_0^+$, then Q is stable. This follows by considering $\mathbb{C}_0^+$ to be the union of closed half discs B_1 and B_2 centered at $\pm j\omega_r$ and their complement in $\mathbb{C}_0^+$. Let the radius of the half discs be small enough so that for $s\in B_1\cup B_2$, $|1-P(s)R(s)|<0.5$. Then for sufficiently small value of ζ, $|s^2+2\zeta\omega_r s+\omega_r^2|$ will dominate $|2\zeta\omega_r s(1-PR)|$ on the boundary of the half discs and by Rouché's theorem D will have no zeros in $B_1\cup B_2$. In the complement of $B_1\cup B_2$ if ζ is sufficiently small, then $|s^2+\omega_r^2|>0$ dominates the other terms in D. Hence D has no zeros in $\mathbb{C}_0^+$ and Q is a stable filter. The controller corresponding to Q in Eq. (8.3) is

$$K=\frac{2\zeta\omega_r s}{s^2+\omega_r^2}R=\frac{\left(2\zeta\omega_r s\Big/\left(s^2+2\zeta\omega_r s+\omega_r^2\right)\right)}{1-\left(2\zeta\omega_r s\Big/\left(s^2+2\zeta\omega_r s+\omega_r^2\right)\right)}R=\frac{F}{1-F}R,$$

which is implemented in this dissertation (Figure 7.14).

Although the control scheme proposed in this work has been related to a Q filter, the Q filter depends on the plant model. It cannot be implemented when the plant model is unknown. Consequently the adaptive schemes in [54], wherein the Q filter is suitably updated and implemented, cannot be directly utilized for improving the closed loop performance in the present framework. Suitable modifications to these schemes will be explored in the future.

The testbed model was classified as belonging to the class of NPRLS under reasonable assumptions on the stability of the beam system in the testbed and strength of the actuator. Providing rigorous mathematical justification for these assumptions will require a detailed study of the models by developing new tools for their analysis. In this regard results developed for a simplified beam system, presented in Appendix A, will be helpful.

For plants in the class of NPRLS, the magnitude of the perturbations can be large depending on the stability margin of the associated semigroup. Hence NPRLS is in fact a class of nonlinear infinite dimensional systems. Interconnected system of nonlinear partial differential equations model many physical processes such as fluid flow in tubular networks. Developing general results for interconnection of plants belonging to NPRLS, as has been done in the finite dimensional case, can provide a framework for modeling and controlling such networks.

In this work, the plant gain used for controller design is obtained experimentally in the absence of steel in the mold. During production the frictional forces on the mold due to the presence of steel influences these gains. These influences were claimed to be small based on reasonable heuristic arguments. Measuring the value of the mold friction can help quantify this claim. Mold friction is a valuable parameter from a metallurgical standpoint which cannot be measured directly. Developing observers to estimate its value will be useful.

The stability of the state matrix obtained by discretizing the coupled partial differential equations modeling the beam in the testbed using a second order finite difference scheme is sensitive to the discretization step size. Since a discretization step size of 0.0251 m and the parameter values in Table 1 gave a stable matrix and the resulting model captured the testbed behavior well in simulation, this issue was not investigated in detail. Preliminary studies however showed that the instability is related to the treatment of the boundary condition in the

numerical scheme. A detailed analysis of this problem will be useful in the numerical study of such systems of PDEs.

REFERENCES

[1] B. A. Francis and W. M. Wonham, "The internal model principle for linear multivariable regulators," *Appl. Math. Optim.*, vol. 2, no. 2, pp. 170-194, 1975.

[2] S. Hara, Y. Yamamoto, T. Omata and M. Nakano, "Repetitive control system: A new type servo system for periodic exogenous signals," *IEEE Trans. Autom. Control*, vol. 33, no. 7, pp. 659-668, 1988.

[3] M. Tomizuka, T-C. Tsao, and K-K. Chew, "Analysis and synthesis of discrete-time repetitive controller," *ASME J. Dyn. Syst. Meas. Contr.*, vol. 111, pp. 353-358, 1989.

[4] T. J. Manayathara, T-C. Tsao, J. Bentsman and D. Ross, "Rejection of unknown periodic load disturbances in continuous steel casting process using learning repetitive control approach", *IEEE Trans. Control Syst. Technol.*, vol. 4, no. 3, pp. 259-265, 1996.

[5] M. R. Bai and T. Wu, "Simulations of an internal model-based active noise control system for suppressing periodic disturbances," *J. Vib. Acoust.*, vol. 120, pp. 111-116, 1998.

[6] L. J. Brown and Q. Zhang, "Periodic disturbance cancellation with uncertain frequency," *Automatica*, vol. 40, pp. 631-637, 2004.

[7] I. D. Landau, A. Constantinescu and D. Rey, "Adaptive narrow band disturbance rejection applied to an active suspension – an internal model principle approach," *Automatica*, vol. 41, pp. 563-574, 2005.

[8] Omata, T., Hara, S., and Nakano, M., "Nonlinear repetitive control with application to trajectory control of manipulators," *J. Robotic Syst.*, vol. 4, no. 5, pp. 631-652, 1987.

[9] J. Ghosh and B. Paden, "Nonlinear repetitive control," *IEEE Trans. Autom. Control*, vol. 45, no. 5, pp. 949-954, 2000.

[10] P. Lucibello, "Comments on "Nonlinear repetitive control"," *IEEE Trans. Autom. Control*, vol. 48, no. 8, pp. 1470-1471, 2003.

[11] E. J. Davison, and A. Goldenberg, "Robust control of a general servomechanism problem: The servo compensator" *Automatica,* vol. 11, pp. 461-471, 1975.

[12] E. J. Davison, "The robust control of a servomechanism problem for linear time-invariant multivariable systems," *IEEE Trans. Autom. Control*, vol. 21, no. 1, pp. 25-34, 1976.

[13] E. J. Davison, "Multivariable tuning regulators: The feedforward and robust control of a general servomechanism problem," *IEEE Trans. Autom. Control*, vol. 21, pp. 35-47, 1976.

[14] H. Logemann and S. Townley, "Low gain control of uncertain regular linear systems," *SIAM J.Contr. Optim.*, vol. 35, no. 1, pp. 78-116, 1997.

[15] T. Hamalainen and S. Pohjlainen, "A finite-dimensional robust controller for systems in the CD-algebra," *IEEE Trans. Autom. Control*, vol. 45, no. 3, pp. 421-431, 2000.

[16] R. Rebarber and G. Weiss, "Internal model based tracking and disturbance rejection for stable well-posed systems," *Automatica*, vol. 39, pp. 1555-1569, 2003.

[17] V. Natarajan and J. Bentsman, "Robust rejection of sinusoids in stable nonlinearly perturbed unmodelled linear systems: Theory and application to servo," *Proceedings of the American Control Conference*, San Francisco, CA, pp. 3289-3294, 2011.

[18] V. Natarajan and J. Bentsman, "Robust periodic reference tracking by stable uncertain infinite-dimensional linear systems," *Proceedings of the American Control Conference*, San Francisco, CA, pp. 1777-1782, 2011.

[19] V. Natarajan and J. Bentsman, "Rejection of sinusoids from nonlinearly perturbed uncertain regular linear systems," *Proceedings of the 50th IEEE Conference on Decision and Control and European Control Conference*, Orlando, FL, pp. 4931-4936, 2011.

[20] V. Natarajan and J. Bentsman, "Rejection of periodic disturbances from the class of nonlinearly perturbed regular linear systems," *to be submitted*.

[21] V. Natarajan and J. Bentsman, "Classifying an industrial servo model as a nonlinearly perturbed regular linear system," *to be submitted*.

[22] H-J. Shin, G-G. Lee, W-Y. Choi, S-M. Kang, J-H. Park, S-H. Kim and B. G. Thomas, "Effect of mold oscillation on powder consumption and hook formation in ultra low carbon steel slabs," *AISTech*, Nashville, TN, 2004.

[23] http://ccc.illinois.edu/ (webpage of continuous casting consortium at the University of Illinois at Urbana-Champaign)

[24] H. E. Merrit, *Hydraulic control systems*, Wiley and Sons, NY, 1967.

[25] D. H. Kim and T-C. Tsao, "A linearized electrohydraulic servovalve model for valve dynamics sensitivity analysis and control system design," *ASME J. Dyn. Syst. Meas. Contr.*, vol. 122, pp. 179-187, 2000.

[26] Meirovitch, L., 1967, *Analytical methods in vibrations*, The Macmillan company, London, 1967.

[27] M. R. Sirouspour and S. E. Salcudean, "On the nonlinear control of hydraulic servo-systems," *Proceedings of the 2000 IEEE International conference on Robotics and Automation,* San Fransisco, CA, pp. 1276-1282, 2000.

[28] Thayer, W. J., 1965, "Transfer functions for Moog servovalves," *Technical Bulletin 103*, Moog Inc. Controls division, East Aurora, NY.

[29] R. K. Miller and A. N. Michel, 1980, "On the response of nonlinear multivariable interconnected feedback systems to periodic input signals," *IEEE Trans. Circuits Syst.*, vol. 27, no. 11, pp. 1088-1097, 1980.

[30] M. Green and D. J. N. Limebeer, *Linear robust control*, Prentice-Hall, Englewood Cliffs, 1995.

[31] E. Freitag and R. Busam 2005, *Complex analysis*, Springer, NY, 2009.

[32] G. Weiss, "Transfer functions of regular linear systems. Part I: Characterization of regularity," *Trans. Amer. Math. Soc.*, vol. 342, no. 2, pp. 827-854, 1994.

[33] G. Weiss and R. Curtain, "Dynamic stabilization of regular linear systems," *IEEE Trans. Autom. Control*, vol. 42, no. 1, pp. 4-21, 1997.

[34] G. Weiss, "The representation of regular linear systems on Hilbert spaces," *Control and Estimation of Distributed Parameter Systems*, F. Kappel, K. Kunisch, and W. Schappacher, Eds., Basel: Birkhauser Verlag, vol. 91, pp. 401–416, 1989.

[35] A. Pazy, *Semigroups of linear operators and applications to partial differential equations,* Applied Mathematical Sciences, vol. 44, Springer, 1983.

[36] G. Weiss, "Admissibility of unbounded control operators," *SIAM J.Contr. Optim.,* vol. 27, no. 3, pp. 527-545, 1989.

[37] J. U. Kim and Y. Renardy, "Boundary control of the Timoshenko beam," *SIAM J.Contr. Optim.,* vol. 25, no. 6, pp. 1417-1429, 1987.

[38] O. Morgul, "Dynamic boundary control of Timoshenko beam," *Automatica,* vol. 28, no. 6, pp. 1255-1260, 1992.

[39] D-H Shi, S. H. Hou, D-X. Feng, "Feedback stabilization of a Timoshenko beam with an end mass," *Int. J. Control,* vol. 69, no. 2, pp. 285-300, 1998.

[40] C-G Zhang, "Boundary feedback stabilization of the undamped Timoshenko beam with both free ends," *J. Math. Anal. Appl.,* vol. 326, pp. 488-499, 2007.

[41] S. Shoukui, "Boundary stabilization of nonuniform Timoshenko beam," *Appl. Math. J. Chinese Univ. Ser. B*, vol. 14, no. 4, pp. 467-474, 1999.

[42] F. Ammar-Khodja, S. Kerbal and A. Soufyane, "Stabilization of the nonunifrom Timoshenko beam," *J. Math. Anal. Appl.,*vol. 327, pp. 525-538, 2007.

[43] D-H Shi and D-X Feng, "Exponential decay rate of the energy of a Timoshenko beam with locally distributed feedback," *ANZIAM J.,* vol. 44, pp. 205-220, 2002.

[44] Q. Yan, S. H. Hou, G. Huang and L. Wan, "Stabilization of the nonunifrom Timoshenko beam with coupled locally distributed feedbacks," *J. Syst. Sci. Complex.,* vol. 18, no. 3, pp. 419-428, 2005.

[45] A. Soufyane, "Exponential stability of the linearized nonuniform Timoshenko beam," *Nonlinear Anal.: Real World Appl.,* vol. 10, pp. 1016-1020, 2009.

[46] J. E. Lagnese, G. Leugering, and E. J. P. G. Schmidt, "Control of planar networks of Timoshenko beams," *SIAM J.Contr. Optim.,* vol. 31, no. 3, pp. 780-811, 1993.

[47] Z-J Han and G-Q Xu, "Stabilization and Riesz basis property of two serially connected Timoshenko beams system," *Z. Angew. Math. Mech.,* vol. 89, no. 12, pp. 962-980, 2009.

[48] R. F. Curtain and G. Weiss, "Well posedness of triples of operators (in the sense of linear systems theory)," *Control and Estimation of Distributed Parameter Systems*, F. Kappel, K. Kunisch, and W. Schappacher, Eds., Basel: Birkhauser Verlag, vol. 91, pp. 41–59, 1989.

[49] A. Ellman and R. Piche, "A two regime orifice flow formula for numerical simulation," *ASME J. Dyn. Syst. Meas. Contr.*, vol. 121, pp. 721-724, 1999.

[50] W. Borutzky, B. Barnard and J. Thoma, "An orifice flow model for laminar and turbulent conditions," *Simul. Modell. Pract. Theory*, vol. 10, pp. 141-152, 2002.

[51] J. Hauser and M. V. Sivaselvan, "On the computation of compatible trajectories for hydraulic shaketables," *Proceedings of the American Control Conference,* St. Louis, MO, pp. 5210-5215, 2009.

[52] G. F. Franklin, J. D. Powell and M. Workman, *Digital control of dynamic systems,* Addison Wesley Longman, 1998.

[53] Y. Meng and B. G. Thomas, "Interfacial friction-related phenomena in continuous casting with mold slags," *ISSTesch steelmaking conference*, Indianapolis, IN, pp. 589-606, 2003.

[54] T. T. May, I. M. Y. Mareels and J. B. Moore, *High performance control*, Birkhauser Boston, 1997.

[55] F. Alabau-Boussouira, "Asymptotic behavior for Timoshenko beams subject to a single nonlinear feedback control," *Nonlinear Differ. Equ. Appl.*, vol. 12, pp. 643-669, 2007.

[56] A. Pazy, "On the applicability of Lyapunov's theorem in Hilbert spaces," *SIAM J. Math. Anal.,* vol. 3, no. 2, pp. 291-294, 1972.

APPENDIX A

EXPONENTIAL STABILITY OF A SIMPLIFIED BEAM EQUATION

A simplified beam equation, closely related to the testbed model is shown to be exponentially stable. The tools and results presented in this section could be adapted to rigorously establish Assumption 4 in the dissertation.

A.1 Simplified beam equation

With notation as in Chapter 6, the beam equation is given by the PDEs

$$m_b \frac{\partial^2 y_L}{\partial t^2} + \gamma_y \frac{\partial y_L}{\partial t} = \frac{\partial}{\partial x}\left(k'Ga_b \left(\frac{\partial y_L}{\partial x} - \psi_L \right) \right),$$

$$\frac{I}{a_b} m_b \frac{\partial^2 \psi_L}{\partial t^2} + \gamma_\psi \frac{\partial \psi_L}{\partial t} = \frac{\partial}{\partial x}\left(EI \frac{\partial \psi_L}{\partial x} \right) + k'Ga_b \left(\frac{\partial y_L}{\partial x} - \psi_L \right),$$

$$m_b \frac{\partial^2 y_R}{\partial t^2} + \gamma_y \frac{\partial y_R}{\partial t} = \frac{\partial}{\partial x}\left(k'Ga_b \left(\frac{\partial y_R}{\partial x} - \psi_R \right) \right),$$

$$\frac{I}{a_b} m_b \frac{\partial^2 \psi_R}{\partial t^2} + \gamma_\psi \frac{\partial \psi_R}{\partial t} = \frac{\partial}{\partial x}\left(EI \frac{\partial \psi_R}{\partial x} \right) + k'Ga_b \left(\frac{\partial y_R}{\partial x} - \psi_R \right).$$

The boundary conditions are

$$y_L(-l) = 0, \quad k'Ga_b \left(\frac{\partial y_R(l)}{\partial x} - \psi_R(l) \right) + M \frac{\partial^2 y_R(l)}{\partial t^2} + \gamma_M \frac{\partial y_R(l)}{\partial t} = 0,$$

$$y_L(0) = y_R(0) = 0, \ \frac{\partial \psi_L(-l)}{\partial x} = \frac{\partial \psi_R(l)}{\partial x} = 0, \ \psi_L(0) = \psi_R(0), \ \frac{\partial \psi_L(0)}{\partial x} = \frac{\partial \psi_R(0)}{\partial x}.$$

Note that the effect of gravity is not included in the equations and the boundary condition at the mold end is unchanged. The boundary condition at actuator end is changed to drop the actuator dynamics. The beam is assumed to be hinged at this end.

With α, β, α_1, α_2, d_1, d_2, d_3, L_l^2, L_r^2, H_l^n, H_r^n, and $H_{r,0}^n$ as defined in Chapter 6 and $H_{l,0}^n = \left\{ f : f \in H^n(-l,0), f(-l) = f(0) = 0 \right\}$ (different from Chapter 6), consider the space

$$Z = \left\{ \begin{array}{l} (f_1, f_2, f_3, f_4, f_5, f_6, f_7, f_8, a_1) \in H_{l,0}^1 \times L_l^2 \times H_l^1 \times L_l^2 \times H_{r,0}^1 \times L_r^2 \times H_r^1 \times L_r^2 \times \mathbb{R} \\ \text{with } f_3(0) = f_7(0) \end{array} \right\}.$$

Henceforth z_1 and z_2 will be generically used to represent elements of Z with their components being $(f_1, f_2, f_3, f_4, f_5, f_6, f_7, f_8, a_1)$ and $(g_1, g_2, g_3, g_4, g_5, g_6, g_7, g_8, b_1)$, respectively. The inner product on Z is defined as

$$\begin{aligned} \langle z_1, z_2 \rangle_Z = \alpha \int_{-l}^{0} f_{1,x} g_{1,x} \mathrm{dx} + \int_{-l}^{0} f_2 g_2 \mathrm{dx} + \int_{-l}^{0} f_3 g_3 \mathrm{dx} + \beta \int_{-l}^{0} f_{3,x} g_{3,x} \mathrm{dx} + \int_{-l}^{0} f_4 g_4 \mathrm{dx} + \alpha \int_{0}^{l} f_{5,x} g_{5,x} \mathrm{dx} \\ + \int_{0}^{l} f_6 g_6 \mathrm{dx} + \int_{0}^{l} f_7 g_7 \mathrm{dx} + \beta \int_{0}^{l} f_{7,x} g_{7,x} \mathrm{dx} + \int_{0}^{l} f_8 g_8 \mathrm{dx} + \frac{1}{\alpha_2} a_1 b_1. \end{aligned}$$

The norm on Z is induced by this inner product and the completion of Z with respect to this norm follows directly since the H^1-norm of a function dominates its infinity norm.

The state operator *A* associated with the beam equation is defined as follows. The domain of A, $D(A)$, is given by

$$D(A) = \left\{ \begin{array}{l} z_1 \in H_{l,0}^2 \times H_{l,0}^1 \times H_l^2 \times H_l^1 \times H_{r,0}^2 \times H_{r,0}^1 \times H_r^2 \times H_r^1 \times \mathbb{R} \text{ and} \\ f_{3,x}(-l) = 0, f_3(0) = f_7(0), f_{3,x}(0) = f_{7,x}(0), f_{7,x}(l) = 0, \\ f_4(0) = f_8(0), a_1 = f_6(l) \end{array} \right\}.$$

The density of $D(A)$ in Z follows from the usual arguments using infinitely differentiable functions and Sobolev embedding. If $z_1 \in D(A)$ and $z_2 = Az_1$ then,

$$g_1 = f_2,\ g_2 = \alpha f_{1,xx} - d_1 f_2 - \alpha f_{3,x},$$

$$g_3 = f_4,\ g_4 = \alpha\alpha_1\left(f_{1,x} - f_3\right) + \beta f_{3,xx} - d_2 f_4,$$

$$g_5 = f_6,\ g_6 = \alpha f_{5,xx} - d_1 f_6 - \alpha f_{7,x},$$

$$g_7 = f_8,\ g_8 = \alpha\alpha_1\left(f_{5,x} - f_7\right) + \beta f_{7,xx} - d_2 f_8, \text{ and}$$

$$b_1 = \alpha\alpha_2\left(f_7(l) - f_{5,x}(l)\right) - d_3 a_1.$$

A.2 Exponential stability of the beam equation

The wellposedness of the beam equation can be established as in Chapter 6 and is not discussed here. Let the semigroup associated with the beam equation be $S(t)$. The exponential stability of $S(t)$ is established next. For brevity of notation, the subscripts *l* and *r* are dropped from the y and ψ without causing ambiguity. Also C will represent a generic constant taking different value in different equations. Consider the state space representation of the beam equation,

$$\begin{aligned} z_t &= Az, \\ z(0) &= z_0. \end{aligned} \tag{A.1}$$

Consider the energy function along the trajectory of Eq. (A.1),

$$E(t) = \int_{-l}^{0} + \int_{0}^{l}\left(m_b y_t^2 + \frac{Im_b}{a_b}\psi_t^2 + k'Ga_b\left(\psi - y_x\right)^2 + EI\psi_x^2\right)\mathrm{dx} + My_t(l)^2.$$

Lemma A1: Let $z_0 \in D(A)$. *Then* $E_t(t) \le 0$.

Proof: If $z_0 \in D(A)$, then the trajectory of Eq. (A.1) is a continuous function of time on $D(A)$ with the graph norm and a continuously differentiable function of time on Z. Therefore taking the time derivative of $E(t)$ gives

$$\frac{1}{2}E_t(t) = \int_{-l}^{0} + \int_{0}^{l} \left(m_b y_t y_{tt} + \frac{Im_b}{a_b}\psi_t \psi_{tt} + EI\psi_x \psi_{xt} \right) \mathrm{dx} + \int_{-l}^{0} + \int_{0}^{l} k'Ga_b(\psi - y_x)(\psi_t - y_{xt})\,\mathrm{dx} + My_t(l)\,y_{tt}(l).$$

By substituting for the terms y_{tt} and ψ_{tt} from the PDEs gives

$$\frac{1}{2}E_t(t) = \int_{-l}^{0} + \int_{0}^{l} y_t\left(-\gamma_y y_t + k'Ga_b(y_{xx} - \psi_x)\right)\mathrm{dx} + \int_{-l}^{0} + \int_{0}^{l} \psi_t\left(-\gamma_\psi \psi_t + EI\psi_{xx} + k'Ga_b(y_x - \psi)\right)\mathrm{dx}$$
$$+ \int_{-l}^{0} + \int_{0}^{l} \left(k'Ga_b(\psi - y_x)(\psi_t - y_{xt}) + EI\psi_x\psi_{xt}\right)\mathrm{dx} + y_t(l)\left(-\gamma_M y_t(l) - k'Ga_b(y_x(l) - \psi(l))\right).$$

Using integration by parts and the appropriate boundary conditions of the PDE system it follows after simplification that

$$\frac{1}{2}E_t(t) = \int_{-l}^{0} + \int_{0}^{l} \left(-\gamma_y y_t^2 - \gamma_\psi \psi_t^2\right)\mathrm{dx} - \gamma_M y_t^2(l).$$

Hence, $E_t(t) \le 0$. □

Lemma A2: There exist constants γ_1 and γ_2 such that for any $z_0 \in Z$,

$$\gamma_1 \left\| S(t)z_0 \right\|_Z^2 \le E(t) \le \gamma_2 \left\| S(t)z_0 \right\|_Z^2 .$$

Proof: Note that

$$\left\| S(t)z_0 \right\|_Z^2 = \left\| z(t) \right\|_Z^2 = y_t^2(l)/\alpha_2 + \int_{-l}^{0} + \int_{0}^{l} \left(\alpha y_x^2 + y_t^2 + \psi^2 + \beta\psi_x^2 + \psi_t^2\right)\mathrm{dx}.$$

The existence of γ_2 such that $E(t) \le \gamma_2 \left\| S(t)z_0 \right\|_Z^2$ follows easily. $\gamma_1 \left\| S(t)z_0 \right\|_Z^2 \le E(t)$ for some γ_1 if for some C,

$$C\left(\int_{-l}^{0}+\int_{0}^{l}\left(\left(\psi-y_x\right)^2+\psi_x^2\right)\mathrm{dx}\right)\geq\int_{-l}^{0}+\int_{0}^{l}y_x^2\,\mathrm{dx}\,.$$

The last inequality follows from Lemma A3 presented next. □

Lemma A3: Let $f,g\in H^1(-l,l)$ *with* $f(-l)=f(0)=0$. *Then* $\exists C_0>0$ *such that*

$$C_0\left(\int_{-l}^{l}(f_x-g)^2\,\mathrm{dx}+\int_{-l}^{l}g_x^2\mathrm{dx}\right)\geq\int_{-l}^{l}f_x^2\mathrm{dx}\,.$$

Proof: Following [55] define the function w on $[-l,0]$ by

$$w_x=-g+\frac{1}{l}\int_{-l}^{0}g\,\mathrm{dx}\,,\ w(-l)=0\,.$$

It follows from Poincare inequality that

$$\int_{-l}^{0}w_x^2\,\mathrm{dx}=\int_{-l}^{0}g^2\,\mathrm{dx}-\frac{1}{l}\left(\int_{-l}^{0}g\,\mathrm{dx}\right)^2\leq C\int_{-l}^{0}g_x^2\,\mathrm{dx}\,.$$

Therefore

$$\int_{-l}^{0}g^2\,\mathrm{dx}\ \leq\ C\int_{-l}^{0}g_x^2\,\mathrm{dx}+\frac{1}{l}\left(\int_{-l}^{0}(g-f_x)\mathrm{dx}\right)^2\ \leq C\int_{-l}^{0}g_x^2\,\mathrm{dx}+C\int_{-l}^{0}(g-f_x)^2\,\mathrm{dx}.$$

Let $g_0=\int_{-l}^{0}g\,\mathrm{dx}=g(x_0)$ for $x_0\in[-l,0]$. Then clearly

$$g_0^2\ \leq\ C\int_{-l}^{0}g_x^2\,\mathrm{dx}+C\int_{-l}^{0}(g-f_x)^2\,\mathrm{dx}.$$

Also for $x\in[-l,l]$, $g(x)=g_0+\int_{x_0}^{x}g_x\,\mathrm{dx}$. Hence it follows that

$$\int_{-l}^{l}g^2\,\mathrm{dx}\ \leq\ Cg_0^2+C\int_{-l}^{l}g_x^2\,\mathrm{dx}\ \leq\ C\int_{-l}^{l}g_x^2\,\mathrm{dx}+C\int_{-l}^{l}(g-f_x)^2\,\mathrm{dx}.$$

This completes the proof of the lemma. □

Along the trajectory of Eq. (A.1) define the functions

$$G(t) \equiv G(z(t)) = \int_{-l}^{0} + \int_{0}^{l} \left(m_b y y_t + \frac{I m_b}{a_b} \psi \psi_t \right) \mathrm{dx} + M y(l) y_t(l),$$

and $F(t) = \frac{\mu t E(t)}{2} + G(t)$, where $\mu > 0$ is a constant that must be chosen. Using Jensen's inequality it can be shown that $\left| G(z(t)) \right| \le C \left\| z(t) \right\|_Z^2$ where C is independent of the trajectory.

Lemma A4: Let $z_0 \in D(A)$. *There exists* $T > 0$ *independent of* z_0 *such that* $\forall t \ge T$, $F_t(t) \le 0$.

Proof: Since $z_0 \in D(A)$, taking the time derivative of $F(t)$ as in Lemma A1 gives

$$F_t = \frac{\mu}{2}(E + tE_t) + \int_{-l}^{0} + \int_{0}^{l} \left(m_b \left(y_t^2 + y y_{tt} \right) + \frac{I m_b}{a_b} \left(\psi_t^2 + \psi \psi_{tt} \right) \right) \mathrm{dx} + M \left(y_t^2(l) + y(l) y_{tt}(l) \right),$$

$$= \frac{\mu}{2} \int_{-l}^{0} + \int_{0}^{l} \left(m_b y_t^2 + \frac{I m_b}{a_b} \psi_t^2 + k' G a_b (\psi - y_x)^2 + EI \psi_x^2 \right) \mathrm{dx} + \frac{\mu M}{2} y_t^2(l)$$

$$+ \mu t \int_{-l}^{0} + \int_{0}^{l} \left(-\gamma_y y_t^2 - \gamma_\psi \psi_t^2 \right) \mathrm{dx} - \mu t \gamma_M y_t^2(l)$$

$$+ \int_{-l}^{0} + \int_{0}^{l} \left(m_b y_t^2 + y \left(-\gamma_y y_t + k' G a_b (y_{xx} - \psi_x) \right) \right) \mathrm{dx}$$

$$+ \int_{-l}^{0} + \int_{0}^{l} \left(\frac{I m_b}{a_b} \psi_t^2 + \psi \left(-\gamma_\psi \psi_t + EI \psi_{xx} + k' G a_b (y_x - \psi) \right) \right) \mathrm{dx}$$

$$+ M y_t(l)^2 + y(l) \left(-\gamma_M y_t(l) - k' G a_b (y_x(l) - \psi(l)) \right),$$

Next using integration by parts and the appropriate boundary conditions it follows that

$$F_t = \int_{-l}^{0} + \int_{0}^{l} \left(y_t^2 \left(\frac{\mu m_b}{2} - \frac{\mu \gamma_y t}{2} + m_b \right) + EI\psi_x^2 \left(\frac{\mu}{2} - 1 \right) \right) \mathrm{dx}$$

$$+ \int_{-l}^{0} + \int_{0}^{l} \left(k'Ga_b \left(\psi - y_x \right)^2 \left(\frac{\mu}{2} - 1 \right) + \psi_t^2 \left(\frac{\mu I m_b}{2a_b} - \frac{\mu \gamma_\psi t}{2} + \frac{I m_b}{a_b} \right) \right) \mathrm{dx}$$

$$+ \left[y_t^2 (l) \left(\frac{\mu M}{2} - \frac{\mu \gamma_M t}{2} + M \right) \right] - \left\{ \gamma_M y(l) y_t (l) + \int_{-l}^{0} + \int_{0}^{l} \left(-\gamma_y y y_t - \gamma_\psi \psi \psi_t \right) \mathrm{dx} \right\}.$$

Choose $\mu < 1$. Then for a sufficiently large T independent of the specific trajectory, the integral terms with y_t^2, ψ_t^2, $\left(\psi - y_x\right)^2$ and ψ_x^2 are negative if $t > T$. The terms in the square bracket are also negative. The remaining terms in the curly bracket can be dominated as follows:

$$\left| -\gamma_M y(l) y_t (l) + \int_{-l}^{0} + \int_{0}^{l} \left(-\gamma_y y y_t - \gamma_\psi \psi \psi_t \right) \mathrm{dx} \right|$$

$$\le C \left(y_t^2 (l) + \int_{-l}^{0} + \int_{0}^{l} \left(y_t^2 + \psi_t^2 \right) \mathrm{dx} \right) + \delta \left(y^2 (l) + \int_{-l}^{0} + \int_{0}^{l} \left(y^2 + \psi^2 \right) \mathrm{dx} \right)$$

$$\le C \left(y_t^2 (l) + \int_{-l}^{0} + \int_{0}^{l} \left(y_t^2 + \psi_t^2 \right) \mathrm{dx} \right) + C\delta \left(\int_{-l}^{0} + \int_{0}^{l} \left(y_x^2 + \psi^2 \right) \mathrm{dx} \right)$$

$$\le C \left(y_t^2 (l) + \int_{-l}^{0} + \int_{0}^{l} \left(y_t^2 + \psi_t^2 \right) \mathrm{dx} \right) + C\delta \left(\int_{-l}^{0} + \int_{0}^{l} \left(\left(\psi - y_x \right)^2 + \psi_x^2 \right) \mathrm{dx} \right).$$

Here the first inequality is using Hölder's inequality, the second inequality is using Jensen's inequality and the third inequality is using Lemma A3. If δ is chosen small enough, for sufficiently large T, all these terms are dominated by the other negative terms in F_t. Hence for $t > T$, $F_t < 0$. From the proof T is independent of the specific trajectory. □

Theorem A1: $S(t)$ *is an exponentially stable semigroup.*

Proof: Let $z_0 \in D(A)$. For any $t \le T$, where T is as in Lemma A4

$$F(t)=\frac{\mu t}{2}E(t)+G(t) \;\le\; \frac{\mu t\gamma_2}{2}\|z(t)\|^2+C\|z(t)\|^2$$
$$\le \frac{\mu T\gamma_2}{2}R\|z_0\|^2+CR\|z_0\|^2$$
$$\le \bar{C}\|z_0\|^2,$$

where $R=\sup_{t\le T}\|S(t)\|_{op}$. But from Lemma A4 $F_t<0$, for $t>T$. Hence, it follows that $F(t)\le \bar{C}\|z_0\|_Z^2$ for all t. Therefore,

$$\left|\frac{\mu t}{2}E(t)+G(t)\right|\le \bar{C}\|z_0\|_Z^2,\ \forall t,$$
$$\Rightarrow \gamma_1\mu t\|z(t)\|^2-C\|z(t)\|_Z^2<\bar{C}\|z_0\|_Z^2,\ \forall t,$$
$$\Rightarrow \|z(t)\|^2<\frac{2\bar{\bar{C}}\|z_0\|_Z^2}{\gamma_1\mu t},\ \forall t:\gamma_1\mu t>2C.$$

Hence for $t>2C/\gamma_1\mu$, $\|z(t)\|_Z=\|S(t)z_0\|_Z<\bar{\bar{C}}\|z_0\|_Z/\sqrt{t}$. Thus $S(t)z_0$ is a bounded function that decays like $1/\sqrt{t}$. Since $\bar{C}$ and $\bar{\bar{C}}$ are independent of $z_0\in D(A)$, by the density of $D(A)$ in Z this decay is true for all $z_0\in Z$. Hence the cube of the response to initial condition is integrable for all $z_0\in Z$. From [56] it follows that $S(t)$ is an exponentially stable C_0-semigroup. □